T.R.
EGE UNIVERSITY
Graduate School of Natural and Applied Sciences

INVESTIGATION OF THE EFFECTS OF CENTROSOME DEFECTS ON THE DEVELOPMENT OF PROSTATE CANCER

PhD Thesis

Aadil JAVED

Department of Biotechnology

İzmir
2022

T.R.
EGE UNIVERSITY
Graduate School of Natural and Applied Sciences

INVESTIGATION OF THE EFFECTS OF CENTROSOME DEFECTS ON THE DEVELOPMENT OF PROSTATE CANCER

Aadil JAVED

Supervisor : Prof Dr. Kemal Sami KORKMAZ

Department of Biotechnology
Biotechnology Third Cycle Programme

İzmir
2022

EGE UNIVERSITY GRADUATE SCHOOL OF NATURAL AND APPLIED SCIENCES

DECLARATION OF COMPLIANCE WITH THE CODE OF ETHICS

In accordance with the relevant provisions of the EU Graduate Education Regulations, this thesis titled "Investigation of the effects of centrosome defects on the development of Prostate cancer", which I submitted as a Doctorate Thesis, is my own work, and all the results, information and documents I have presented are my own work that I have obtained within the scope of this thesis work, that I have cited all the information and comments that were not obtained through this thesis work, and that I have duly provided them in the list of sources, that I have not acted in violation of patent and copyright rights during the thesis work and writing, I declare that I have not submitted my thesis in another thesis study or at another university, that I have acted in accordance with the scientific ethical rules at all stages from the planning to the writing of this thesis, and that I will accept all kinds of legal consequences if the opposite arises.

10/06/2022

Aadil JAVED

ABSTRACT

INVESTIGATION OF THE EFFECTS OF CENTROSOME DEFECTS ON THE DEVELOPMENT OF PROSTATE CANCER

JAVED, Aadil

Doctorate (Ph.D.) Thesis, Department of Biotechnology

Thesis Supervisor: Prof. Dr. Kemal Sami KORKMAZ

June 10, 2022, 181 Pages

In this study, we characterized HN1 using *in silico* approaches as a putative disordered protein with gene expression high in Prostate cancer samples as compared to normal Prostate tissues. *HN1* co-expression network from Prostate cancer tissues highlighted that HN1 is involved in centrosome and cell cycle related pathways. The native protein levels of HN1 were found significantly higher in Prostate cancer cell lines such as LNCaP and PC-3 as compared to normal Prostate epithelial cells (RWPE1). This indicates that HN1 is a cancer related protein manifesting in tumorous cells. HN1 expression was enriched in S-phase of the cell cycle and its overexpression also resulted in higher S-phase populations in different Prostate cell lines. HN1 rescue using Tet-ON system in HN1 silenced cells showed that HN1 is a centrosome clustering protein in Prostate cancer cells. Moreover, *HN1* overexpression influences APC/C activity indicated in changes in Fluorescent-based Cell Cycle Indicator (FUCCI) probes in PC-3 cells. Lastly, HN1 overexpression increases migration and invasion of Prostate cancer cells. In summary, HN1 is a cell cycle regulatory protein involved in centrosome regulation and is enriched in tumor cells as compared to normal Prostate cells.

Key words: Prostate Cancer, Centrosome, Cell Cycle, HN1

ÖZET

SENTROZOM HATALARININ PROSTAT KANSERİ GELİŞİMİNE OLAN ETKİLERİNİN ARAŞTIRILMASI

JAVED, Aadil

Doktora Tezi

Tez Danışmanı: Prof. Dr. Kemal Sami KORKMAZ

Haziran 10, 2022, 181 Sayfa

Bu tez çalışmasında, normal Prostat dokularına kıyasla Prostat kanseri örneklerinde yüksek gen ekspresyonuna sahip olduğu gösterilen ve yapısal olarak düzensiz bir protein olan *HN1'i* öncelikle *in siliko* yaklaşımlar kullanarak tanımladık. Prostat kanseri dokularında *HN1* ortak ekspresyon ağının, HN1'in sentrozom ve hücre döngüsü ile ilgili yollarda yer aldığını gösterdik. HN1'in doğal protein seviyelerinin, normal Prostat epitel hücreleri (RWPE1) ile karşılaştırıldığında LNCaP ve PC-3 gibi Prostat kanseri hücre hatlarında önemli oranda yüksek olduğunu bulguladık. Bu durum HN1'in tümörlerin gelişimi ile ilgili bir protein olabileceğini düşündürdü. Ayrıca, HN1 ifadesi hücre döngüsünün S-fazında yüksekti ve vektörler ile aşırı ekspresyonu sonucunda farklı Prostat hücre hatlarında daha yüksek S-faz popülasyonları ile sonuçlandı. HN1 susturulmuş hücrelerde Tet-ON sistemi kullanarak HN1 ifadesi kurtarma deneyi gerçekleştirildiğinde, HN1'in Prostat kanseri hücrelerinde bir sentrozom kümeleme proteini olduğunu görüldü. Yine HN1 aşırı ifadesi ile PC-3 hücrelerinde - Floresan bazlı Hücre Döngüsü Göstergesi (FUCCI) - problarındaki değişikliklerde belirtilen APC/C aktivitesininde etkilendiği gösterildi. Son olarak, çalışmalarımızda HN1 aşırı ifadesi ile Prostat kanseri hücrelerinin göçünü ve istilasını arttırdığını gösterdik. Özetle, HN1, sentrozom düzenlemesinde yer alan bir hücre döngüsü düzenleyici proteindir ve normal Prostat hücrelerine kıyasla tümör hücrelerinde ifadesi artmaktadır.

Anahtar kelimeler: Prostat Kanseri, Sentrozom, Hücre Döngüsü, HN1

PREFACE

This study has been compiled owing to the untiring efforts of Prof. Dr. Kemal Sami Korkmaz as he managed the finances and day-to-day activities of our laboratory. I believe HN1 is truly a carcinogenic gene and functions in the regulation of key mechanisms inside the cell cycle, therefore, driving the passion of our team to continuously work. The period it took to complete this study was not a smooth ride as the world faced a once in a century-pandemic. Personally, I was able to persevere due to the undying support of my family. I lost my grandmother (Nano), and my nephew (Hashir) and it pains me to remember that I could not be there to see them one last time. I hope the study puts HN1 on the radar of cell biology-related investigations so that the sacrifices we make for the sake of knowledge become worth the efforts.

I dedicate this study to my Mama, Papa, Nano, and Hashir

İzmir

10/06/2022

Aadil JAVED

CONTENTS

APPROVAL iii

DECLARATION OF COMPLIANCE WITH THE CODE OF ETHICS v

ABSTRACT vii

ÖZET ix

PREFACE xi

CONTENTS xiv

LIST OF FIGURES xx

INDEX OF TABLES xxiii

INDEX OF SYMBOLS AND ABBREVIATIONS xxiii

1. INTRODUCTION 1

1.1. Aims Of The Study 2

1.2. Significance Of The Study 2

2. LITERATURE REVIEW 4

2.1. Prostate Cancer 4

2.1.1. Introduction To Prostate Cancer 4

2.1.2. Genetic Basis Of Prostate Cancer 5

2.1.3. Androgen Receptor And Its Involvement In Prostate Cancer 8

2.2. Centrosome In Cancer 10

2.2.1. Structure And Function Of Centrosome 10

2.2.2. Centriole Duplication Cycle 11

2.2.3. Centrosome Abnormalities In Cancer 12

2.2.4. Centrosome Amplification And Its Consequences 15

2.2.5. Centrosome Clustering 16

CONTENTS (CONTINUED)

2.3. Cell Cycle 18

2.3.1. Overview Of Cell Cycle 18

2.3.2. Cyclin Dependent Kinases In Cell Cycle Control 19

2.3.3. E3 Ligase Complexes In Cell Cycle Control 22

2.4. Hematological And Neurological Expressed 1 24

2.4.1. HN1 In Historical Context 24

2.4.2. HN1 In Different Cancers 26

2.4.3. HN1 In Prostate Cancer Cell Lines 28

2.5. Tet-On Inducible Expression System 29

2.6. Fluorescent Ubiquitination Based Cell Cycle Indicator (Fucci) System 31

3. MATERIALS AND METHODS 33

3.1. *In Silico* Approaches For HN1 33

3.1.1. Disorder Prediction Tools 33

3.1.2. *HN1* Co-Expression Network Analysis 33

3.1.3. Genomics And Transcriptomics Data Analysis Of *HN1* In Prostate Cancer 34

3.2. Bacterial Culture And Recombinant DNA Preparation 35

3.2.1. Competent Cell Preparation 35

3.2.1.1. Materials 35

3.2.1.2. Method 35

3.2.2. Plasmid And Ligation Reaction Transformation 36

3.2.2.1. Materials 36

3.2.2.2. Method 36

3.2.3. Colony PCR And Restriction Digestions 37

CONTENTS (CONTINUED)

3.2.3.1. Materials 37

3.2.3.2. Method 37

3.2.4. Agarose Gel Electrophoresis 38

3.2.4.1. Materials 38

3.2.4.2. Method 38

3.2.5. Plasmid DNA Isolation (Alkaline Lysis Method) 39

3.2.5.1. Materials 39

3.2.5.2. Method 39

3.2.6. Plasmid DNA Isolation (Hi-Speed Midi-Prep) 40

3.2.6.1. Materials 40

3.2.6.2. Method 41

3.2.7. Inserting HM-HN1 And HN1-Venus In pCW57 Plasmid 41

3.3. General Mammalian Cell Culture Methods 43

3.3.1. Materials 43

3.3.2. Thawing, Growing, Seeding, Counting, And Storing Adherent Cell Lines 44

3.4. DNA And siRNA Transfections In Prostate Cell Lines 46

3.4.1. Materials 46

3.4.2. Method 46

3.5. Cell Proliferation Assay 47

3.6. Cell Cycle Distribution Assay 48

3.6.1. Materials 48

3.6.2. Method 48

3.7. Protein Isolation And Western Blotting 49

CONTENTS (CONTINUED)

3.7.1. Chemicals And Solutions 49

3.7.2. Antibodies For Western Blotting 50

3.7.3. Method Of Protein Isolation And SDS-PAGE 51

3.7.4. Method For Western Blotting 53

3.8. Immunofluorescence Microscopy 54

3.8.1. Materials 54

3.8.2. Antibodies For Immunofluorescence 55

3.8.3. Method 55

3.9. Lentivirus Production 57

3.9.1. Materials 57

3.9.2. Method 57

3.10. Stable Cell Line Generation 58

3.10.1. Materials 58

3.10.2. Method 58

3.11. Cell Cycle Synchronization Approaches 59

3.12. Apoptosis Assay And Live Cell Flow Cytometry 60

3.12.1. Materials 60

3.12.2. Method 61

3.13. Cell Migration And Invasion Assay 61

3.13.1. Materials 61

3.13.2. Method 61

4. RESULTS 63

4.1. *In Silico* Analysis On HN1 63

CONTENTS (CONTINUED)

4.1.1. HN1 Is A Putative Disordered Protein 63

4.1.2. *HN1* Co-Expression Network Identifies Its Potential Role In Cell Cycle And Centrosome Related Pathways 65

4.1.3. STRING Interaction Network For *HN1* Co-Expressed Genes In PRAD 69

4.1.4. *HN1* Is Overexpressed In Prostate Cancer 70

4.2. Plasmid DNA And siRNA Transfections In Prostate Cell Lines 71

4.2.1. Effect Of Altered HN1 Expression On Proliferation 71

4.2.2. Effect Of Altered HN1 Expression On Cell Cycle Distribution 72

4.2.3. HN1 Depletion And Overexpression In DU-145 Cells 74

4.2.4. HN1 Depletion In DU-145 Leads To Disruption Of Γ-Tubulin 75

4.2.5. Effect Of *HN1* Overexpression On Cell Cycle Related Proteins 77

4.3. Analyzing Native HN1 Protein In Prostate Cancer Cells 79

4.3.1. Cyclohexamide (CHX) Chase Assay 79

4.3.2. HN1 Protein Levels In Cell Cycle Synchronized Prostate Cancer Cells 80

4.4. HN1 Inducible Tet-ON System 83

4.4.1. *HN1* Cloning In Tet-ON Inducible Expression System 83

4.4.2. Validating HN1 Inducible System By Western Blotting 84

4.4.3. Effect Of HN1-Induction By Doxycycline In HN1-Inducible Stable Prostate Cancer Cell Lines 85

4.4.4. HN1 Rescue After Depletion By siRna In HN1-Inducible PC-3 Cells 86

4.4.5 Effect Of *HN1* Overexpression On Cyclin B1 In HN1-Inducible PC-3 Cells .. 90

4.4.6. HN1 Induced PC-3 Cells Are Protective Against Apoptotic Inducers 91

4.4.7. *HN1* Overexpression After G2 Induces An Early Exit From Mitosis 93

CONTENTS (CONTINUED)

4.4.8. Wound Healing Assay In HN1 Inducible PC-3 Cells 95

4.5. *HN1* Overexpression In FUCCI Cells 96

4.5.1. Generating And Validating FUCCI-PC3 Cells 96

4.5.2. Deciphering APC/C Activity Using Live FUCCI Cells 99

4.5.3. Effect Of *HN1* Overexpression On FUCCI-PC3 Cells 101

4.6. HN1-Venus Induction Using Tet-ON Inducible Expression System 104

4.6.1. Constructing And Validating pCW57-HN1-Venus Transgene Plasmid System 104

4.6.2. Effect Of HN1 Overexpression Using Pcw57-HN1-Mvenus 106

5. DISCUSSION 110

5.1. HN1 Is A Disordered Protein Expressed Highly In Prostate Cancer 110

5.2. HN1 Is Involved In Regulating Centrosomes In Prostate Cancer 111

5.3. HN1 Is A Cell Cycle Regulatory Protein In Prostate Cancer Cells 114

5.4. *HN1* Expression Promotes Tumorigenic Profile Of PC-3 Cells 116

6. CONCLUSION AND FUTURE RECOMMENDATIONS 119

REFERENCES 121

RESUME 142

ACKNOWLEDGEMENT 145

LIST OF FIGURES (CONTINUED)

Figure 2.1: Difference between normal Prostate and enlarged Prostate 5

Figure 2.2: Commonly mutated genes in Prostate cancer 7

Figure 2.3: The general relationship of AR with Prostate Cancer progression 9

Figure 2.4: General structure of centrosome 11

Figure: 2.5 Centrosome duplication cycle is aligned with the cell cycle. 12

Figure 2.6: Simplified centrosome amplification pathways in cancers. 14

Figure 2.7: The consequences of centrosome amplification during cell cycle. 16

Figure 2.8: Centrosome clustering of supernumerary centrosomes 17

Figure 2.9: Overview of cell cycle regulation and cell cycle checkpoints..... 19

Figure 2.10: Regulation of Cell Cycle by Cyclin Dependent Kinases..... 21

Figure 2.11: The interplay of APC/C and SCF complexes..... 23

Figure 2.12: The mechanism of Tet-ON system. 30

Figure 2.13: The map of pCW57.1 plasmid for Tet-ON system. 31

Figure 2.14: Overview of the FUCCI reporter system..... 32

Figure 4.1: *In silico* approaches predict HN1 as a disordered protein 64

Figure 4.2: Enrichment of HN1 co-expression network in CoExpedia database and PRAD dataset..... 66

Figure 4.3: Protein-protein interaction map of HN1 co-expressed genes in PRAD .. 70

Figure 4.4: HN1 is overexpressed in Prostate cancer. 71

Figure 4.5: Effect of HN1 alteration on proliferation of Prostate cell lines..... 72

Figure 4.6: Cell Cycle Distribution Analysis of altered HN1 levels in Prostate cells 73

Figure 4.7: Effect of altered HN1 expression on proliferation and cell cycle distribution of DU-145 cells 75

LIST OF FIGURES (CONTINUED)

Figure 4.8: HN1 depletion in DU-145 cells causes disruption of γ-tubulin by siRNA transfection 76

Figure 4.9: HN1 depletion in metaphase DU-145 cells, result in dysregulation of spindle assembly. 77

Figure 4.10: Effect of altered HN1 expression on different cell cycle related proteins 79

Figure 4.11: Cyclohexamide (CHX) chase assay for HN1 in different Prostate cancer cell lines 80

Figure 4.12: Cell cycle synchronization approaches show that HN1 levels fluctuate in cell cycle in PC-3 cells. 82

Figure 4.13: LNCaP, DU-145, and PC-3 cells have HN1 levels fluctuating throughout the cell cycle. 83

Figure 4.14: *HN1* was cloned into pCW57.1 expression plasmid 84

Figure 4.15: HN1 induction upon Doxycycline treatment in PC3-pCW57-HMHN1 cells was validated. 85

Figure 4.16. HN1 inducible PC-3 and LNCaP cells show differential response to HN1 induction for cell proliferation. 86

Figure 4.17: Schematic representation of HN1 rescue experiment in HN1-inducible PC-3 cells 87

Figure 4.18: HN1 rescue causes centrosome clustering like phenotype in PC-3 cells 88

Figure 4.19: HN1 alteration or rescue causes nuclear abnormalities 89

Figure 4.20: HN1 rescue did not rescue the centrosomal defects in PC-3 cells 90

LIST OF FIGURES (CONTINUED)

Figure 4.21: HN1 induction in HN1-inducible PC-3 cells show reduction in cyclin B1 levels 91

Figure 4.22: The effect of *HN1* overexpression on apoptotic inducing factor Bax. .. 91

Figure 4.23: The *HN1* overexpressed PC-3 cells are protective against apoptotic inducers 92

Figure 4.24: The *HN1* overexpression in G2 synchronized cells show early exit from mitosis 94

Figure 4.25: Cell cycle distribution analysis for cells released into G1 after G2 synchronization 95

Figure 4.26: Effect of *HN1* overexpression on the migration of PC3 cells 96

Figure 4.27: Validating FUCCI and lentiviral packaging plasmids by restriction digestion. 97

Figure 4.28: Validation of FUCCI-PC3 cells using nocodazole treatment and immunofluorescence microscopy 98

Figure 4.29: FUCCI- PC3s were validated using flow cytometry 99

Figure 4.30: FUCCI cells can be used for deciphering APC/C activity 101

Figure 4.31: *HN1* overexpression leads to stabilization of an indirect measure of APC/C activity 102

Figure 4.32: HN1 induction after G2 using Tet-ON system in FUCCI-PC3 cells showed early exit from mitosis 103

Figure 4.33: *HN1* insertion in pcDNA4-TO-Venus by PCR and restriction cloning 104

LIST OF FIGURES (CONTINUED)

Figure 4.34: *HN1*-Venus insertion in pCW57 vector and validation by microscopy and western blotting. 105

Figure 4.35: Effect of HN1-mVenus on CP110 and cyclin F using doxycycline in Tet-inducible system 107

Figure 4.36: Effect of HN1-mVenus on geminin using doxycycline in Tet-inducible system 107

Figure 4.37: Effect of *HN1* overexpression on Invasion capability of PC3 cells was measured using cell invasion assay 109

LIST OF TABLES

Table 3.1: Cell lines, media composition and sources used in the study 44

Table 4.1: TCGA PRAD dataset contains *HN1* co-expressed centrosomal genes ... 67

Table 4.2: TCGA PRAD dataset contains *HN1* co-expressed cell cycle genes..... 68

Table 4.3: TCGA PRAD dataset contains *HN1* co-expressed kinesin family genes 69

LIST OF SYMBOLS AND ABBREVIATIONS

Symbols	Explanation
°C	Degree Centigrade
bp	Base pair
C	Cysteine

LIST OF SYMBOLS AND ABBREVIATIONS (CONTINUED)

E	Glutamate
F	Phenylalanine
g	Gram
G	Glycine
H	Histidine
I	Isoleucine
kb	Kilobase
L	Leucine
M	Methionine
mA	Milli-Ampere
ml	Milli-liters
mm	Milli-meters
mM	Milli-Molar
N	Normal Solution
ng	Nanogram
P	Proline
pmol	Picomole
T	Threonine
Thr	Threonine

LIST OF SYMBOLS AND ABBREVIATIONS (CONTINUED)

Tyr	Tyrosine
V	Valine
V	Volt
W	Tryptophan
Y	Tyrosine
α	alpha
β	beta
γ	gamma
μ	micro
μl	Micro-liters
μM	Micro-Molar

Abbreviations	Explanation
ADP	Androgen Deprivation Therapy
AKT1	AKT Serine/Threonine Kinase 1
APC	Adenomatous Polyposis Coli
APC/C	Anaphase promoting complex/cyclosome
APC1	Anaphase Promoting Complex Subunit 1
APS	Ammonium Persulphate
AR	Androgen Receptor

LIST OF ABBREVIATIONS (CONTINUED)

ATC	Anaplastic Thyroid Cancer
ATCC	American Type Culture Collection
ATEs	Androgen response elements
ATM	Ataxia-Telangiectasia Mutated
ATP	Adenosine triphosphate
ATR	Ataxia telangiectasia and Rad3 related
AURKA	Aurora Kinase A
BCA	Bicinchoninic Acid
BP	Biological Process
BRCA2	Breast Cancer Associated 2
BSA	Bovine Serum Albumin
BUB1	Budding Uninhibited By Benzimidazoles 1 Homolog
CAV1	Caveolin-1
CC	Cellular Compartment
CDC20	Cell Division Cycle 20
CDC25A	Cell Division Cycle 25A
CDC6	Cell Division Cycle 6
CDKs	Cyclin-dependent kinases
cDNA	Complementary DNA

LIST OF ABBREVIATIONS (CONTINUED)

CDT1	Chromatin licensing and DNA replication factor 1
CEP164	Centrosomal Protein of 164 kDa
Cep97	Centrosomal Protein 97
CHK1	Checkpoint Kinase 1
CHK2	Checkpoint Kinase 2
CIP/KIP	CDK Interacting Protein/Kinase Inhibitory Protein
CP110	Centriolar Coiled-Coil Protein Of 110 kDa
CPAP	Centrosomal protein 4.1-associated protein
CPC	Chromosome Passenger Complex
CRPC	Castration-Resistant Prostate Cancer
CSPC	Castration-Sensitive Prostate Cancer
CTNNB1	Catenin Beta 1
DDR	DNA Damage Response
dH_2O	Distilled Water
DHFR	Dihydrofolate Reductase
DHT	dihydrotestosterone
DMEM	Dulbecco's Modified Eagle Medium
DMSO	Dimethyl Sulfoxide
DNA	Deoxyribonucleic Acid

LIST OF ABBREVIATIONS (CONTINUED)

dNTPs	Deoxynucleoside Triphosphates
DU-145	Duke University 145 (Prostate Cancer Cell Line, Brain Metastasized)
E. Coli	*Escherchia Coli*
E2Fs	E2F family of transcription factors
ECL	Enhanced chemiluminescence
EGF	Epidermal Growth Factor
EGFR	Epidermal Growth Factor Receptor
Emi1	Early Mitotic Inhibitor 1
EMT	Epithelial Mesenchymal Transition
ESTs	Expressed Sequence Tags
ETG	ETS-related gene
ETS	Erythroblast Transformation Specific
ETV1	ETS Variant Transcription Factor 1
FBS	Fetal Bovine Serum
FBXW7	F-box/WD repeats carrying protein 7
FITC	Fluorescein isothiocyanate
FOXA1	Forkhead box protein A1
FUCCI	Fluorescent Ubiquitination Cell Cycle Indicator
FUCCI-PC3	PC-3 cells stabilized for FUCCI probes

LIST OF ABBREVIATIONS (CONTINUED)

FZR1	Fizzy related 1
G_0	G (not) / Gap Phase zero (Senescent phase)
G1	Gap Phase 1
G2	Gap Phase 2
GEO	Gene Expression Omnibus
GEPIA	Gene Expression Profiling Interactive Analysis
GO	Gene Ontology
GSK-3β	Glycogen Synthase Kinase 3 beta
GTEx	Genotype-Tissue expression
H2AX	H2A histone family member X
HCC	Hepatocellular Carcinoma
HEC1	Highly Expressed in Cancer 1
HEK293T	Human Embryonic Kidney 293T
HeLa	cervical carcinoma cell line (Henrietta Lacks)
HGNC	HUGO Gene Nomenclature Committee
HN1	Hematological and Neurological Expressed 1
HN1L	Hematological and Neurological Expressed 1 Like
HNRNPA1	Heterogeneous Nuclear Ribonucleoprotein A1
HOXA11-AS1	Homeobox A 11 Antisense Strand 1

LIST OF ABBREVIATIONS (CONTINUED)

HR	Hazard Ratio
hrEGF	Human Recombinant Epidermal Growth Factor
HUGO	Human Genome Organisation
I-TASSER	Iterative Threading ASSEmbly Refinement
IPTG	Isopropyl β-d-1-thiogalactopyranoside
KIFC1	Kinesin Family Member C1
KLK3	Kallikrein 3
LB	Lysogeny Broth
LLS	Log-Likelihood Score
LNCaP	Lymph Node Cancer of the Prostate
M	Mitosis
mAG	Monomeric Azami Green
MAD2	Mitotic Arrest Deficient 2
MF	Molecular Function
miRNA	Micro-RNA
mKO2	Monomeric Kusabira-Orange
MPS1	Monopolar Spindle 1
mRNA	Messenger RNA
MT1-MMP	Membrane-Type 1 Matrix Metalloproteinase

LIST OF ABBREVIATIONS (CONTINUED)

MTOC	Major Microtubule Organizing Centers
MYC	Myelocytomatosis Viral Oncogene
MYCN	MYCN Proto-Oncogene
MYT1	Myelin transcription factor 1
NCOR1	Nuclear Receptor Corepressor 1
NEB	New England Biolabs
NEPC	Neuroendocrine Prostate Cancer
NF-κB	Nuclear factor kappa B
NKX3.1	NK3 Homeobox 1
OD	Optical Density
PAGE	Polyacrylamide Gel Electrophoresis
PBS	Phosphate Buffered Saline
PC-3	Prostate Cancer Cell Line (Bone Metastasized)
PC3-pCW57	PC-3 cells stabilized for pCW57 viruses
PC3-pCW57-HMHN1	PC-3 cells stabilized for pCW57-HMHN1 viruses
PCC	Pearson Correlation Coefficient
PCM	Pericentriolar Material
PCR	Polymerase Chain Reaction
pCW57-HMHN1	pCW57 Plasmid containing HM-HN1 (ORF) insert

LIST OF ABBREVIATIONS (CONTINUED)

PEI	Polyethylenimine
$pH3^{S10}$	Phospho-Histone 3 (Serine 10)
PI	Propidium Iodide
PI3K	Phosphoinositide 3-kinase
PI3K3CA	Phosphatidylinositol-4,5-Bisphosphate 3-Kinase, Catalytic Subunit Alpha
PI3KCB	Phosphatidylinositol-4,5-Bisphosphate 3-Kinase, Catalytic Subunit Beta
PLK4	Polo-Like Kinase 4
PLKs	Polo-Like Kinases
PMSF	Phenylmethylsulfonyl Fluoride
PONDR	Predictor of Natural Disordered Regions
PRAD	Prostate Adenocarcinoma
PSA	Prostate Specific Antigen
PTEN	Phosphatase And Tensin Homolog
PVDF	Polyvinylidene Difluoride
RB1	Retinoblastoma Transcriptional Corepressor 1
Ring-Box 1	Ring-Box 1
RIPA	Radioimmunoprecipitation assay
RPM	Revolutions per Minutes

LIST OF ABBREVIATIONS (CONTINUED)

RPMI	Roswell Park Memorial Institute medium
RRM1	Ribonucleotide Reductase M1
rtTA	Reverse Tetracycline-Controlled Transactivator
RWPE-1	Prostate Epithelial Cells Transformed By HPV
S	Synthesis Phase
SAC	Spindle Assembly Checkpoint
SAGE	Serial Analysis Of Gene Expression
SAS-6	Spindle Assembly Abnormal Protein 6 Homolog
SAS4	Spindle Assembly Abnormal Protein 4
SCF complex	Skp, Cullin, F-box containing complex
SDS	Sodium Dodecyl Sulphate
SFRP1	Secreted Frizzled Related Protein 1
SGOL1	Shugoshin-like 1
siRNA	Small interfering RNA
SKP2	S-phase kinase-associated protein 2
SLBP	Stem-Loop Binding Protein
SOB	Super Optimal Broth
SPOP	Speckle-type POZ protein
STAMP2	Six Transmembrane Prostate Protein 2

LIST OF ABBREVIATIONS (CONTINUED)

STRING	Search Tool for the Retrieval of Interacting Genes/Proteins
SVs	Splice Variants
TAE	Tris-Acetate EDTA
TB	Transforming Buffer
TBS	Tris-Buffered Saline
TBS-T	Tris-Buffered Saline-Tween 20
TCGA	The Cancer Genome Atlas
TE	Tris-EDTA
TEMED	Tetramethylethylenediamine
Tet-ON	Tetracycline ON
TetO	Tetracycline Operator Sequence
tetR	Tetracycline Repressor
TGF-β	Transforming Growth Factor β
TMPSS2	Transmembrane Protease Serine 2
TP53	Transformation-related Protein 53
TPM	Transcripts Per Million
TRE	Tetracycline Response Element
Tris	Trisma Base
tTA	Tetracycline-Controlled Transactivator

UTR	Untranslated Region
UV	Ultraviolet
VP16	Virion Protein 16
WBCs	White Blood Cells
WNT	Wingless/Integrated
ZBTB16	Zinc Finger And BTB Domain Containing 16
β-actin	Beta-Actin
β-catenin	Beta-Catenin
βTrCP	Beta-Transducin Repeat Containing Protein
γ-tubulin	Gamma Tubulin

1. INTRODUCTION

Prostate cancer is a disease that is characterized by the genetic changes occurring in Prostate cells leading to uncontrolled growth and eventually metastasis to other organs of the body including lymph nodes, bones, and even the brain. There are many genetic events that trigger the growth changes in Prostate cells, many of which are known. However, there are certain factors, which remain uncharacterized (Wang et al., 2018). Centrosomes in mammalian cells organize spindle microtubules for equal distribution of genetic material to daughter cells. The centrosome errors either structural or numerical are associated with mitotic and genomic infidelity associated with various cancers. Moreover, centrosome duplication is an event that is intricately linked with the progression of the cell cycle. The cell fate of proliferation depending on the decision of G1 to S phase transition directly affects the decision to duplicate centrosomes. Therefore, cell cycle and centrosome cycles are interlinked. These tightly regulated systems have been studied vastly in the progression of cancer as well (Lin et al., 2022). In the context of Prostate cancer, centrosome and cell cycle irregularities are common. Therefore, components of these cycles influence the progression of normal cells to tumorous. There have been numerous studies detailing the accounts of cell cycle and centrosome cycle involvement in Prostate cancer with the majority of components being enriched in overexpressed forms (Schatten & Ripple, 2018). However, there is still a lot to be discovered.

Hematological and Neurological Expressed 1 (HN1) is a highly conserved gene often expressed in mammalian cells and was previously characterized as regulated by Androgen receptor (AR) in Prostate Cancer cells (Varisli et al., 2012). It has been reported as a prognostic factor for various cancers recently, therefore, there is a growing interest in understanding *HN1* and its role in carcinogenesis (Liu et al., 2020; Chen et al., 2020). The co-expression network of a gene identifies the genes expressed simultaneously with a gene in a given circumstance and can be used to identify the possible mechanisms and functions of a gene product (Serin et al., 2016). The levels of HN1 at transcript and protein levels have not been reported in Prostate cancer samples. Therefore, *in silico* approaches utilizing transcriptomics data provide an important tool in determining if *HN1* is involved in carcinogenesis of Prostate cancer. Moreover, HN1 has

previously been identified as an interacting partner of centrosome marker γ-tubulin, and HN1 silencing leads to the multiplication of γ-tubulin foci (Varisli, 2012, Ozturk, 2016). However, a rescue experiment to determine the impact of HN1 restoration on this phenotype has not been performed and can help identify HN1 as an integral part of centrosome regulation.

An inducible expression system in mammalian cells provides a unique opportunity to investigate the temporal dynamics of the function of an unknown gene product (Kallunki et al., 2019). Since the previous studies indicate that HN1 is involved in the cell cycle pathway, *HN1* can be cloned into a tetracycline-inducible expression system to determine the alterations in cell cycle dynamics controlled by HN1. Furthermore, the Fluorescent-based Cell Cycle Indicator (FUCCI) system is another tool specifically applied to understand the cell cycle dynamics (Zielke & Edgar, 2015), which can be used in combination with the inducible expression system to find the role of HN1 in the cell cycle.

1.1. Aims Of The Study

- Elucidate if the amino-acid sequence of HN1 protein, predicts any indication of it being a disordered protein.
- Using *in silico* approaches, identify and narrow down the key cellular mechanisms for the function of HN1 in the context of Prostate cancer.
- Identify and differentiate the native protein levels of HN1 in different phases of the cell cycle in different cell lines of the Prostate.
- Illustrate any difference in cell proliferation and cell cycle distribution upon alteration of *HN1* expression in different cell lines of Prostate cancer.
- Identify the impact of HN1 rescue on the phenotype of supernumerary centrosomes in Prostate cancer cells.
- Illustrate using the FUCCI reporter system the impact of *HN1* overexpression on the cell cycle indicator probes.
- Investigate the impact of *HN1* overexpression on the invasion and migration of Prostate cancer cells.

1.2. Significance Of The Study

The co-expression network of *HN1* in Prostate cancer can determine the potential pathways of HN1 and the data obtained from *in silico* approaches can help narrow down the *in vitro* investigations. Since the cell cycle is an integral

pathway altered in cancer cells, HN1 being a component of cell cycle regulatory machinery has the potential of being used as insightful information for future studies in cancer biology. The Tet-ON inducible expression system and FUCCI system provide unique tools to understand the temporal function of HN1 in the cell cycle pathway. Therefore, this study even though being a continuation of previous studies on HN1 encompasses new technologies to understand the role of HN1.

2. LITERATURE REVIEW

2.1. Prostrate Cancer

2.1.1. Introduction To Prostate Cancer

The growth of cells in the human body is a coordinated event that involves the organization of cells in tissues and organs with specialized cells performing their functions within the limits of their confined environment depending on their structure and function. The cell division leads to the multiplication of cells to replace the injured or dead cells and if cell division becomes impaired, it leads to cancer development causing tissue-specific or organ-specific impacts on the body if remained unchecked can metastasize to other parts of the body and may lead to hindrance in the function of vital organs and death (Sunchu & Cabernard, 2020). There are many different kinds of cancers that can occur depending on the origin of tissue of the cancerous growth of cells, which is unusual and uncontrollable due to the inaction of several internal mechanisms of the cellular division. One of which is Prostate cancer which develops in the Prostate glands situated under the urinary bladder in men, functioning to produce the fluid known as seminal fluid required for the transportation and provision of sperms in men (Banerjee et al., 2018). The acini (cluster of cells) embedded in stroma and ducts form the normal glands of the Prostate, which form a basement membrane or a basal epithelium layer that surrounds the columnar epithelium (Fine & Reuter, 2012). The stromal cells are anchored in the extracellular matrix containing the myocytes, which help in promoting contractility along with the prevention of fluid stagnation (Sanches et al., 2021). The fibroblasts contained within the stroma assist in supporting the ducts of the Prostate gland and irregularities of the paracrine signaling of fibroblasts and epithelial cells in the Prostate have been associated with changing the pattern of ducts in Prostate Cancer (Bonollo et al., 2020).

Prostate Cancer is characterized as the enlargement of the Prostate gland as shown in figure 2.1. The epithelial cells in the Prostate are known to express higher levels of the *Androgen Receptor* (*AR*) gene, which transcribe and translate to form Androgen Receptor proteins that drive the development of the epithelium and growth of these cells. Therefore, normal and cancerous Prostate cells depend on androgens, which activate the receptors and cause activation of transcription machinery dependent on AR, for which one of the target genes is Prostate Specific

Antigen (*PSA*) functioning as a serine protease and is significantly higher in the case of Prostate cancer in men and can be used for initial diagnosis of the disease (Filella et al., 2018). In terms of mortality and incidence, Prostate cancer ranks among the top five cancers in the world, and in 2015 alone, there were 1.6 million cases of Prostate cancer in men were reported (Pernar et al., 2018). There is a global variation in the incidences of Prostate cancer as African-American men are at significantly higher risk for developing the disease and dying as a result of Prostate cancer (Barsouk et al., 2020).

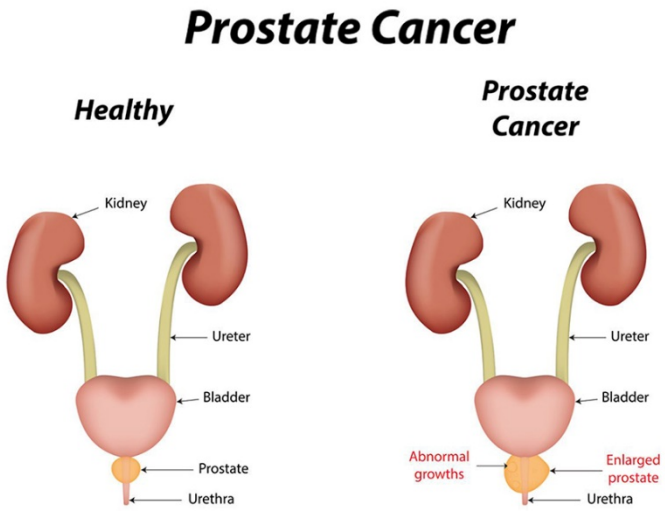

Figure 2.1: Difference between normal Prostate and enlarged Prostate in healthy and Prostate Cancer anatomy.

2.1.2. Genetic Basis Of Prostate Cancer

Like many other cancers, the cancer of the Prostate also involves the accumulation of the somatic mutations over the age in the epithelial cells and these mutations occur usually in tumor suppressors and oncogenes, further altering the cellular homeostasis originating from functional defects caused by altered protein translation and gene transcription (Cheng et al., 2019). These mutations are known to occur in genes that regulate the processes of cell death, cell proliferation, DNA damage response, and cell growth (Robinson et al., 2015). The localized form of the disease is associated with the fusion of two distinct regions in the genome including the transcription factor family of erythroblast transformation specific (ETS) and AR-regulated promoters (Carver et al., 2009). For example, Prostate biopsy specimens from white men showed almost 50 % and

31 % of black and Asian men exhibit the fusion of *ETS-related gene* (*ETG*) and transmembrane protease serine 2 (*TMPSS2*), implicating a genetic phenomenon of racial disparity of Prostate Cancer incidences (Blackburn et al., 2019).

In primary Prostate cancers, the gain of function mutation of *FOXA1*, a fusion of *ETV1* and *TMPRSS2,* and loss of function mutation of SPOP is strongly apparent (Armenia et al., 2018). The genetic instability associated with the development of Prostate cancer is promoted in *SPOP* mutation carrying models (Blattner et al., 2018). *FOXA1* gene acts as an oncogene and drives the metastatic progression of advanced Prostate cancer as it increases the transcription of *AR* (Adams et al., 2019). The *MYCN* and *AURKA* gene amplification mutations are strongly associated (in almost 40 % of cases) with a rare form of Prostate Cancer known as Neuroendocrine Prostate Cancer (NEPC) (Beltran et al., 2011). The metastatic development along with the clinical progression and biochemical failure resulting from the disease are associated with higher genetic instability arising from chromoplexy, chromothripsis, and kataegis, which can indicate the aggressiveness of the disease. These mutational phenomena constitute the gene methylation and copy number amplifications as the genetic signatures underlying the genetic instability (Fraser et al., 2017; Perdomo et al., 2018). There is high heterogeneity in Prostate Cancer, as the genes that drive the disease in its initial stages cannot be targeted directly for therapy. However, as the disease progresses, the targetable alterations such as the one in *ATM*, in the non-indolent form of the disease exhibited in 10 % of the patients can be used for targeting its signaling pathway (Fraser et al., 2017). Figure 2.2 adapted from Rebello et al shows the genetic alterations in specific genes in comparison to the stage of the progression of Prostate Cancer from benign to metastatic forms.

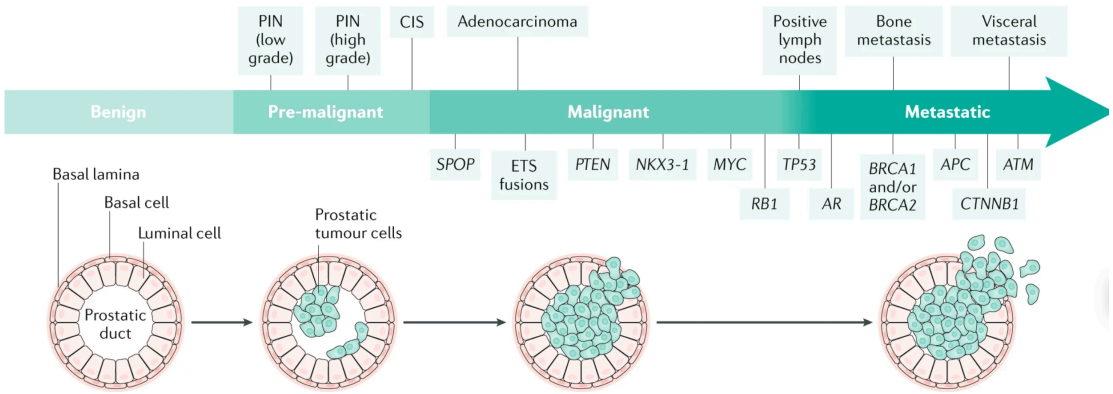

Figure 2.2: Commonly mutated genes in Prostate cancer are shown according to their enrichment at different disease stages.

The involvement of bone sites and lymph nodes in advanced disease forms encompasses the metastatic cancer of the Prostate in which the disease is no longer confined to the organ of origin and includes Castration-Sensitive Prostate Cancer (CSPC) and Castration-Resistant Prostate Cancer (CRPC). CRPC progression exhibits multiple sites of metastasis after Androgen Deprivation Therapy (ADP) (Stopsack et al., 2020). CRPC is further characterized by the loss of function mutations such as deletions or inactivating mutations in genes that function in repressing the transcription of AR e.g. *NCOR1* and *ZBTB16* alongside the gain of function mutations including amplification of *FOXA1* which is a positive regulator of *AR* (Robinson et al., 2015).

The progression from CSPC to CRPC involves further mutations in genes that regulate the growth of the cells (figure 2.2). *PTEN* is a tumor suppressor, which undergoes loss of function mutations that are enriched in CRPC (Frazer et al., 2017). Moreover, the gain of function mutations in *AKT1*, *PI3K3CA*, and *PI3KCB* are also associated with advanced Prostate Cancer in which the PI3K pathway is altered, which can be targeted for therapy (Robinson et al., 2015; Carver et al., 2011). Gain of function mutations in *CTNNB1* and loss of function mutations in *APC* as part of the WNT signaling pathway is also important in determining the aggressive fate of the Prostate Cancer (Grasso et al., 2012). Other important genetic factors directly linked with Prostate cancer are located on chromosome 8q including loss of *NKX3.1* tumor suppressor and gain of *MYC* oncogene (Grasso et al., 2012; Robinson et al., 2015). During tumor development, the *MYC* is expressed at higher levels without copy number variations illustrating a transcriptional axis involved in the regulation of tumorigenesis that can be

targeted for therapy, especially in *PTEN* mutated cancers (Hubbard et al., 2016). The mechanisms which function in controlling the genetic stability are either deleted or lost in the progression of Prostate Cancer and are considered the pivotal events in driving the lethal forms of cancer. The major regulators of the cell cycle such as *RB1* and *TP53* have also been shown as mutated in CRPC (Stopsack et al., 2020; Mateo et al., 2020). Loss of these genes is also significantly associated with poor outcomes of the disease or overall survival from the disorder (Figure 2.2).

DNA Damage Response (DDR) pathways are guardians of the genomic fidelity in dividing cells and somatic mutations occurring in DDR genes are also found prevalent. The sensitivity to ionizing radiation along with intercalators of DNA strands and higher copy number amplifications resulting from deficiencies in the homologous repair pathway may originate from mutations in double-strand break repair genes. These mechanisms can render some therapies ineffective (Abida et al., 2017). The *ATM* and *BRCA2* are two genes involved in the homologous repair pathways that are continuously mutated in advanced Prostate Cancer with lesser-mutated forms present in localized tumors of the Prostate (Mateo et al., 2020).

2.1.3. Androgen Receptor And Its Involvement In Prostate Cancer

AR is the most studied gene in the context of Prostate cancer. Androgen receptor (AR) translocates to the nucleus from the cytoplasm upon binding to androgens including dihydrotestosterone (DHT) in the luminal epithelium of the gland. In the nucleus, AR elicits transcriptional responses after binding to the target genes on their androgen response elements (AREs) (Tan et al., 2015). The neoplastic cells with increased proliferation rates exhibit higher levels of AR in the lumen of the Prostate (Mills, 2014). The neoplasia contains cells growing in an unregulated manner. The transcription factor function of AR defines the cellular homeostasis by activating genes responsible for the function of the Prostate such as *PSA* and *KLK3* (Lamb et al., 2014). AR drives tumorigenesis by promoting the transcriptional program of the growth-related genes (Tan et al., 2015). Androgen-deprivation therapy (ADT) causes changes in AR manifesting as changes in its expression and post-translational modifications. For example, the factors regulating AR expression are changed, leading to overexpression of *AR*, or

the *AR* gene is amplified causing *AR* overexpression (Chan et al., 2014). Moreover, a gain of function mutations located in the ligand-binding domain can trigger a constitutively active form of AR to remain active without proper signals inside the cellular environments along with the mutations occurring in domains that define the ligand specificity of the receptor. These changes lead to AR becoming active in the presence of other ligands such as glucocorticoids and estrogens (Robins, 2012). The post-translational modifications of AR can render it sensitive to androgen at low levels after the removal of testes by castration (Van der Steen et al., 2013). AR splice variants occurring after alternative splicing for the production of short variants (SVs) of AR known as AR-SVs lacking ligand-binding domains remain active and perform constitutive transcription of target genes (Antonarakis et al., 2016). The higher expression of AR is an indicator of transition from CSPC to CRPC and can also trigger resistance from therapy to block the targeting of androgen signaling (Snow et al., 2019). These mechanisms of AR involvement in Prostate cancer progression are highlighted in figure 2.3 adapted from Rebello et al 2021.

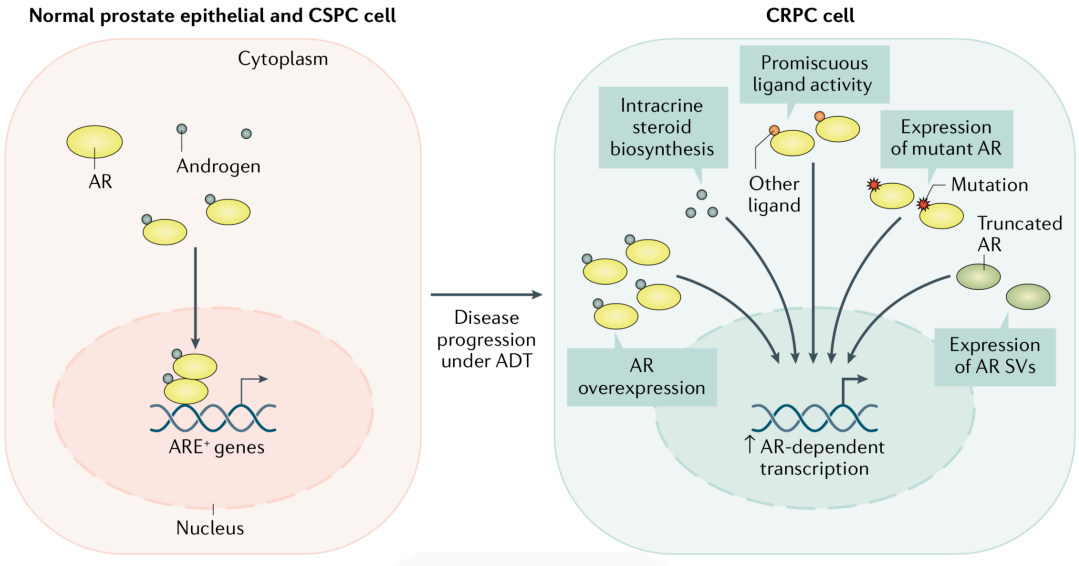

Figure 2.3: The general relationship of Androgen Receptor (AR) with Prostate Cancer progression.

2.2. Centrosome In Cancer

2.2.1. Structure And Function Of Centrosome

In mammalian cells, the centrosomes consist of centriole pairs that are localized near the nucleus in interphase cells the centriole pairs are oriented perpendicularly and the overall structure is embedded within a pericentriolar material or matrix (PCM) composed of coiled-coiled proteins (Figure 2.4). The centrosomal matrix contains numerous centrosomal proteins such as pericentrin and γ-tubulin ring complexes along with centrin proteins (Schatten & Sun, 2015). The centrosome-associated proteins are linked with the matrix surrounding the centrosomes (figure 2.4a). The primary function of the centrosomes in mammalian cells is to act as major microtubule organizing centers (MTOC) of the cells. The microtubule organization function of the centrosome is assisted by other proteins, which help in the nucleation of microtubules such as Aurora kinases, Polo-like kinases (PLKs), pericentrin, and γ-tubule among others. The microtubule anchoring proteins in the centrosome include dynactin, centriolin, ninein, and katanin act as microtubule releasing proteins (Martin & Akhmanova, 2018). The centrosome is a membrane-less organelle in mammalian cells and this feature allows the centrosomes to remain dynamic throughout the cell cycle and interact with the cytoplasmic components due to the activity of microtubules that are organized in centrosomes. The general structure of the centrosome is given in figure 2.4 adapted from Schatten, & Sun, 2018.

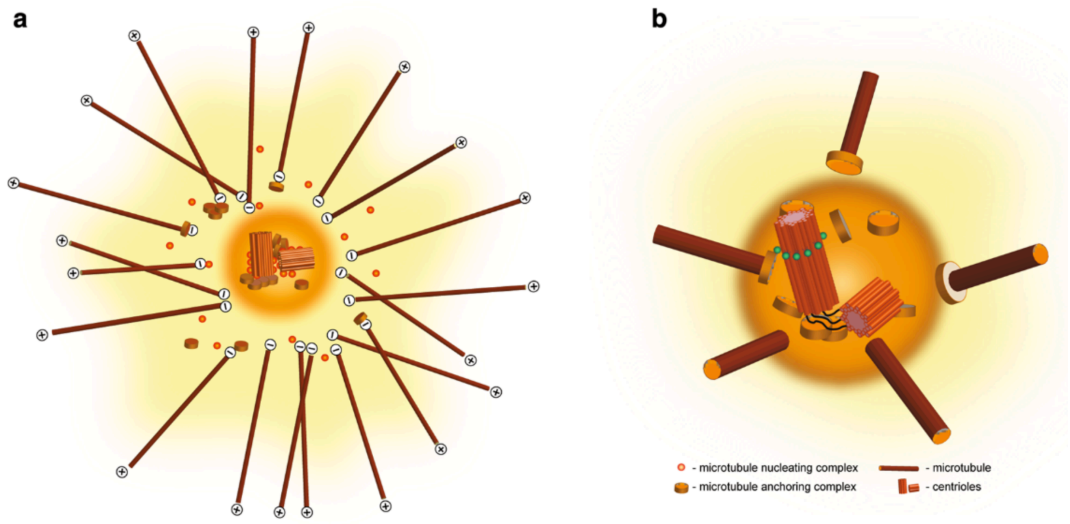

Figure 2.4: General structure of centrosome. The centrosome anchor the minus end directed microtubules (a), and the centrioles are interlinked by linker and oriented in a perpendicular manner (b).

2.2.2. Centriole Duplication Cycle

The cell cycle progression is coupled with the centrosome duplication cycle and these pathways are tightly regulated. The fidelity of chromosome or genetic material being distributed equally in two daughter cells is ensured by these events (Fırat-Karalar & Stearns, 2014). Two centrioles in a G_0/G1 phase of the cell cycle are one mother centriole and another daughter centriole. The centriole linker connects these two centrioles and is quite flexible at the proximal ends of centrioles (Agircan et al., 2014). When G1 cells start to transition into the S phase at the G1/S transition, a procentriole assembles from the already existing centriole at the proximal end, where it is orthogonally arranged. The procentriole is attached throughout the S and G2 phases to the parent centriole and grows in length. Before the G2 phase ends, the centriole linker present between the two parental centrioles is broken off so that the centrosomes can separate and move to opposite poles in mitosis for the formation of spindle poles required for equal distribution of chromosomes in daughter cells after cell division (Banterle & Gönczy, 2017). In mitosis, the cartwheel structure of newly formed centrioles is targeted for degradation, and daughter centrioles are disengaged from parental centrioles (Jana, 2021). The duplication cycle is completed as centrioles in the daughter cells are linked with centriole linkers at the proximal ends (Loncarek & Bettencourt-Dias, 2018). The centriole duplication cycle is illustrated in figure 2.5.

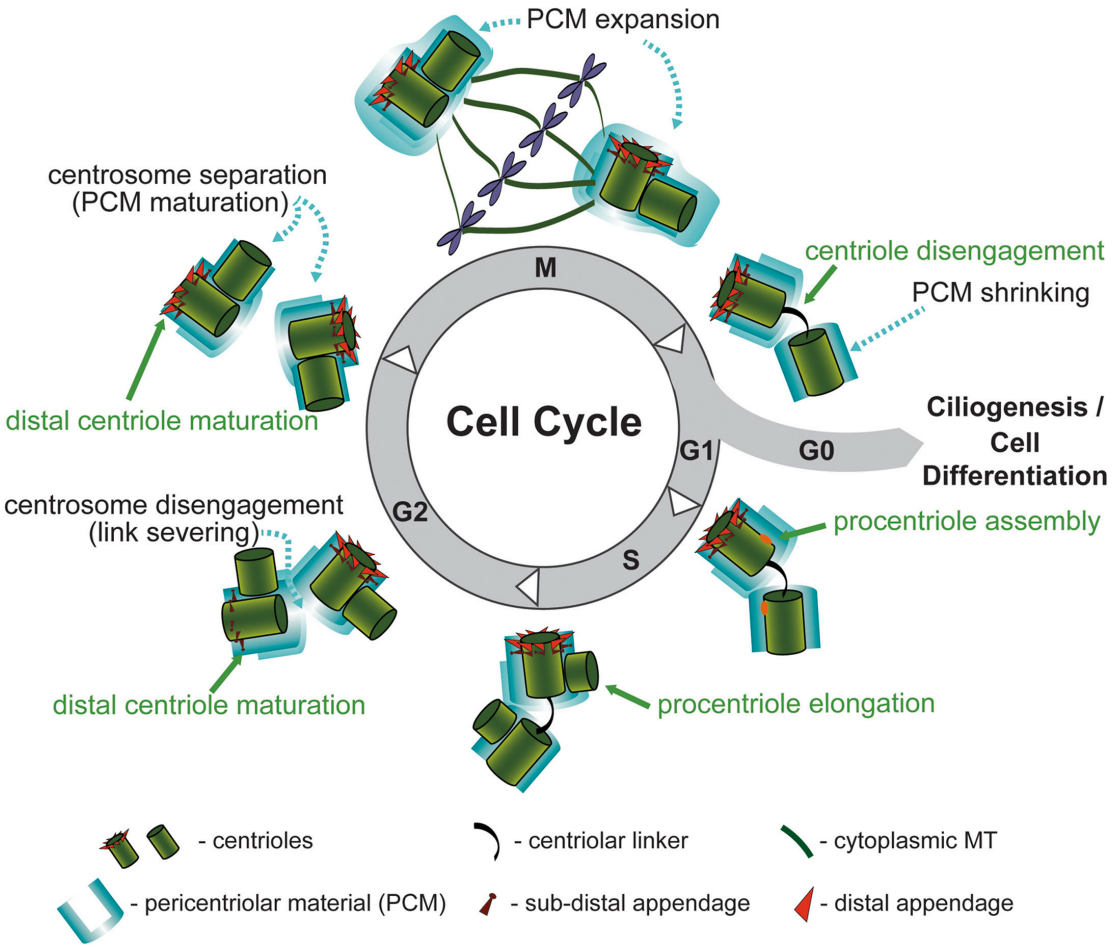

Figure: 2.5 Centrosome duplication cycle is aligned with the cell cycle.

2.2.3. Centrosome Abnormalities In Cancer

Abnormalities in centrosomes have been described in a variety of cancers including multiple myeloma, pancreatic cancer, ovarian cancer, colon cancer, breast cancer, and Prostate cancer (Godinho & Pellman, 2014). In some cancers such as gastrointestinal and breast cancers, low-grade lesions have shown centrosomal abnormalities which suggest that centrosome errors can be the cause of the initiation of carcinogenesis (Chan, 2011). In some cases, the advanced form of the cancers such as urothelial cancers exhibit the amplification of the centrosomes and are associated with the recurrence of the disease and can indicate the advanced stage of cancer (Yamamoto et al., 2004). In the case of Prostate cancer, the disease progression along with the distant metastasis is correlated with centrosome amplification (Pihan et al., 2001). There are two types of centrosomal abnormalities occurring in human cancers including the structural and numerical

errors of the centrosomes. The structural defects consist of further two types such as centriole structure abnormalities and errors in the accumulation of PCM (Godinho & Pellman, 2014).

The overexpression or lower expression of centrosomal components such as SAS4/CPAP, which constitute the centriolar structure, can elucidate the structural abnormalities of the centrosomes (Kohlmaier et al., 2009). The increase in PCM as measured by pericentriolar markers can also deduce structural defects (Nigg, 2006). However, centrosomal amplification can also be interpreted by measuring the amount of PCM, which is a numerical defect of the centrosomes (Godinho et al., 2014). Since centrosome amplification is frequently studied in cancers, many mechanisms have been defined that can lead to catastrophic phenotypes including de novo centriole assembly, overduplication of centrioles, cell-cell fusion, mitotic slippage, and cytokinesis failure (Godinho et al., 2009). There is a diversity of proteins involved in centrosome amplification in cancer including tumor suppressor genes. The dysregulation of the centrosome duplication pathway mentioned previously is the major route for centrosome amplification (Brownlee & Rogers, 2013). The conserved process of centrosome duplication is controlled by the activity of Polo Like Kinase 4 (PLK4) and its overexpression has been associated with extra centrioles (Coelho et al., 2015). PLK4 autophosphorylates and is regulated further by $SCF^{\beta TrCP}$ (Guderian et al., 2010). The protein essential for cartwheel structure SAS-6 is controlled by proteasomal degradation and is involved in the centriole biogenesis with irregularities contributing to centrosome amplification (Arquint & Nigg, 2016).

Cep97 and CP110 are other capping proteins regulating the length of the centrioles. CP110 regulation from $SCF^{Cyclin\ F}$ further implicates the role of proteolysis in controlling the centrosome duplication cycle (Zhao et al., 2021). PLK1 and Aurora A kinases are centrosome maturation factors, which assist in the accumulation of PCM. The altered expression and activities of these important mitotic kinases result in centrosome amplification and carcinogenic profiles in cancer cells (Hoffmann, 2021). The centrosome-related carcinogenesis arising in p53 null cells shows that p53 is involved in regulating PLK4 expression, which in turn is affected by proteasome-mediated degradation. Therefore, p53 mutated models exhibited higher numerical centrosomal defects (Coelho et al., 2015). The clinically relevant centrosomal abnormalities lead to chromosomal instability

leading to multipolar mitoses. The two mechanisms underlying centrosomal anomalies are illustrated in figure 2.6 adapted from Cosenza & Krämer, 2016. Excess seeding occurring in the vicinity of maternal centrioles leads to supernumerary centrioles, causing centriole overduplication. On the other hand, centrosomes can get accumulated due to the presence of multiple replicated centrosomes consisting of pairs of mother and daughter centrioles. These mechanisms are mutually exclusive as the overduplication results from irregularities in the duplication cycle and centrosome accumulation can be the result of other faulty processes including mitosis (mitotic slippage) and cytokinesis (cytokinesis failure) (Cosenza & Krämer, 2016).

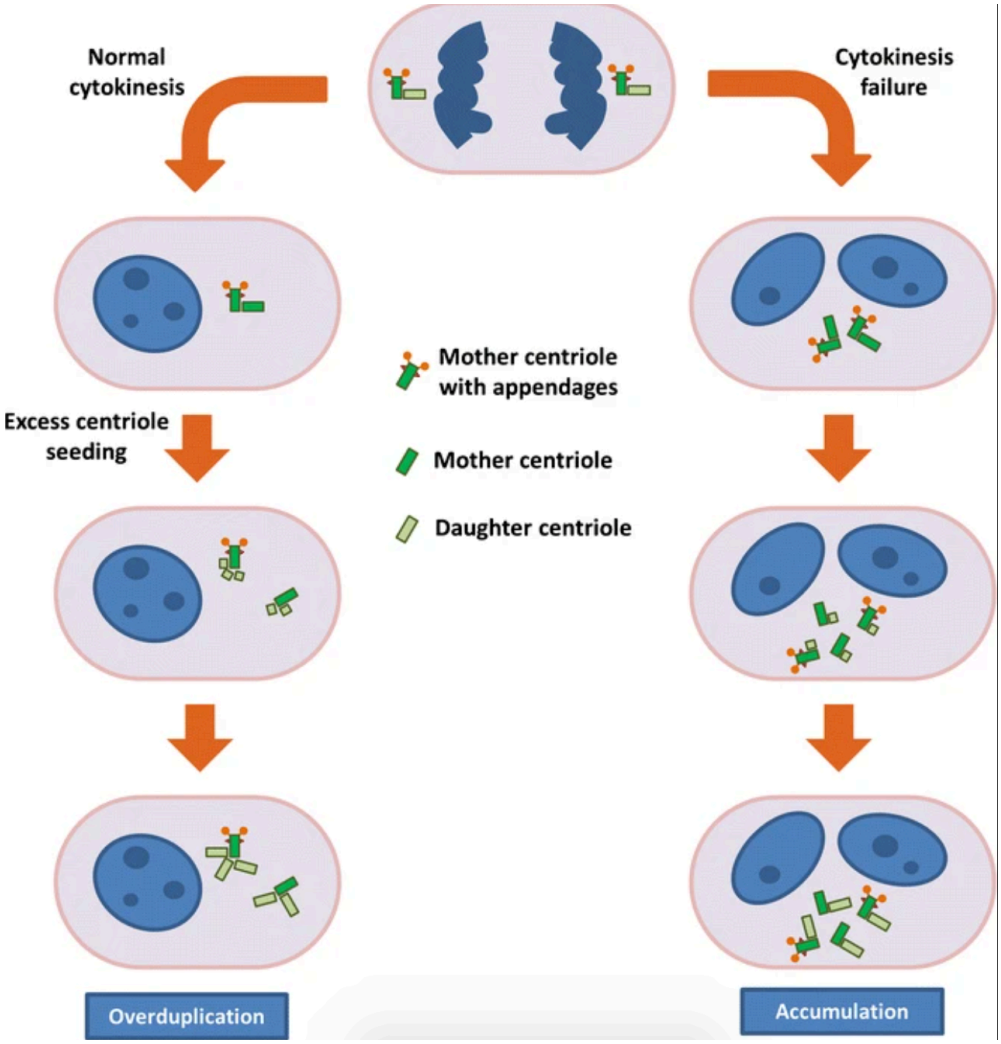

Figure 2.6: Simplified centrosome amplification pathways in cancers.

2.2.4. Centrosome Amplification And Its Consequences

The consequences of centrosome amplification can be manifested in different ways depending on the cell cycle phase including interphase or mitosis. During mitosis, chromosome segregation errors can result from centrosome amplification, which further can lead to aneuploidy, which has a direct correlation with chromosome instability and cancer (Zyss & Gergely, 2009). Supernumerary centrosomes tend to cluster together during the formation of the poles and may lead to the multipolar distribution of microtubules and their consequent attachments to the chromosomes known as merotelic kinetochore-microtubule attachments (Silkworth et al., 2009). The merotelic attachments are able to avoid the spindle assembly checkpoint (SAC) and can lead to missegregation, which is not arrested, causing aneuploidy (Cimini, 2008). At the cytokinetic furrow, lagging chromosomes can get trapped due to amplified centrosomes, acting as a source of DNA damage, further generating genomic instability required for carcinogenesis (Janssen et al., 2011). Extensive DNA damage and abnormal DNA replication can result from micronuclei formations, which encapsulate the lagging chromosomes (Krupina et al., 2021).

Another consequence of centrosome amplification is the asymmetric cell division, which is independent of the mechanisms involving chromosome segregation or aneuploidy (Kulukian et al., 2015). Moreover, amplified centrosomes and their effects are not limited to mitosis as extra centrosomes in interphase cells can affect the signaling via cilia which originate from centrioles (Mahjoub & Stearns, 2012). The cellular polarity is a direct function of microtubule nucleation from centrosomes, and in amplified centrosomes, the nucleation capacity is increased, leading to changed polarity, which further enhances the migration and invasiveness of cancer cells. In interphase cells increased nucleation of microtubules changes the Rho GTPases and promotes carcinogenic potentials of cells (Ogden et al., 2013; Kushner et al., 2016). Supernumerary centrosomes are also known to alter the signaling pathways within the cells as centrosomes act as a resting place or a converging point for different pathways. The over duplicated centrosomes provide maximal interphase for different components of the cell cycle and other pathways to get altered (Bose & Dalal, 2019; Jewett & Pearson, 2021). Most importantly, the amplified centrosomes provide a quantifiable trait, which can be used for determining the

clinically feasible attributes such as the metastatic potential of various cancers (Mittal et al., 2021). Various consequences of amplified centrosomes have been shown in figure 2.7 adapted from Godinho & Pellman, 2014.

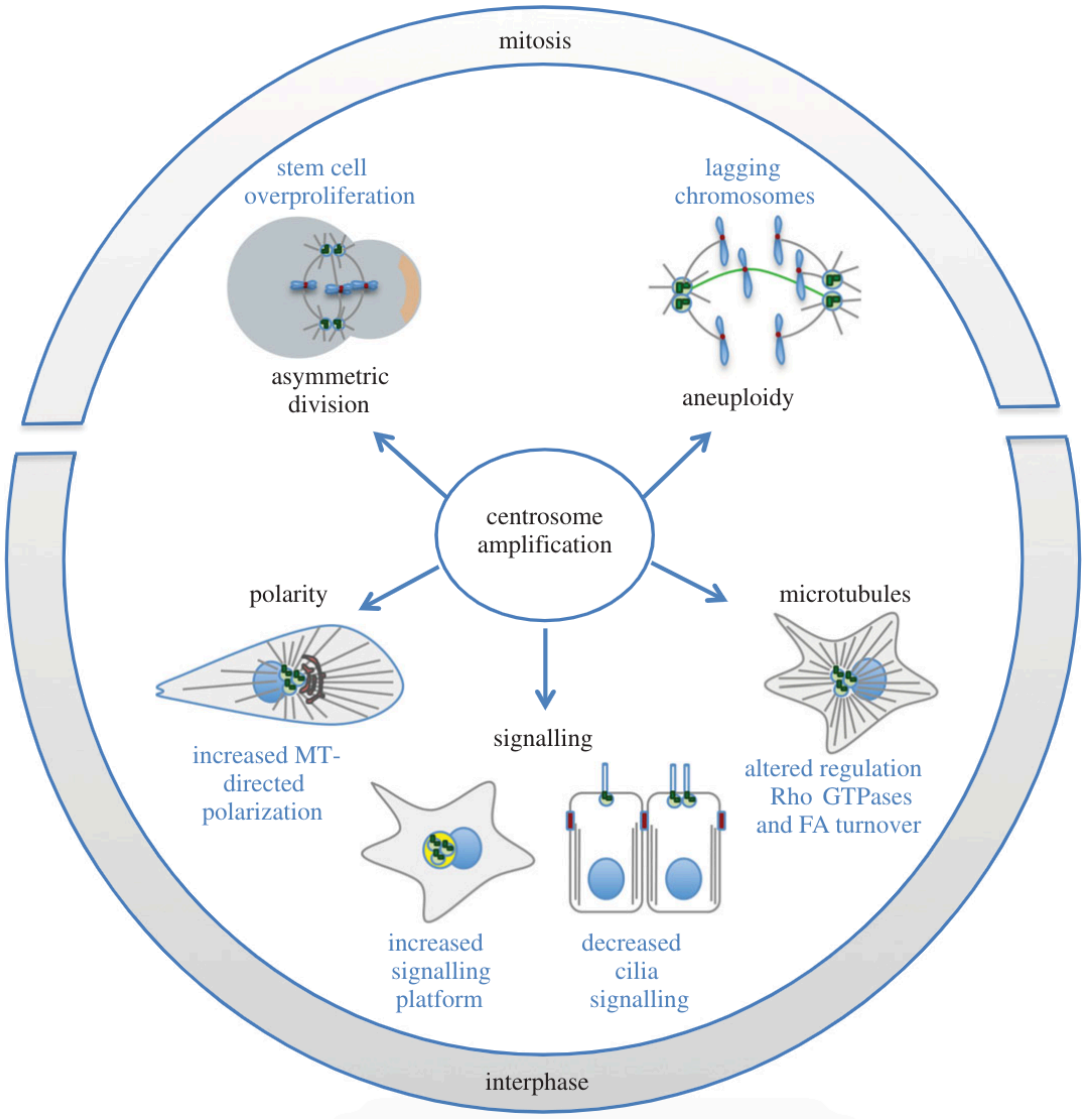

Figure 2.7: The consequences of centrosome amplification depending on phases of cell cycle.

2.2.5. Centrosome Clustering

Supernumerary centrosomes marked by the presence of multiple centrosomal cores can lead to the formation of multiple spindles and can cause tumorigenesis by promoting chromosomal instability; have been observed in various tumors (Kalkan et al., 2022). Multipolar spindles can also lead to cell death as catastrophic CIN can reduce the viability of the living cells (Rodrigues-Ferreira & Nahmias, 2020). Therefore, cancer cells employ a method of

centrosome clustering of supernumerary centrosomes to enable the pseudo-bipolar assemblies for cell division (Krämer et al., 2011). Therefore, centrosome clustering provides a mechanism for cancer cells to divide even in the presence of lethal traits such as multiple centrosomes as shown in figure 2.8 adapted from Kramer et al., 2011.

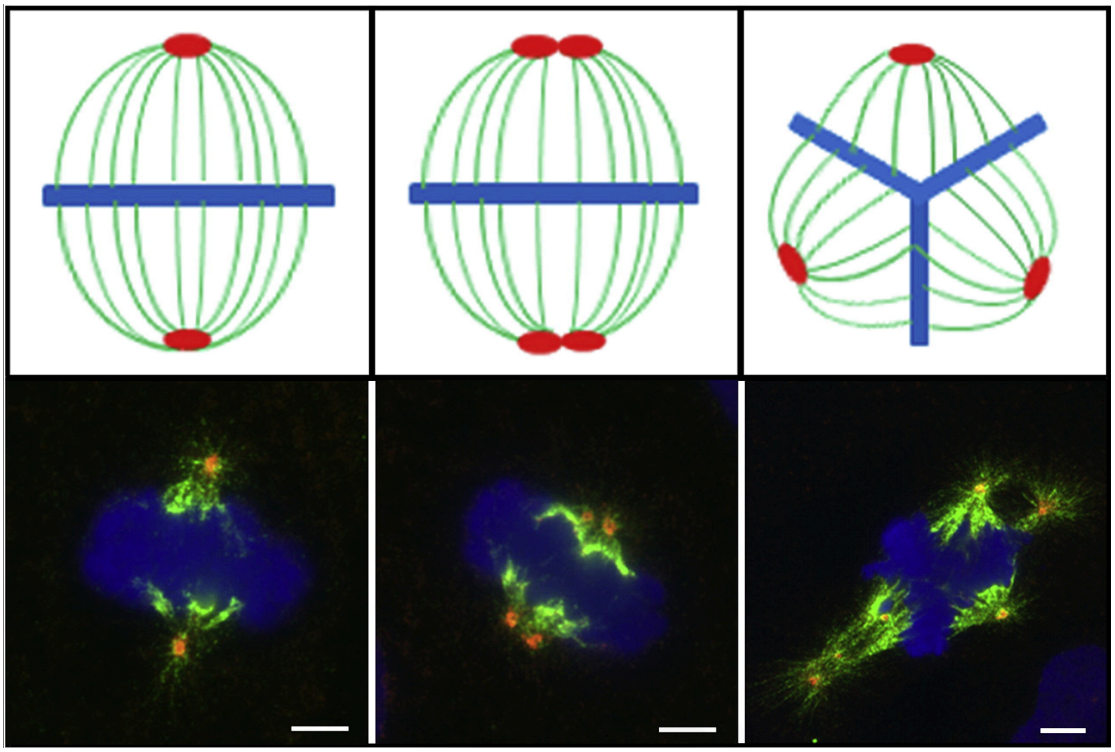

Figure 2.8: Centrosome clustering of supernumerary centrosomes. The left panel shows the normal bipolar assembly of metaphase plate with one centrosome at each pole, the middle panel shows supernumerary centrosomes clustered together to form bipolar spindle assembly and the right panel shows the catastrophic phenotype of multipolar spindle formation with amplified centrosomes.

Clustered supernumerary centrosomes forming bipolar spindle assemblies are not only prevalent in tumors, primary binuclear hepatocytes with polyploidy also contain this feature (Faggioli et al., 2011). Neuroblasts with PLK4 overexpression and treatment with cytochalasin D exhibit clustered centrosomes with a bipolar array of spindles (Ryniawec & Rogers, 2021). The prevention of multipolar spindles requires the action of spindle tension and a cohort of proteins take part in carrying out this function including HEC1, survivin, CEP164, SGOL1, and mitotic kinases (Leber et al., 2010). The astral microtubules exert forces that cause cortical pulling of the spindle poles in interphase cells observed in Drosophila (Kwon et al., 2008). The correction of microtubule attachments that

merotelic at the kinetochore requires the activity of chromosome passenger complex (CPC) and can reduce the spindle tension (Sabat-Pośpiech et al., 2019). Interestingly, minus end-directed kinesin family of microtubule motor proteins, are considered centrosome-clustering proteins as kinesin-like protein KIFC1 phosphorylation by ATM and ATR kinases are required for centrosome clustering (Fan et al., 2021).

2.3. Cell Cycle

2.3.1. Overview Of Cell Cycle

The cell cycle of a eukaryotic cell has an interphase containing three phases G1, S, and G2 phases, and the mitosis (M) phase carrying cytokinesis (Alberts et al., 2002). During the interphase of the cell cycle, the growth of cells occur due to the accumulation of the nutrients required for the subsequent mitosis along with the replication of cellular contents including organelles and DNA. The mitosis then occurs to divide the cells into two daughter cells carrying genetic material and organelles (Carlton et al., 2020). There are several cell cycle checkpoints to ensure the correct progression of the cell cycle in terms of cellular components and division as shown in figure 2.9 adapted from Ben-Salem & Venkadakrishnan, 2021. Cyclin-dependent kinases (CDKs) are activated by different cyclins due to their sequential expression throughout the cell cycle (Satyanarayana & Kaldis, 2009). The mitogenic signaling gives rise to the activation of cyclin D in the G1 phase of the cell cycle, which in turn functions in activating the CDK4/6 causing the phosphorylation of retinoblastoma protein (RB) (Giacinti & Giordano, 2006). The E2F transcription factors are then released to activate the cyclin E and cyclin A transcriptions which leads to further phosphorylation of RB. There are internal CDK inhibitors in cells with families including INK4 and CIP/KIP, which bind the complexes of cyclin-CDKs to inhibit phosphorylation of RB and cause eventual prevention of E2F release. These mechanisms cause the replication machinery to be arrested, hence a checkpoint for the cell cycle control (Ekholm & Reed, 2000). The mitotic checkpoint is triggered due to various interactions of cyclin B-CDK1 complexes, which inhibit the RB by phosphorylations from S to G2/M transition. Cyclin B-CDK1 complex assists in nuclear envelope breakdown, chromosome condensation, and mitotic spindle formations. The phosphorylations of tumor

suppressor RB control the checkpoints as hyperphosphorylations due to altered signaling in tumor cells render the growth of cells independent of outside or mitogenic signals (Moser et al., 2018).

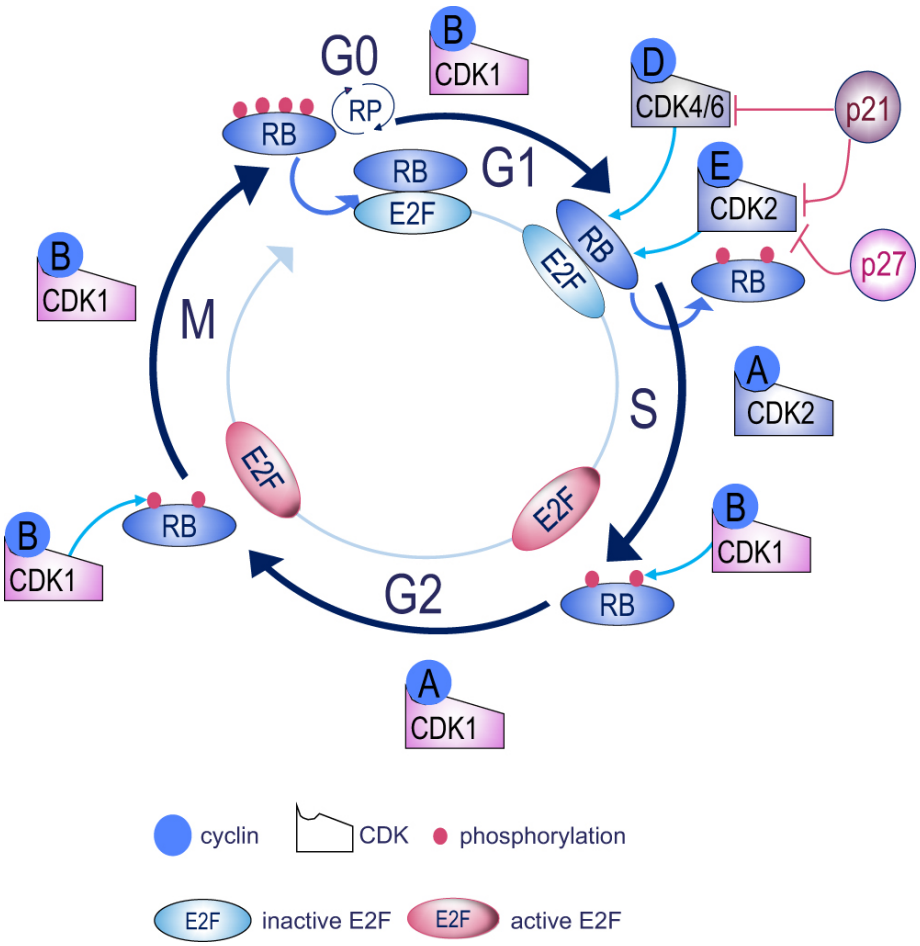

Figure 2.9: Overview of cell cycle regulation and cell cycle checkpoints.

2.3.2. Cyclin Dependent Kinases In Cell Cycle Control

The cells in adult tissues carrying diploid DNA usually reside in a state of quiescence marked by the G_0 phase that is either permanent or temporary depending on the functionality of the cells. When cells enter a new cell cycle after mitosis, growth factors or hormones trigger a cascade of signaling events that converge on CDK4 or CDK6 to cause the cells to go through another round of cell cycle upon entry into the S phase. The cyclin D protein with fluctuating levels throughout the cell cycle binds the CDK4/6 to form complexes and can be inhibited by the aforementioned inhibitors in figure 2.9 (Malumbres & Barbacid, 2001). Activated cyclin D-CDK4/6 complexes phosphorylate RB along with p130 and p107, which in hypophosphorylated forms function in recruiting repressors of

E2F transcription factors for inhibiting the G1 to S transition. Cyclin C/CDK3 complexes are also involved in RB phosphorylations which can lead to entry into the S phase directly from Go which is either a reversible or permanent phase depending on the cell type (Ren & Rollins, 2004). The downstream target genes of E2F activated upon RB phosphorylated by CDK4/6 include *CCNE*, *CCNA*, and *CCNB* encoding cyclin E, cyclin A and cyclin B respectively. Other proteins activated upon this cascade include dihydrofolate reductase (DHFR), ribonucleotide reductase M1 (RRM1), RRM2, and Polo-like kinase 1 (PLK1), spindle checkpoint protein MAD2, and mitotic checkpoint serine-threonine kinase (BUB1). These proteins function in the progression of the cell cycle (Asghar et al., 2015). In late G1, E2F factors activate cyclin E1 and cyclin E2, which bind CDK2 to activate the cyclin E/CDK2 complex, activating CDK2, which before cyclin E binding, is kept sequestered in p27 and p21 bound forms. These inhibitors are also marked for ubiquitin-mediated degradation upon activation of CDK2. CDK2 is further activated by cell division cycle 25A (CDC25A), which dephosphorylates CDK2 (Ditano et al., 2021). CDK2 phosphorylates a range of substrates for progressing the cell cycle and carrying out different functions such as histone synthesis (Nuclear protein activator of histone transcription, centrosome duplication, and DNA replication (Chi et al., 2020). The schematic control of cell cycle-regulated by CDKs is shown in figure 2.10 adapted from Ding et al., 2020.

The activation of CDK4/6 and CDK2 and their downstream targets render the fate of the cell cycle independent of the mitogenic signals, therefore, the restriction point is passed at this point. When the S phase nears its end, cyclin A displaces cyclin E from CDK2 and F-box/WD repeats carrying protein 7 (FBXW7) leading to proteasomal degradation of cyclin E (Siu et al., 2012). The termination of the S phase is led by E2F1 and CDC6 phosphorylations by CDK2 bound with cyclin A, causing entry into the G2 phase of the cell cycle. CDK2 is also involved in the activation of CDK1, which drives the G2/M transition. Cyclin B activates CDK1 and CDK1 phosphorylations causing nuclear envelope breakdown, chromosome condensation, and mitotic spindle assembly in mitosis. Anaphase promoting complex/cyclosome (APC/C) degrades cyclin B and decreases CDK1 activity in anaphase during spindle assembly checkpoint (SAC) (Gavet & Pines, 2010). High fidelity of genomic integrity is ensured upon the

realization of the critical events dependent on the cell cycle progression and mitotic-onset, which is enabled by CDK1 rendering it the most important of the cyclin-dependent kinases (Santamaría et al., 2007). CDK1 activity is further controlled by Myelin transcription factor 1 (MYT1), G2 checkpoint kinase (WEE1), and CDC25C phosphatase. CDK1 is inhibited by phosphorylations at Tyr15 by Wee1, and Thr14 and Tyr15 by MYT1, and these phosphates are removed by CDC25C for activation of CDK1 (Potapova et al., 2009).

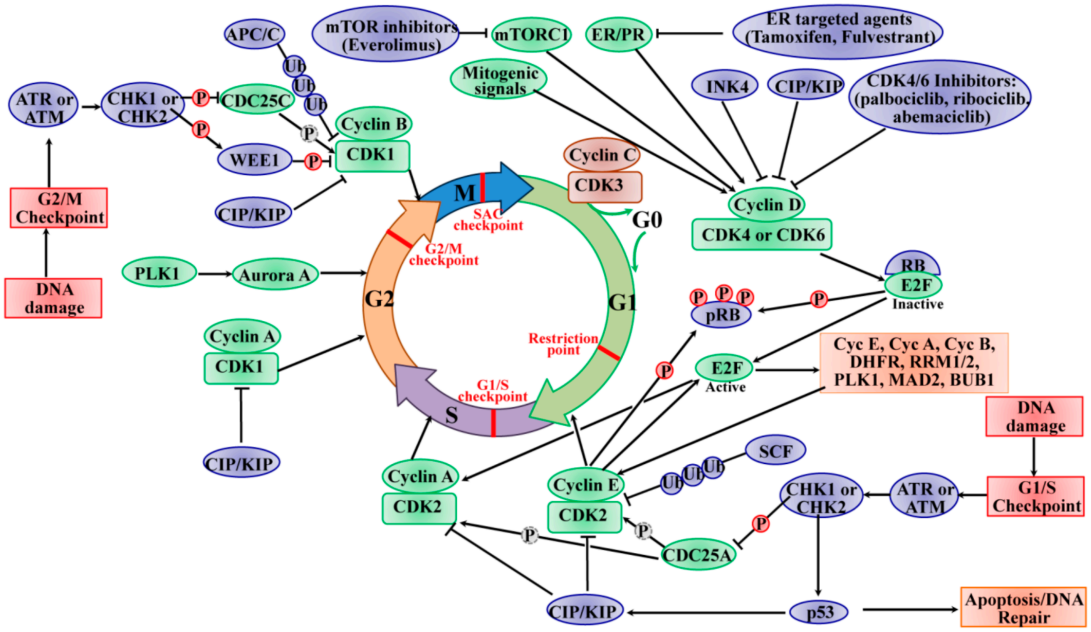

Figure 2.10: Regulation of Cell Cycle by Cyclin Dependent Kinases

DNA damage during the cell cycle causes cells to arrest for repairing the damage before entering the mitosis. These checkpoints occur before and after DNA synthesis in G1 and G2 phases. The DNA damage signaling involves checkpoint kinases CHK1 and CHK2 along with Ataxia telangiectasia mutated kinase (ATM), Ataxia telangiectasia, and Rad3 related kinase (ATR), and phosphatidylinositol 3-kinase (PI3K) (Bensimon et al., 2011). CHK1/CHK2 axis is activated upon phosphorylations from ATM/ATR kinases, which detect the DNA damage (Zhao & Piwnica-Worms, 2001). CHK2 upon activation from upstream kinases leads to p53 activation, causing the G1 arrest to repair the damaged DNA (Mustofa et al., 2020). Cyclin E-CDK2 complex activity is reduced upon activation of p21 by p53, as DNA repair machinery is upregulated upon p21 activation. Eventually, apoptosis is triggered if the stress of DNA

damage is not repaired properly (Koniaras et al., 2001). CHK1 also triggers G2 arrest by phosphorylating CDC25A to induce proteolysis by ubiquitination. Another substrate of CHK1 is WEE1, which is another mechanism for G2 arrest of the cell cycle (Otto & Sicinski, 2017). Mitotic checkpoint also known as spindle assembly checkpoint (SAC), functions in monitoring the metaphase plate for correcting the chromosome alignment. The checkpoint is regulated by monopolar spindle 1 (MPSI) also known as TTK protein kinase, which regulates the recruitment of checkpoint proteins to the kinetochore complexes. The genome integrity and appropriate chromosome segregation are regulated by the phosphorylation of substrates of TTK (Musacchio, 2015). The passage of SAC brings the APC/C complex into play, which stimulates the degradation of securing and cyclin B to initiate mitosis (Thu et al., 2018). The checkpoints present at various time points throughout the cell cycle ensure the genomic and mitotic fidelity of the cells entering the new cell cycle, and the convergence of various signaling pathways and these checkpoints on CDKs indicate the importance of cyclins and CDKs in the cell cycle progression.

2.3.3. E3 Ligase Complexes In Cell Cycle Control

The cell cycle progression depends on CDK activity and the ordered manner of the activity of different CDKs is maintained by timely events of activation and degradation of CDK activators and inhibitors along with the degradation of cyclins (Pack et al., 2019). There are two important families of E3 ubiquitin ligases that control the regulation of CDKs by mediating the proteolytic degradation in mammalian cells. These are known as APC/C and SCF protein complexes, which have been studied in great detail (Vodermaier, 2004). The cullin-RING E3 ubiquitin ligase is a multi-subunit machine known as APC/C, which assists in mitosis and G1 to regulate the progression of the cell cycle until the cells enter the S phase (Barford, 2011). There are two co-activators named CDC20 and CDH1 (Fizzy related 1, FZR-1) for the temporal activity of APC/C. These activators are structurally relevant and are sequentially activated for the regulation of mitosis and G1. CDC20 engages with APC/C for its activation when the auto-inhibition of APC1 is relieved by phosphorylation (Qiao et al., 2016). Cyclin B1 along with securin are marked for degradation by APC/C^{CDC20} for the onset of anaphase and chromosome segregation (Chang et al., 2003; Hagting et

al., 2002). CDH1 phosphorylated by CDK1 is activated upon degradation of cyclin B1 by APC/C^{CDC20}, thereby rendering these sequential events important in the regulation of mitosis (Crasta et al., 2008). CDC14 is another factor, which de-phosphorylates and activates the APC/C^{CDH1} at the onset of anaphase (van Leuken et al., 2009). Therefore, CDC14 activation and cyclin B1 degradation for suppression of CDK1 leads to robust APC/C^{CDC20} to APC/C^{CDH1} transition at the build-up of metaphase to anaphase transition as shown in figure 2.11 adapted from Dang et al., 2021.

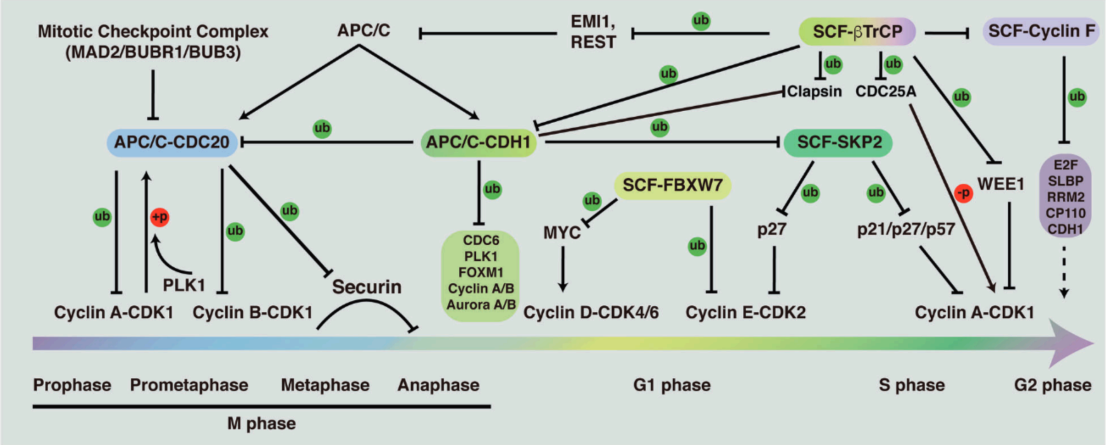

Figure 2.11: The interplay of APC/C and SCF complexes in regulation of the cell cycle.

G1 maintenance and exit from mitosis are irreversible mechanisms controlled by CDH1 activation and degradation of its substrates such as SKP2, FOXM1, CDC20, PLK1, and cyclin B1 (Li & Zhang, 2009). At G1/S transition, CDH1 inactivated is facilitated by several mechanisms including Emi1 accumulation, E2 enzyme UBE2C degradation, and phosphorylation of CDH1 by CDK (Li & Zhang, 2009). Therefore APC/C is active from mitosis to the end of G1 due to its activators CDC20 and CDH1 in a sequential manner (figure 2.11). There is another complex containing three core subunits of Cullin, SKP1, and RBX1 along with other F-box proteins, named as SCF complex. It degrades a large number of substrates as compared to APC/C and contains many co-factors including Cyclin F, βTrCP, FBXW7, and SKP2 among others (Thompson et al., 2021). APC/C^{CDH1} in G1 suppresses SKP2 and its ligase activity (Bashir et al., 2004). By the end of G1, CDK2 phosphorylates SKP2, and enzymatic activity of CDH1 is reduced and SKP2 is protected from degradation from APC/C^{CDH1},

thereby rendering SCF^{SKP2} ligase complex activated (Rodier et al., 2008). CDK2 inactivates p27 by phosphorylation, leading to its ubiquitination and subsequent degradation by SKP2 (Wu et al., 2012). P27 inhibition of CDK2 along with the phosphorylations of RB is also relieved as a result of SKP2 activation, causing the activation of G1 to S transition in a positive feedback loop manner. SKP2 also control p21 and p57 members of CIP/KIP and leads to their proteasomal degradation (Rubin et al., 2020). As mentioned previously, cyclin A replaces cyclin E to associate with CDK2, and cyclin E degradation is dependent on SKP2 activity for the initiation of DNA synthesis in the S phase. Therefore, SKP2 is important in cell cycle regulation (Nakayama et al., 2000). The transcriptional engines dedicated to progressing the cell cycle E2Fs, are inhibited due to ubiquitination mediated by Cyclin F, which is another co-activator of SCF, at the entry into G2 (Clijsters et al., 2019). In G2 cells, cyclin F also degrades SLBP to reduce the accumulation of H2AX in the presence of genotoxic stress in the cells (Dankert et al., 2016). Other substrates of $SCF^{cyclin\ F}$ include CP110 and RRM2 for controlling centrosome homeostasis along with genomic integrity (D'Angiolella et al., 2010, 2012). The timely progression of mitosis is controlled by βTrCP, which modulates cyclin F (Mavrommati et al., 2018).

At mitotic entry CDK1 is activated as it binds to cyclin A, to initiate the chromosome condensation (Gong & Ferrell, 2010). Subsequently, during pro-metaphase activated APC/C^{CDC20} degrades cyclin A, and in metaphase, cyclin B is degraded by APC/C^{CDC20} (Lara-Gonzalez et al., 2019). This temporal degradation of cyclin A and cyclin B indicates that SAC is involved in cyclin B degradation, whereas cyclin A destruction is independent of SAC (Dang et al., 2021). MAD2, a spindle assembly checkpoint protein inhibits APC/C^{CDC20} activity to occur before metaphase to limit the degradation of cyclin B before metaphase where spindle assembly takes place (Schrock et al., 2020) as shown in figure 2.11 adapted from Dang et al., 2021.

2.4. Hematological And Neurological Expressed 1

2.4.1. HN1 In Historical Context

In 1997, Tang et al reported a novel 1.4-kb cDNA clone that was isolated from a blood islands-derived primitive erythroid cell hgtll cDNA library of a murine day 9 yolk sac, which was expressed in many fetal and adult tissues

including the highest levels in hematopoietic cells and fetal brain tissue. The same study also reported the tissue mRNA distribution, chromosomal localization, and nucleotide sequence of *HN1* as well. Furthermore, a significant homology between HN1 and murine expressed sequence tags (ESTs) along with human-derived ESTs from cDNA libraries (infant, fetal, adult brain, fetal spleen and liver, white blood cells (WBCs), endothelial cells. Prostate gland, lung, testes, and placenta) was also observed. Cells of hematopoietic origins including 10-day yolk sac blood-derived circulating erythroblasts showed the highest expression of HN1, with day 17 fetal brains also showing relatively higher expression as compared to the adult brain, which had considerably lower expression. On this rationale, the gene encoding cDNA product was designated as hematological and neurologic-expressed sequence 1, HN1 (Tang et al, 1997). The serial analysis of gene expression (SAGE) method then also identified mRNA of *HN1* in primary cultured microglial cells and N9 microglial cell line (Inoue et al, 1999). Earlier genetic mapping studies reported that human chromosome position 17q25 encompasses several genes that are important in disorders including hereditary neuralgic amyotraphy and tylosis associated with esophageal cancer (Risk et al, 2002) along with tumorigenesis of sporadic breast cancer and ovarian cancer (Kalikin et al, 1999). Mouse HN1 encoding a 154 amino acid peptide was not placed in a known protein family owing to the absence of any known domain. However, it showed considerable homology to mouse cDNA D17Ertd441w, identified earlier in an extensive study on mouse development, from a fertilized egg cDNA library (Ko et al, 2000). The genomic sequence of this homolog was included in the T-complex region of chromosome 17 in mice, which is reported to be involved in male reproduction and embryonic development (Silver, 1993). The homolog of HN1 encoded a 190 amino acid peptide with 30 % identity with *HN1* as reported by Zhou et al in 2004 and named *Hematological and Neurological Expressed 1-Like (HN1L)*. They also reported 30 orthologues and paralogues of HN1 and HN1L across various invertebrates and vertebrates with their sequences being highly conserved in phylogeny. In light of this data, the *HN1* gene family term was established for being evolutionarily conserved in nature and contained *HN1*, *HN1lL*, and their various pseudogenes as well (Zhou et al, 2004).

2.4.2. HN1 In Different Cancers

In a study involving gene expression arrays performed for selecting potential markers for epithelial ovarian cancer, *HN1* was one of the four genes that were 3-fold upregulated and distinguished tumor samples from normal ovarian surface epithelial cells (Lu et al, 2004). HN1 mRNA has also been reported in vitro in a murine glioma cell line (GL261) and in vivo in murine brain tumors along with human U118MG and U87MG cell lines in vitro and human brain tumors (high-grade malignant gliomas) (Laughlin et al, 2009). The study that showed the aforementioned expressions of *HN1* also revealed that HN1 depletion had no effect on cell proliferation; however, the tumors established from depleted HN1 GL261 cells were smaller in volume as compared to those with control cells. In situ hybridization and immunohistochemistry analysis indicated that HN1 expression was concentrated on the edges of tumors (Laughlin et al, 2009). Since cells proliferate quickly in that area and certain factors like membrane-type 1 matrix metalloproteinase and matrix metalloproteinase 2 (MT1-MMP/MMP2 play a key role in various interactions, the presence of HN1 in that area warrants further studies as such factors have been critical in appropriating invasive ability of cancer (Seiki, 2003).

The origination process of cancer has also been associated with the altered expression micro-RNAs. miRNA microarray and real-time PCR analysis depicted that miR-132 was significantly deregulated in Ductal carcinoma in situ of invasive breast cancer and its overexpression inhibited the proliferation and colony formation in breast cancer cell line (Li et al, 2013). *HN1* has been identified as one of the target genes of miR-132 in breast cancer where miR-132 binds to the 3' UTR of HN1 transcript, leading to subdued tumorigenic phenotypes including in vitro and in vivo invasion, proliferation, metastasis, and migration (Zhang et al, 2014). Moreover, higher expression of the *HN1* gene was also significantly associated with worse overall survival in breast cancer patients, thereby illustrating the potential impact of miR-132 in regulating *HN1* by controlling the oncogenic effects of higher expression of HN1 as a therapeutic strategy in breast cancer pathology (Zhang et al, 2014). One of the popularly recognized oncogene *MYC* has been known to be overexpressed in various tumors as it influences the processes of proliferation, apoptosis, and eventually tumorigenesis (Facchini & Penn, 1998). It has been demonstrated that patients with breast cancer had a

positive correlation between *MYC* and *HN1* and studies in breast cancer cell lines also suggested that overexpression of *HN1* enhanced the expression of *MYC* and the genes activated by *MYC* including *CDK4, CCND1, p21, CAV1, and SFRP1*. However, downregulation of MYC showed reverse effects *in vitro* in breast cancer cell lines. Based on the observations of that study, it was concluded that HN1 potentially increased the stability of MYC and acted upstream of *MYC* by suppressing the activity of GSK3β, which functions by destabilizing MYC. Hence, it could be suggested that *HN1* plays its role in the stimulation of breast cancer via *MYC* expression, further implying its significance as a potential therapeutic target in breast cancer (Zhang et al, 2017).

In HEK293T, A549, and HUVEC cells, 3‘UTR sequences of *HN1* have been investigated. It is reported that short 3‘UTR sequences are expressed in cancer cells and long 3‘UTR sequences of *HN1* are expressed in senescent cells showing the regulation of alternative polyadenylation of HN1 as a mechanism of the function of HN1. The lengthening of 3‘UTR of *HN1* was a function of a splicing factor known as HNRNPA1 (Jia et al., 2019). In endometrial cancer cell lines, HN1 gave a response to metformin, a pharmacological agent for therapy. In endometrial cancer, HN1 expression has been associated with cancer patients as higher expression portrays a poor prognosis for the disease (Bateman et al., 2020). Moreover, *HN1* is overexpressed in thyroid cancer, showing a poor prognosis for cancer. It is reported that HN1 increases the tumorigenesis, invasion, and migration of thyroid cancer ATC cells by regulating the stability of microtubules as it interacts with Stathmin 1. The depletion of HN1 in ATC cells leads to a decrease in EMT induced by TGF-beta (Pan et al., 2021). *HN1* overexpression has also been reported as a poor prognosis marker of liver cancer where the E2F target, G2, and DNA repair pathways are associated with HN1 expression (Liu et al., 2020). In liver cancer cells, HN1 acts as a downstream target of c-Met and can be considered a biomarker for HCC (Chen et al., 2020). In cervical cancer, HN1 is upregulated and can be considered an independent prognostic marker as it induces lymph node metastasis and lymphangiogenesis by activation of the NF-κB pathway (Chen et al., 2020).

2.4.3. HN1 In Prostate Cancer Cell Lines

HN1 has been identified as a novel gene that is associated with castration-resistant Prostate cancer (CRPC) in a study that analyzed the transcriptome of human LNCaP cancer cells while progressing to CRPC. High expression of *HN1* was detected along with 14 other genes that were associated with metastasis of Prostate cancer (Romanuik et al, 2010). Expression of *HN1* has been reported in Prostate cancer cell lines PC-3 and LNCaP, while it was not upregulated in DU-145 cells. It was revealed that HN1 expression was responsive to epidermal growth factor (EGF) in PC-13 cells. HN1 depletion in PC-3 cells resulted in increased Akt(S473), GSKβ (S9, Y216) phosphorylations, c-myc expression, nuclear accumulation of cyclin D1, accumulation of β-catenin, prolongation of the G1 phase of cell cycle and increased tetraploidy. Moreover, ectopic expression of *HN1* showed a reduced proliferation rate and accumulation of cells in G2/M. In conclusion, HN1 was considered a potential regulator of key cellular processes including Akt/β-catenin/GSK3β pathways, cell cycle regulation, and other eventualities of these pathways (Varisli et al, 2011). Further studies in Prostate cancer cell lines revealed that HN1 depletion resulted in translocation of androgen receptor (AR) to the nucleus by increased Akt(S473) phosphorylation. On the other hand, *HN1* overexpression caused increased ubiquitination mediated degradation of AR and subsequently downregulation of AR downstream genes like *NKX3.1, STAMP2, KLK3, and KLK4*. In LNCaP cells (androgen sensitive) *HN1* overexpression reduced colony formation and androgen-mediated (R1881) growth, however in androgen insensitive PC-13 and DU-145, it increased the colony formation without affecting the proliferation of cells (Varisli et al, 2012).

Since *HN1, AR and EGFR* have been reported as highly expressed genes in Prostate adenocarcinoma and stimulation of *AR* without androgens gives a survival advantage to Prostate cancer cells post androgen ablation therapy, HN1 could be placed at a crossroads in intervention therapies that involve targeting AR in cancers refractory to hormones (Lonergan & Tindall, 2011). Another study in Prostate cancer cell lines demonstrated that the overexpression of *HN1* led to b-catenin degradation, dysregulation in E-cadherin interactions, and actin re-organization causing migration in vitro. The role of HN1 as a potential regulator of β-catenin signaling, cell growth, and migration in Prostate cancer cells was established (Varisli et al, 2015). E-cadherin and β-catenin have been known as

adhesion molecules that function in maintaining the normal epithelial phenotype of cells and dysregulated epithelial cell adhesion leading to invasive phenotype is involved in one of the major hallmarks of cancer i.e. metastasis. In Prostate carcinoma, loss of expression of these proteins has been reported in higher grades of the disease (Junior et al, 2010). Therefore, HN1 induction altering the interactions between cadherin and catenin could be important in the context of tissue morphology, development, integrity, and cellular polarity as well (Varisli et al, 2015). Furthermore, HOXA11-AS1 is a competing endogenous RNA, which functions in regulating HN1 by sponging miR-24-3p, a microRNA regulating HN1 in Prostate cancer cells (Cheng et al., 2021).

2.5. Tet-On Inducible Expression System

The control of eukaryotic gene expression by inducible promoters for studying the function of individual genes has been reported several times. There are promoters that respond to external stimuli such as metal ions or hormones, however with secondary undesirable effects. The first bacterial system of Isopropyl β-d-1-thiogalactopyranoside (IPTG) induction was tested in mammalian cells with minimal induction. Meanwhile, a tetracycline-based tet system in mammalian HeLa cells showed good results for induction of gene expression (Gossen & Bujard, 1992). The tetracycline repressor (tetR) recognizes the response element (TRE) consisting of several repeats of 19 nucleotides known as tetracycline operator sequence (tetO). The regulation of transcription in bacterial systems depends on the binding of tetracycline (or Doxycycline) to tetR instead of TRE. Therefore, the TREs are placed upstream of the minimal promoters to develop the tetracycline-dependent-promoters and are used in mammalian expression systems (Das et al., 2016).

The tetracycline OFF system indicates that the expression under the influence of tetO-carrying promoters is reduced in the presence of tetracycline. The tetracycline-controlled transactivator (tTA) developed after fusing the C-terminal domain of VP16 (virion protein 16) with the tetR is used for the tetracycline OFF system. When tetracycline is absent, tetO sequences remain bound to tetR segment of the tTA, while the activation fragment continues to promote the transcription. However, when tetracycline is present, it remains bound to tetR, which inhibits the binding of tTA to tetO, causing a reduction in

transcription and hence the tet-OFF system (Kallunki et al., 2019). Moreover, the residues of tetR required for inducing the repression of transcription were mutated to produce rTetR, which assists the transcription in the presence of tetracycline (Gossen et al., 1995). Furthermore, VP16 fusion with rTetR to produce a transactivator known as reverse tetracycline-controlled transactivator (rtTA) leads to a new system known as Tet-ON system as shown in figure 2.12, where the transcription is activated in the presence of tetracycline or Doxycycline (Kallunki et al., 2019). There are many expression plasmids available that can be used for inducing or repressing the expression of the desired gene. The pCW57.1 is one of the examples of an all-in-one Tet-ON system for making stable cell lines and inducing the expression of the desired gene by cloning a gene of interest in the plasmid and generating lentiviral particles (Barger et al., 2015). The general map of pCW57.1 is shown in figure 2.13.

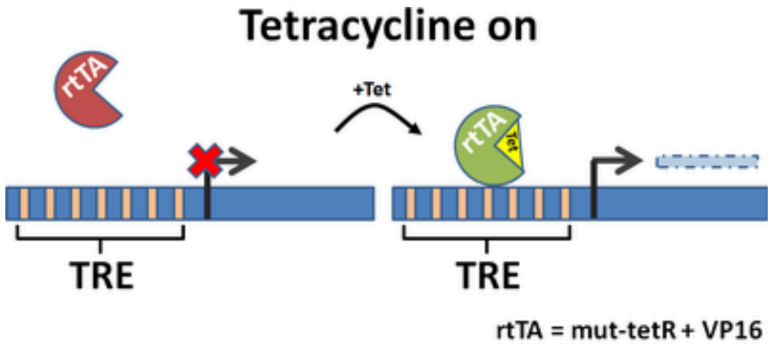

Figure 2.12: The mechanism of Tet-ON system.

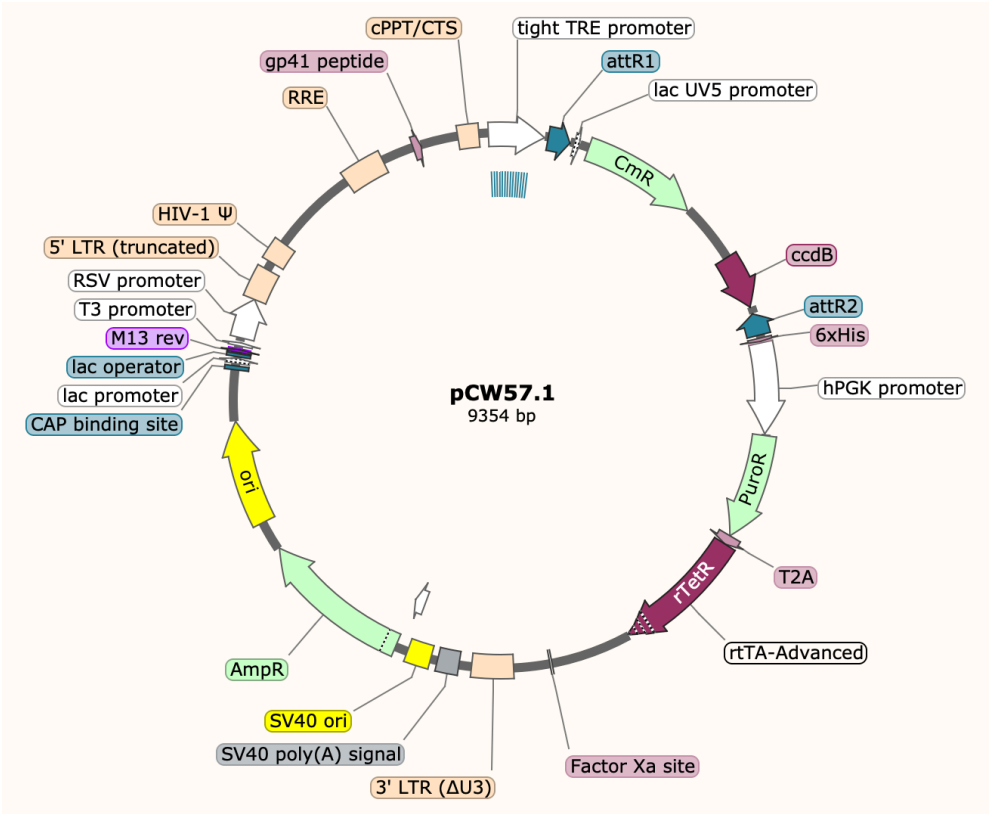

Figure 2.13: The map of pCW57.1 plasmid for Tet-ON inducible expression system.

2.6. Fluorescent Ubiquitination Based Cell Cycle Indicator (FUCCI) System

The Fluorescent Ubiquitination-based Cell Cycle Indicator (FUCCI) system was introduced in 2008 as a reporter system to monitor the living cells in different phases of the cell cycle (Sakaue-Sawano et al., 2008). A number of groundbreaking discoveries have since been made in the field of cell proliferation using this technology. The system applies two principal components of the DNA replication system including the inhibitor named Geminin and its substrate functioning as a licensing factor known as Cdt1. These proteins and their levels oscillate during the cell cycle and oppose each other in the pattern of DNA replication (Arias & Walter, 2007). The native levels of Cdt1 in eukaryotic cells are high in G1 and before S and go down immediately after the start of the S-phase due to proteasomal degradation by SCF^{SKP2} (Li et al., 2003). Meanwhile, Geminin functions to inhibit Cdt1 and remains high in S and G2 phases, and goes down in mitosis and G1 phases (Luo & Kessel, 2004). SCF^{SKP2} and APC/C^{CDH1} sequentially activate and affect the levels Cdt1 and Geminin in a negative manner respectively. The SCF^{SKP2} ligase complex is activated during S and G2 phases and degrades Cdt1, while APC/C^{CDH1} is activated during mitosis and G1 phases and

degrades Geminin in this time period (Li & Zhang, 2009). SCF^{SKP2} also acts as a substrate of APC/C^{CDH1} implying a tight control of the progression of the cell cycle (Bashir et al., 2004). As shown in the figure 12.14 (A, B) adapted from Zielke & Edgar, 2015, shows that the FUCCI system contains fluorescent proteins fused with Cdt1 and Geminin in their degron forms. The system heavily relies on the activities of SCF^{SKP2} and APC/C^{CDH1} for appropriate visualization of cells in different phases of the cell cycle (Zielke & Edgar, 2015).

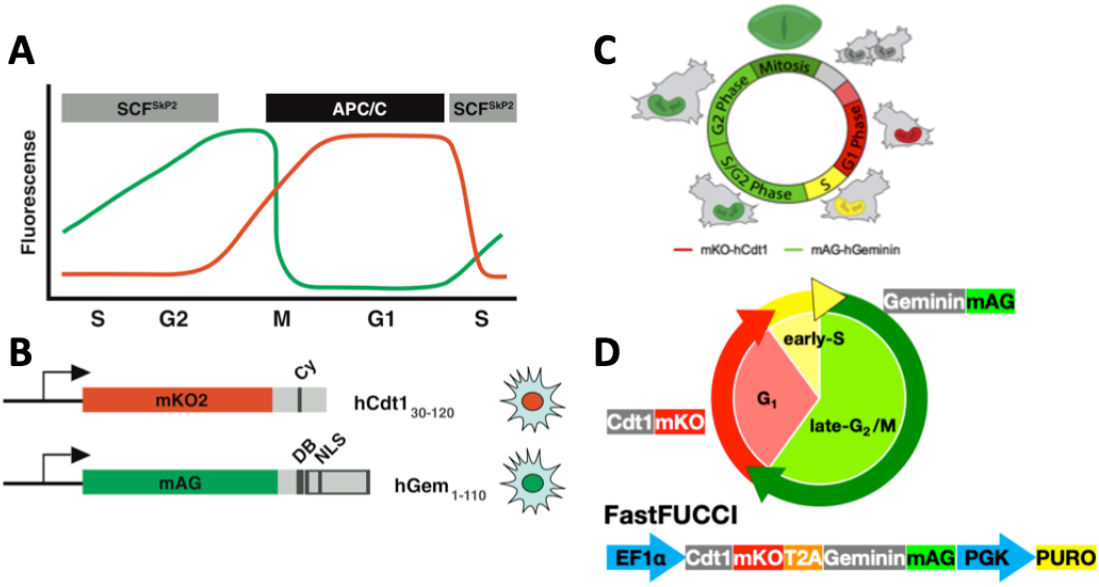

Figure 2.14: Overview of the FUCCI reporter system. (A) The SCF^{SKP2} and $APC/^{CDH1}$ activities fluctuate during cell cycle and inhibit each other. The green color fluorescence marked by Geminin expression shows the activity of SCF^{SKP2}, while orange color fluorescence exhibits the expression of Cdt1 and identifies as the activity period of APC/C^{CDH1}. (B) The degron sequences of hCdt1 and hGem fused with mKO2 and mAG tags showing orange and green fluorescence respectively in the nucleus are illustrated. (C) The relevant expression of Cdt1 and Geminin degrons in nucleus of a cycling cell fused with mKO2 and mAG fluorescence tag. (D) The example of a FUCCI reporter known as FastFUCCI and the coding features in a lentiviral plasmid.

3. MATERIALS AND METHODS

3.1. *In Silico* Approaches For HN1

3.1.1. Disorder Prediction Tools

The HN1 protein structure was modeled by using different platforms including Iterative Threading ASSEmbly Refinement (I-TASSER) (Yang et al., 2015), ROBETTA (Ovchinnikov et al., 2016), and QUARK (Lee et al., 2017) and visualized in PyMol software (Baugh et al., 2011) by applying energy minimization using Powell method. HN1 amino acid composition was compared against known disordered protein to establish a pattern showing disorder-promoting residues being enriched in the protein. Predictor of Natural Disordered Regions (PONDR) score is a measure of disordered-ness in a protein, and the HN1 PONDR score was determined and plotted to reveal the disordered regions in the protein sequence (Xue et al., 2010). The absolute mean net charge for HN1 protein was plotted against known ordered and disordered proteins. A mathematical representation of HN1 as a disordered protein is described. The description is based on the relationship between mean hydrophobicity and the mean net charge of the protein.

3.1.2. *HN1* Co-Expression Network Analysis

The co-expression database "CoExpedia" search platform (Yang et al., 2017) was used to extract the co-expressed genes of *HN1* from the Gene Expression Omnibus (GEO) database. HUGO Gene Nomenclature Committee (HGNC) Symbol of *Hematological and Neurological Expressed 1, "HN1"* was searched in CoExpedia through its online portal to collect all the co-expressed genes from the available human GEO datasets in the CoExpedia database. Furthermore, *HN1* co-expressed genes (479) were applied for enrichment analysis for Gene Ontology (GO) for molecular function (MF), biological process (BP), and cellular compartment (CC) by using FunRich version 3.1.3 (Pathan et al., 2015) for human Taxon ID: 9606. To narrow down the *HN1* co-expression network in the context of Prostate cancer, *HN1* similar genes were detected from The Cancer Genome Atlas (TCGA) Prostate Adenocarcinoma (PRAD) expression dataset from the Gene Expression Profiling Interactive Analysis (GEPIA) database (Tang et al., 2017). A Pearson correlation coefficient value of more than

0.5 is used as a threshold for implementing a stringent analysis of the *HN1* co-expression pattern. 176 genes were identified and used for gene enrichment analysis using FunRich version 3.1.3 as described above. A Pearson correlation coefficient (PCC) value of more than 0.5 was used as a cut-off for *HN1* similar genes to further process the enrichment of the network. The significant association of co-expression was marked by $p < 0.05$ for PCC described in the GEPIA database.

To determine the protein-protein interaction network in Prostate cancer, the protein list of all the *HN1* co-expressed genes was uploaded onto the Search Tool for the Retrieval of Interacting Genes/Proteins (STRING) database, which provides a user to determine the protein-protein interactions based on co-expression and experimental data extracted from literature (Szklarczyk et al., 2015). The disconnected nodes were excluded from the final network as the confidence score of 0.9 was selected as a threshold for the construction of the protein-protein interaction. The interaction score was based on the active interaction sources, co-expression and experiment-based means inside the edges of the network, and evidence as to the selected options of the STRING network.

3.1.3. Genomics And Transcriptomics Data Analysis Of *HN1* In Prostate Cancer

The disease-free survival analysis of *HN1* expression within the PRAD tumor dataset of TCGA described in the GEPIA database was conducted. The survival plot was based on a Cox PH model on 246 samples of low expression of HN1 and 246 samples of high expression of HN1. The Hazard Ratio indicator *p(HR*) value was significant for the plot for differentiation of samples based on the high and low expression for the indicated time for disease-free survival.

The c-Bioportal database was used for screening Prostate cancer for mutations in HN1, as it contains datasets and studies from which genomic profiling data can be extracted from normal and Prostate cancer patients (Gao et al., 2013). The threshold for screening the studies was made stringent with minimum cases set as 100 and minimum mutation rate set as 1 % for the analysis. The comparison of different mutations such as amplification and deep deletion was made dependent on the occurrence of mutation in the *HN1* gene in the cancer patient described by the studies screened from the threshold values.

GEPIA database was again searched for mining the transcriptomics data on HN1 in normal tissues and Prostate cancer samples. The data from normal tissues were extracted from TCGA normal and The Genotype-Tissue expression (GTEx) datasets, and data from Prostate cancer patients were derived from the PRAD dataset of TCGA. The comparison of normal and cancer data is described in the form of a box plot with parameters of $\log_2(TPM + 1)$ for log scale, jitter size at 0.04, p-value cut-off as 0.01, and $|Log_2FC|$ Cutoff as 1.

3.2. Bacterial Culture And Recombinant DNA Preparation

3.2.1. Competent Cell Preparation

3.2.1.1. Materials

- *E. Coli* DH5α strain
- Transforming Buffer: 55 mM $MnCl_2$, 15 mM $CaCl_2$, 250 mM KCl, 10 mM PIPES (piperazine-1,2-bis[2-ethanesulfonic acid) (pH=6.7) dissolved in deionized water
- SOB media: 20 g tryptone + 5 g yeast extract + 0.5 g Nacl + 10 ml 250 mM KCl, dissolved in 950 ml deionized water and pH set at 7.0 and volume made to 1 litre, autoclaved. After autoclaving, 5 ml sterile 2 M $MgCl_2$ solution, stored at 4 °C.
- Spectrophotometer
- Transparent cuvettes
- Shaking incubator
- Erlenmeyer flasks (250 ml, 500 ml, 1000 ml, 2000 ml)
- Refrigerated centrifuge (Eppendorf)
- Dimethyl sulfoxide (DMSO) (Sigma, Germany)
- Eppendorf tubes
- Sterile pipettes and Pipettor
- Mini-pipettes and mini-pipetters
- Falcon tubes (50 ml)
- Dry ice, Ice-box
- Refrigerators (+4 °C, -20°C, -80°C)

3.2.1.2. Method

Chemically competent bacterial cell populations were prepared as described previously (Inoue et al., 1990). Transforming buffer solution along with SOB media was prepared. An *E. Coli* strain of DH5α was taken from frozen stock

and streaked on an LB agar plate and incubated overnight at 37°C in an incubator. A single colony of the bacteria was selected and grew on a shaking platform in 250 ml SOB media until the OD_{600} (Optical Density) reached 0.7. The bacterial culture was then placed on ice for 10 minutes prior to centrifugation at 2500g for 15 minutes at 4°C. After centrifugation, the supernatant was removed and the pellet was suspended in an 80 ml TB buffer placed on ice. The same method of centrifugation was repeated again and the supernatant was removed. The pellet was then suspended in 20 ml TB containing 7 % DMSO and chemically competent bacteria cells were then aliquoted on dry ice in Eppendorf tubes containing 200 µl competent cells per tube and stored at -80°C.

3.2.2. Plasmid And Ligation Reaction Transformation

3.2.2.1. Materials

- Chemically Competent Cells
- Ice, icebox
- Plasmid DNA or Ligation reaction mixture
- Eppendorf tubes
- Water bath
- Incubator
- LB media: 10 g tryptone + 5 g yeast extract + 0.5 g NaCl dissolved in 1 litre de ionized water and autoclaved
- Agar (Sigma, Germany)
- Mini-centrifuge (Eppendorf, Germany)
- Cell spreader (glass)
- Plastic petri dishes (disposable)
- Ampicillin (Sigma, Germany)

3.2.2.2. Method

The chemically competent cells stored at -80°C were taken out and placed on ice for 15-20 minutes. The plasmid DNA (1µl/50µl competent cells) or DNA ligation reaction mixture (1µl/50µl competent cells) was added to competent cells and tubes were then slightly hit from the side and placed back on the ice for additional 15-20 minutes. The tubes were then taken out from the ice and placed in a water bath set at 42°C for 45 seconds and immediately placed back on the ice

for at least 2 minutes. The fresh LB media was added to competent cells to make the volume 1 ml and cells were transferred to a larger tube such as a 15 ml falcon tube. The LB media containing transformed bacterial cells was then incubated on a shaker for 45 minutes on a shaker at 37°C. After incubation, LB containing bacterial cells were centrifuged in an Eppendorf tube and pelleted after a short spin for 10 seconds at 12000g at room temperature. The supernatant is removed until 100 µl of liquid remains. The cells are re-suspended using a pipette and spread over a petri dish containing LB agar (with 100 µg/ml Ampicillin) using a glass spreader. The transformed bacteria were then allowed to grow overnight in the form of colonies on an agar plate at 37°C in an incubator.

3.2.3. Colony PCR And Restriction Digestions

3.2.3.1. Materials

- Bacterial colonies
- *Taq* PCR master mix (Qiagen)
- PCR tubes
- Primers (Forward and Reverse):
  LNCX Forward= AGCTCGTTTAGTGAACCGTCAGATC
  HN1 Forward= CAGAATTCCATGACCACAACCACCAC
  HN1 Reverse= TGTGGCGGCCGCTACCCAAGACGAGGCTGG
- PCR grade water
- Thermal cycler (BioRad)
- Plasmid DNA
- Restriction enzymes: BamH1, EcoR1, EcoRV, HindIII, Mme1, Nhe1, Not1, Sal1, Xba1, Xho1 (New England Biolabs)
- Restriction enzyme buffers: Buffer 2.1, Buffer 3.1, Cut-smart buffer (New England Biolabs)
- Eppendorf tubes
- Incubator

3.2.3.2. Method

The individual colonies obtained after an overnight culture of transformed chemically competent cells were picked and added to 10 µl LB (100 µg/ml Ampicillin) and incubated at 37°C for 30 minutes. In the meantime, the polymerase chain reaction (PCR) mixture was prepared using the Taq PCR

Master kit (Cat. No./ID: 201445). Briefly, for a 20 µl reaction, 10 µl master mix (2X), 1 µl of the forward primer and reverse primer (0.5 µM final concentration in 20 µl reaction), 7 µl PCR grade water, and 1 µl of colony mixture were added to a PCR tube. The colony PCR reaction conditions were as given below:

Initial Denaturation: 4 minutes at 94°C

Cycling 3-steps: 35 cycles

Denaturation: 50 seconds at 94°C

Annealing: 50 seconds at 58°C

Extension: 50 seconds at 72°C

Final Extension: 10 minutes at 72°C

The plasmid DNA was digested with appropriate restriction enzymes procured from New England Biolabs (NEB), and the recommended protocol was applied for each enzyme separately. Briefly, the enzyme reaction was set up by adding the DNA, buffer (specific for each enzyme), and water into an eppendorf tube, followed by the enzyme and placed in an incubator at 37°C for at least half an hour up to overnight.

3.2.4. Agarose Gel Electrophoresis

3.2.4.1. Materials

- Agarose (Sigma, Germany)
- TAE buffer: Trizma base 4.84 g + glacial acetic acid 1.14 ml + 0.5 M EDTA (2 ml) dissolved in 1 litre deionized water and pH set at 8.0 with acetic acid
- Erlenmeyer flask (250 ml)
- Microwave oven
- Ethidium Bromide
- Agarose gel casting tray and tank
- Voltage supplier system
- DNA loading buffer
- DNA ladder: 100 bp or 1 kb+

3.2.4.2. Method

1 % agarose gel was prepared by mixing the 70 ml TAE (1X) buffer with 1 g agarose powder in an erlenmeyer flask and heating the mixture in a microwave oven for 30 seconds or until the mixture dissolved completely.

Ethidium bromide (2 µl of 1 % solution) was then added to the mixture and mixed by swirling the flask. The hot solution of agarose gel in TAE buffer with ethidium bromide was then poured into gel apparatus containing gel casting tray with appropriate combs. The gel was then casted after 30-minute wait and comb was then carefully removed from the gel. The tank was then filled with 1X TAE buffer prior to loading the samples mixed with 6X DNA loading dye. Each experiment contained a DNA ladder as appropriate control for correct sizes of DNA bands. The gel was run for 80-90 minutes at 90 volts. The DNA bands were then imaged using a gel doc system equipped with UV light and camera attached to the system.

3.2.5. Plasmid DNA Isolation (Alkaline Lysis Method)

3.2.5.1. Materials

- Solution I: 10 mM EDTA (pH=8.0), 25 mM Tris-HCl (pH=8.0), 50 mM glucose in TE buffer, stored at 4 °C
- Solution II: 1 % SDS in 0.2 N NaOH solution
- Solution III: 60 ml 5mM potassium acetate + 11.5 ml glacial acetic acid + 28.5 ml deionized water to form 5 M acetate and 3 M potassium solution, stored at 4°C
- Falcon tubes
- LB media
- Eppendorf tubes
- Ampicillin (Sigma, Germany)
- Minicentrifuge
- Vortex
- Ethanol
- TE buffer
- RNAse (NEB, UK)

  Incubator

3.2.5.2. Method

A single colony picked from the antibiotic selection on agar plate brown in 5 ml overnight culture in antibiotic-containing media (5 ml) was used for alkaline lysis. 1.5 ml of the culture was centrifuged at 12000g for 30 seconds at room temperature to collect the cell pellet after removing the supernatant. The cell pellet was dissolved in ice-cold 100 µl Solution I and vortexed for suspending the pellet

in the solution completely. The 200 µl of Solution II was added to the homogenized cellular suspension and mixed by inverting the tube 6 times and placed on ice. 150 µl of Solution III was then added to the lysed cells and mixed by using a vortex for 10 seconds and placed on ice for 5 minutes prior to centrifugation at 12000g for 5 minutes at room temperature. The supernatant was collected in a new tube carefully without touching the pipette with the pellet. The ice-cold 100 % ethanol solution in 2-fold volume to the supernatant was then added and vortexed for mixing and placed at ice for 5 minutes prior to centrifugation at 4°C for 5 minutes to collect the DNA pellet. The ethanol was removed using a pipette and the pellet was washed with 70 % ethanol and the remaining ethanol was removed using dry filter paper without touching the visible DNA pellet. The pellet was further air-dried before adding 50 µl TE buffer containing 20 µg/ml RNAse A. The DNA was then incubated at 37°C for half an hour prior to further screening using restriction digestion and gel electrophoresis.

3.2.6. Plasmid DNA Isolation (Hi-Speed Midi-Prep)

3.2.6.1. Materials

- Erlenmeyer flasks (500 ml)
- Incubator
- LB Media
- Ampicillin (Sigma, Germany)
- Ethanol
- Isopropanol
- QIAGEN Midiprep solutions: P1, P2, P3, QBT, QC, QF
- Buffer TE
- Hi-speed midi tip (Qiagen, Germany)
- QIA-precipitator (Qiagen, Germany)
- Falcon tubes (15 ml, 50 ml)
- Ice and Ice-box
- Vortex
- HM-HN1 (His-Max-HN1) plasmid
- pCW57.1 (Plasmid #41393, Addgene)
- pcDNA4-TO (Plasmid #44118, Addgene)
- Pipettor and Pipette tips

- Mini-centrifuge

3.2.6.2. Method

The purified plasmid DNA ready for transfection into mammalian cells was isolated from bacterial growth culture using a Qiagen Hi-Speed Plasmid Midi-kit. Initially, a bacterial colony selected for isolation was grown in 150 ml LB media containing antibiotics for selection, overnight at 37°C on a shaker. The bacterial cells were pelted using centrifugation for 15 minutes at 6000g at 4 °C. The supernatant was removed and cell pellets were suspended in a total of 6 ml P1 solution (containing RNAse A) and cells were homogenized using a vortex. The cells were lysed using 6 ml P2 solution and inverting 6 times and incubating at room temperature for 5 minutes. At this stage, the lysis proceeded marked by the appearance of blue color. After incubation, 6 ml P3 solution was added to neutralize the lysis and lysed cells were then placed inside the cartridge filters provided with the midi prep kit. The lysate was incubated in the cartridge for 10 minutes. The Hi-Speed midi tip was then calibrated using 4 ml of QBT buffer and lysate was poured into the tip using a cartridge plunger. The flow-through was discarded and the tip was washed with 20 ml QC washing buffer. The flow-through was discarded and DNA was eluted using 5 ml QF elution buffer in a 15 ml falcon tube, which was mixed with 3.5 ml isopropanol and mixed using a vortex. The DNA and isopropanol mixture was incubated at room temperature for 5 minutes prior to filtration through a QIA-precipitator using a 20 ml syringe. The DNA was then washed with 2 ml 70 % ethanol using a 5 ml syringe. The excess of ethanol was removed by passing the air through the precipitator using the same syringe. The purified DNA was eluted using TE buffer and quantified using a nano-drop device (spectrophotometer).

3.2.7. Inserting HM-HN1 And HN1-Venus In pCW57 Plasmid

HN1 was cloned into the pCW57.1 expression plasmid. The pCW57.1 plasmid was cut with Nhe1 and Sal1 to prepare the pCW57.11 (ccdB deleted circularized), which was further digested with Sal1 to obtain vector DNA. HM-HN1 plasmid was digested with Sma1 and Sma1 digested HM-HN1 was further sequentially digested with EcoRV to obtain the fragment containing His-Max-HN1 only. The vector ends were filled with dNTPs using T4 DNA polymerase. The DNA ligation was carried out using T4 DNA ligase. Colony PCR from

colonies obtained from the transformation of ligation reaction with LNCX forward and *HN1* reverse primers using *Taq* polymerase was performed. Different clones of pCW57-HMHN1 were validated by miniprep (alkaline lysis) and using Sal1 + EcoRV double digestion, and Xho1 + Xba1 double digestion. One clone was selected for plasmid isolation from Hi-Speed midi prep and validated by using HindIII digestion.

HN1 was first fused with pcDNA4-TO-mVenus using PCR and restriction cloning. Vector was prepared by digesting pcDNA4TO-Venus with Not1 and EcoR1. The HN1 amplification using primers flanking *HN1* ORF with Not1 and EcoR1 sites using HM-HN1 plasmid as template DNA was performed. The amplified PCR product was then digested with EcoR1 and Not1. T4 DNA ligase used for ligation reaction, which was transformed into chemically competent cells. Colony PCR was performed on colonies that appeared after the transformation of the ligation reaction using T4 DNA ligase (New England Biolabs). *HN1* forward and *HN1* reverse primers were used. The positive clones were propagated for plasmid DNA isolation using the mini-prep method and digested with Not1 and EcoR1 to validate the insertion of the *HN1* fragment in pcDNA4-TO-Venus. The pcDNA4-TO-HN1-Venus and pcDNA4-TO-Venus plasmids were transfected to PC-3 cells and observed under an inverted microscope in a green fluorescence filter and imaged using Leica inverted microscope and camera.

HN1-Venus was then inserted in the pCW57 vector and validated by microscopy and western blotting. The pcDNA4-HN1-Venus was digested sequentially, first with Mme1 and Xba1, and then with EcoR1 to obtain a 1.5 kb insert. The insert ends were filled with dNTPs using T4 DNA polymerase. The colony PCR was performed with LNCX forward and *HN1* reverse primers after ligation reaction (transformed into chemically competent bacteria) containing the insert and vector used for preparing pCW57-HMHN1. The correct clone was then validated by propagating and isolating followed by restriction digestion with BamH1.

3.3. General Mammalian Cell Culture Methods

3.3.1. Materials

- Cryotubes
- 15 ml falcon tubes
- Serologic pipettes (2 ml, 5 ml, 10 ml, 25 ml)
- Automated pipettor
- Tissue culture treated-Cell Culture dishes (6 cm^2, 10 cm^2, 75 T-flask, 15 cm^2, and 6-well plate)
- Centrifuge (Core, Model: NF 1200R, Turkey)
- Cell Culture Incubators (Sanyo, Model: MCO-18AIC, Japan)
- Class II Biosafety Cabinet (Esco, Singapore)
- -86°C Freezer (Thermofisher, Model: Forma 900 series, Germany)
- Liquid Nitrogen Tank
- Water Baths (Wsid, Model: T10AL and WB-6, Germany)
- Aspirator (Vacuum motor pump and Pasteur pipettes)
- Inverted Microscope (Leica, Model: DMIL, Germany)
- • +4°C Fridge (Bosch, Model: KDN49DVONE, Germany)
- pH meter (Hanna, Model: HI 2211, Greece)
- Phosphate Buffer Saline (137 mM NaCl, 2.7 mM KCl, 10 mM Na_2HPO_4, pH=7.4)
- 0.25 % Trypsin/EDTA (Gibco)
- Trypan Blue dye (Sigma, Europe)
- Hemacytometer (Neubauer 0101050, Germany)
- 0.22 µm membrane filter (MF-Millipore™, Europe)
- Eppendorf tubes
- Micropipets (10 µl, 200 µl, 1000 µl)
- Micropipette tips (10 µl, 200 µl, 1000 µl)
- Dimethyl Sulfoxide (DMSO) (Sigma, Europe)

Cell Line	Media Composition	Source of cell line
RWPE-1	Keratinocyte serum free media 5 ng/ml hrEGF (Human Recombinant Epidermal Growth Factor) 0.05 mg/ml Bovine Pituitary Extract (BPE) 1 % Penicillin/Streptomycin (P/S)	ATCC (CRL-11609™)
LNCaP	RPMI 1640 10 % Fetal Bovine Serum (FBS) (inactivated) 1 % L-glutamine (L- glu) 1 % Penicillin/Streptomycin (P/S)	ATCC (CRL-1740™)
LNCaP-104R2	RPMI 1640 10 % Charcoal treated Fetal Bovine Serum (FBS) (inactivated) 1 % L-glutamine (L- glu) 1 % Penicillin/Streptomycin (P/S)	ExpaSy (CVCL_M128)
DU-145, PC-3, HEK293T	DMEM F12 5 % Fetal Bovine Serum (FBS) (inactivated) 1 % L-glutamine (L- glu) 1 % Penicillin/Streptomycin (P/S)	ATCC (HTB-81™, CRL-1435™, CRL-3216™)

Table 3.1. Cell lines, media composition and sources used in the study

3.3.2. Thawing, Growing, Seeding, Counting, And Storing Adherent Cell Lines

Prior to cell culture, cell culture media was placed in a water bath at 37°C for at least 15 minutes. Cells in cryotubes were thawed in a water bath at 37°C for 1-2 minutes and immediately placed in 5 ml warm media (appropriate cell culture media compositions are given in table 3.1) in a 15 ml falcon tube. The cells were centrifuged at 900 rpm for 5 minutes at room temperature to sediment the cells. The cell pellet was then separated from the supernatant by aspirating the supernatant utilizing a Pasteur pipette linked to an aspirating motor. The cell pellet was subsequently resuspended in 1 ml warm media using a sterile pipette slowly without damaging the cells to obtain a homogenous suspension of cells, and plated on the appropriate cell culture dish with suitable volumes of warm media (usually 10 ml warm media in a 10 cm^2 tissue-culture treated petri plate). The cell culture dishes were labeled properly for Cell line name, the number of passage, date of thawing, and initials of the researcher. The cell culture dishes are placed in an incubator for cellular growth at 37°C and 5 % CO_2.

Cells were grown on appropriate cell culture plates in 10 ml cell culture media (described in table 3.1) in an incubator containing 5 % CO_2 and temperature set at 37°C. Cell culture media was changed every 48 hours and contaminations risk along with the morphology were monitored in an inverted light microscope. The cell treatments along with the media changes were carried out in a sterile environment in a safety cabinet. Cells were allowed to grow until the confluency of the cells reached up to 80 % in the cell culture container (petri dishes). Cells were always subjected to pre-warmed media taken from +4°C (from a storage fridge) and placed on a water bath at 37°C for 15 minutes.

When cells reached around 80 % confluency, cells were washed with PBS solution by aspirating culture media and adding PBS (3-4 ml) and aspirating PBS. Cells were harvested by trypsinization using 1 ml Trypsin-EDTA dropwise onto cells and incubated for 3-5 minutes depending on cell type at 37 °C. After incubation, using 7 ml normal cell culture media containing FBS, trypsin was inhibited and cells were continuously homogenized by constant pipetting using a sterile pipette. Cells were placed in a 15 ml falcon tube for subsequent centrifugation at 900 rpm for 5 minutes at room temperature. The supernatant was removed to take out any leftover trypsin and cells were re-suspended in 5 ml fresh culture media for cell counting. The desired amount of cells after cell counting were then seeded to new cell culture plates with appropriate culture media and labeling of the plate with a new passage number. To equally distribute cells in the new dish, the plate was gently moved in an ‘8’ motion constantly for 16 times and placed back in the incubator to continue cell growth.

Each experiment requires a certain amount of cells to be seeded for specific treatments as cells grow in cell culture dishes according to their doubling times. Therefore, before seeding cells, it is important to determine the number of cells in the culture media. A hemocytometer containing 9 squares was used for counting the cells. The Trypan blue solution prepared in PBS and sterilized by filtration through a 0.22 µm membrane filter was used for counting cells. 10 µl of cell suspension after passaging the cells was mixed with 90 µl trypan blue dye solution for 1:10 dilution factor in a 1.5 ml eppendorf tube. A cover glass was placed on the central squares with two chambers of the hemacytometer and 10 µl of cell mixture in dye was placed in both upper and lower chambers underneath the cover glass. The living cells remain impermeable to trypan blue dye and can

be seen as bright circular cells, while dead cells can be observed as dark bluish or violet in an inverted microscope. The cells are counted from the 9 central squares in each section of the hemacytometer and the final count is taken as an average of both counts. The number of cells in 1 ml of culture media can then be described from:

Cells per ml= (Total cells counted X Dilution factor (10) X 10^4) / 9

Cells in culture die due to various reasons including changes in morphology, aging, increasing passages, and the type of media used. The cells therefore can be stored in earlier passages to maintain the metabolic health of the cells that can be investigated later after thawing the cells appropriately. Cells can be stored at -80°C or -190°C by applying a suitable cryo-protective reagent. We utilized DMSO to freeze the cells at 5 % in a culture medium containing a homogenous mixture of cells. Approximately 1 X 10^6 cells in 1 ml were stored in cryotubes and stored at -80°C for a few weeks prior to transferring to a liquid nitrogen tank at -190°C for long-term storage.

3.4. DNA And Sirna Transfections In Prostate Cell Lines

3.4.1. Materials

- Cell lines: RWPE1, LNCaP, DU-145, PC-3
- Cell Culture media
- Cell Culture dishes
- FUGENE HD transfection reagent (Roche, Germany)
- Scrambled control siRNA (Santa Cruz, Germany)
- siRNA-HN1 (sc-93949: Santa Cruz Biotechnology, Germany)
- Inverted microscope
- Cell Culture Incubator

3.4.2. Method

The pcDNA4-His-Max (HM-Vector) and pcDNA4-His-Max-HN1 (HM-HN1) plasmids constructed previously (Varisli et al., 2015) were used for studying *HN1* overexpression by plasmid DNA transfection in this study. FUGENE HD transfection reagent (Roche, Germany) was used for transfecting plasmid DNA in a 1:3 ratio as µg:µl (DNA: Reagent) according to the recommendations from the manual of the transfection reagent. 4 X 10^5 RWPE-1,

LNCaP, and PC-3 cells were seeded for 24 hours in 6 cm^2 cell culture petri dishes in their appropriate media before transfection. The next day, after monitoring the cells under inverted microscope, culture media was aspirated and cells were washed with PBS and replaced with antibiotic-free normal culture media before 2-4 hours of transfection. The FUGENE HD transfection reagent was diluted in serum-free media (3 µl reagent added to 97 µl media) and incubated for 5 minutes at room temperature in an Eppendorf tube. Similarly, 1 µg DNA (HM-Vec or HM-HN1) was diluted separately in serum-free media (100 µl) and incubated at room temperature for 5 minutes. The FUGENE HD dilution was added dropwise to the DNA dilution without the solution touching the walls of the Eppendorf tube. The DNA/Reagent complex formation was then carried out by incubation at room temperature for 15 minutes. After completion of complex formation, the mixture was added to the cells in culture dishes slowly in a drop-wise manner. The plates were then placed back in the incubator for 48 hours for transfections to proceed.

Similarly scrambled siRNA or HN1-specific siRNA (sc-93940) were used in HN1 depletion experiments in RWPE-1, LNCaP, and PC-3 cell lines. The experimental design was set up similar to the one described previously for plasmid DNA transfection. Cells were seeded on the 6-cm2 culture dishes one day prior to transfection. 2-4 hours before transfection, culture media was replaced with antibiotic-free media after washing cells with PBS. FUGENE HD transfection reagent was used. 100 picomole (pmol) of RNA (10 µl) was suspended in 90 µl serum-free media and incubated at room temperature for 5 minutes in Eppendorf tube. 10 µl of FUGENE HD transfection reagent was diluted in 90 µl of serum-free media at room temperature for 5 minutes. After incubator FUGENE HD solution was added dropwise to the RNA mixture. The complex formation was carried out at room temperature for 15 minutes prior to adding the complexes to the cells directly as mentioned previously. The plasmid DNA and siRNA-transfected cells were cultured for 48 hours before harvesting for further processing.

3.5. Cell Proliferation Assay

After transfecting the cells with HM-Vector, HM-HN1 or scrambled control RNA, or siHN1-RNA, and incubation for 48 hours, cells were washed

with PBS and trypsinized prior to re-suspension in normal culture media. The cells were subjected to viable cell count by trypan blue exclusion assay as mentioned in the cell counting method. Briefly, 10 µl cells were added to a 90 µl trypan blue dye solution and counted under a hemacytometer described previously. The total cell count was determined mathematically after approximating the cell amount from 1 ml. Triplicate reading was taken to apply statistical analysis of the *t-test* on the replicate. The *p-value* of less than 0.05 was found significant for variation in the means of the total cell count based on the test sample and the control group.

3.6. Cell Cycle Distribution Assay

3.6.1. Materials

- Cell Lines + Culture Media
- Cell Culture Dishes (6-well plates, 6 cm^2 dishes)
- Triton X-100
- RNAse A
- Propidium Iodide
- PBS solution
- BD Acuri 5 Flow cytometer

3.6.2. Method

48 hours post-transfection with siRNA or plasmid DNA as described previously. RWPE-1, LNCAP, and PC-3 cells were washed with PBS and trypsinized to harvest the cells for flow cytometry. The cells were centrifuged at 1000 rpm for 5 minutes at 4°C and the supernatants were removed by aspiration in a 15 ml falcon tube kept on ice. Cellular pellets were then re-suspended in 5 ml PBS and washed again by centrifugation. The cell pellet was then re-suspended in 1 ml PBS and 4 ml of 100 % ethanol was added dropwise when cells in a 15 ml falcon tube were vortexed gently. The cells were fixed in ethanol and placed at -20°C for at least 24 hours. After 24 hours, cells were pelleted by centrifugation at 1200 rpm for 10 minutes at 4 °C. The supernatant was removed and the pellet was washed with ice-cold PBS and centrifuged again. Cells were subjected to permeabilization by adding 1 ml Triton-X100 (0.2 % in PBS) and re-suspending

for 5 minutes at room temperature on a shaker. Cells were transferred to a 1.5 ml eppendorf tube and centrifuged at 2000g for 5 minutes at 4°C. The supernatant was removed and 500 µl of RNAse A (20 µg/ml in PBS) was added to the cell pellet for re-suspension and incubated at 37°C on a water bath for 30 minutes. The cells were centrifuged again for 5 minutes at 4°C, and the supernatant was removed. The 300 µl of Propidium Iodide (PI) solution (5 µg/ml in PBS) was added to the pellet to re-suspend the cells and kept in dark for 15 minutes at ice prior to reading on a flow cytometer. The cellular populations were analyzed in the FlowJo v10 software package. Triplicate reading was taken to apply statistical analysis of the t-test on the replicates. The *p-value* of less than 0.05 was found significant for variation in the means of the cellular populations in different phases of the cell cycle based on the test sample and the control group.

3.7. Protein Isolation And Western Blotting

3.7.1. Chemicals And Solutions

- RIPA modified buffer recipe:

10 mM Tris.base pH=8.0 (Sigma- T5941, Germany), 0.1% SDS (Sigma- L4390, Germany), 1% triton x-100 (Sigma- T8787, Germany), 0.1% sodium deoxycholate (Sigma- D6750, Germany), 1 mM EDTA (Sigma- K5134, Germany), 1 mM EGTA (Sigma- E3889, Germany), 140 mM NaCl (Sigma- S3014, Germany)

- Protease and Phosphatase inhibitors:

Protease inhibitor cocktail (Roche-04693159001, Germany), Phosphatase inhibitor cocktail (Roche- 04906837001, Germany), NaF 100X (100 mM), (Merck- B815549 606, USA), $NaVO_3$ 100X (200 mM) (Fluka- 72060, Germany), PMSF 100X (100 mM) (Fluka- 93482, Germany)

- 30% acrylamide mixture:

(29% acrylamide (Sigma- A9099, Germany) + 1% N, N-methylenebisacrylamide (Sigma- M2022, Germany). The mixture was prepared in 500 ml dH_2O and filtered with 0.2 micron membrane filter.

- 4X SDS-PAGE separating gel buffer:

1.5 M trisma base (pH: 8.8) (Sigma- T5941, Germany) + 0.4% SDS (Sigma- L4390, Germany), pH 8.8

- 4X SDS-PAGE stacking gel buffer:

0.5 M trisma base (pH: 6.8) (Sigma- T5941, Germany), 0.4% SDS (Sigma- L4390, Germany), pH 6.8

- Ammonium persulfate solution (10%) (Sigma- A9164, Germany)
- TEMED (Sigma- T9281, Germany)
- SDS-PAGE gel 1X running buffer:

  3 g Tris base (Sigma- T6066, Germany), 14.4 g glycine (Biochemika/FLUKA- 50046, Germany), 1.0 g SDS (Sigma- L4390, Germany) added to 1 L dH_2O
- Beta-mercaptoethanol (Sigma, M3148)
- 4X LB loading buffer:

  40 mM trism base (pH 8.0) (Sigma- T6066, Germany), 0.4 mM EDTA (Sigma- K5134, Germany), 4% SDS (Sigma- L4390, Germany), 20% glycerol (Sigma- G5150, Germany), Bromophenol blue 200 µl (Merck- L54971322 525, USA)
- SDS-PAGE gel transfer buffer (1X):

  1000 ml (in dH_2O)=20% methanol (Merck- K34212908503, USA), 3 g trism base (Sigma- T6066, Germany), 14.4 g glycine (Biochemika/FLUKA- 50046, Germany)
- TBS (1X) (pH 8.0), total volume 1L

  12.1 g trisma base (Sigma, T6066), 80.0 NaCl (Sigma, S3014)
- TBS-T: 0.1% Tween 20 (Sigma, E1383) was added to 1X TBS.
- Skimmed milk powder (Saliler, Germany)
- BCA kit (Sigma-088K6138, Germany)
- Quartz cuvette (Hellma- 105.202 QS, Germany)
- Isopropanol (Merck- K35707095 607, USA)

3.7.2. Antibodies For Western Blotting

- Anti-HN1 (produced in rabbit) (Cat #PA5-21779, Invitrogen, USA)
- Anti-Cyclin E (produced in mouse) (sc-377100, Santacruz Biotechnology, USA)
- Anti-Cyclin A (produced in mouse) (sc-271682, Santacruz Biotechnology, USA)
- Anti-Cyclin B1 (produced in mouse) (sc-245, Santacruz Biotechnology, USA)
- Anti-CDK1 (cdc2) (produced in mouse) (sc-8395, Santacruz Biotechnology, USA)
- Anti-CDK2 (produced in mouse) (sc-6248, Santacruz Biotechnology, USA)
- Anti-PLK1 (produced in mouse) (4535, Cell Signaling Technology, USA)

- Anti-CDC20 (produced in mouse) (sc-13162, Santacruz Biotechnology, USA)
- Anti-CDH1 (FZR-1) (produced in mouse) (sc-166714, Santacruz Biotechnology, USA)
- Anti-CDT1 (produced in mouse) (sc-365305, Santacruz Biotechnology, USA)
- Anti-pH3^{S10} (produced in mouse)
- Anti-β-actin (Horse Radish Peroxidase (HRP) Conjugated)
- Anti-Bax (produced in mouse)
- Anti-Rabbit-HRP-Conjugated (Sigma Aldrich, USA)
- Anti-Mouse-HRP-Conjugated (Sigma Aldrich, USA)
- Cassettes for dark room
- X-Ray films
- ECL Reagent (BioRad, Germany)

3.7.3. Method Of Protein Isolation And SDS-PAGE

RIPA modified lysis buffer was used for homogenizing the cellular pellets and isolation of protein from different cell lines used for this study. The protein lysates obtained were then separated and western blotting was performed to illustrate the differences in levels of individual proteins in different samples included in the experiments of the study. The method started when the cells were harvested first by washing away the cell culture media from the cell culture dishes and PBS was used for washing the cells. The cells can be scraped directly within the media or PBS with the help of a sterile cell scraper or trypsinization. The cells were pelleted in an Eppendorf tube after washing with PBS. The RIPA modified buffer was added to the cell pellet according to the size of the pellet. The optimized volume of RIPA modified buffer required to get suitable concentration and purity of protein lysate was 5 to 10 times the volume of the pellet. 100-200 µl of RIPA modified buffer added to the pellet was then pipetted up and down rigorously to homogenize the cell pellet. The freshly prepared RIPA modified buffer contained the various protease and phosphatase inhibitors. The cells were then placed on ice for 45 minutes with subsequent pipetting after every 15 minutes during the course of incubation on ice. The lysates were further homogenized using a sonicator with 25 % power and 50 cycles for 20 seconds at room temperature. The protein lysate was then collected by centrifugation at

12000g at 4°C for 10 minutes and collecting the supernatant in another Eppendorf tube. The protein lysates can be stored at -80 °C for a month.

The downstream applications of the protein lysates collected from different experiments involve equal amounts and concentrations of lysates to be used, therefore, protein lysates were quantified using the BCA protein quantification kit (Sigma, USA). The protocol for protein concentration measurement requires the preparation of a BCA working reagent which was made by mixing 75 µl of solution A and 75 µl of solution B with the 3 µl of solution C for each sample. The protein lysate from each sample was taken at 1 µl volume and added to 149 µl RIPA modified buffer and 150 µl of BCA reagent mixture. The black sample was prepared with the 150 µl RIPA modified buffer and 150 µl BCA reagent mixture without adding protein lysate. The samples were prepared in Eppendorf tubes and incubated at 60°C for 1 hour on either a heat block or water bath. After incubation, the samples were taken out from the heat and placed at room temperature for 3 minutes and subsequent absorbance at 562 nm was measured using UV/Vis spectrophotometer. The protein concentration was then measured based on the function of absorbance reading as:

Protein concentration (µg/µl)= (Absorbance (562)/0.014) X 150 / 1000

To separate the proteins using the SDS PAGE method, the BioRad apparatus for SDS gel casting was used. The two pieces of glass with appropriate width (1 or 1.5 mm) were first cleaned using deionized water, ethanol, and isopropanol sequentially. The gel pore size is dependent on the concentration of acrylamide in the gel mixture, and for this study 12 % SDS separating gels were prepared. First a 10 ml separating gel was prepared and poured within the mounted gel casting apparatus followed by stacking gel. 10 ml of separating gel was prepared by mixing 2.5 ml 4X separating gel buffer with 4 ml acrylamide mixture (29:1 acrylamide: bisacrylamide), 3.4 ml deionized water, 150 µl Ammonium persulphate (APS) solution (1 %), and 5 µl TEMED. The separating gel was poured directly immediately after mixing all the ingredients of the separating gel in a falcon tube into the gel casting apparatus. After pouring the separating gel, 1 ml isopropanol was added on top of the gel solution to remove any bubbles formed in the gel solution. The gel was left for polymerization for 15-20 minutes at room temperature. The isopropanol was removed by tilting the gel casting apparatus. After the separating gel was cast, the stacking gel solution was

prepared in falcon tubes. 2.5 ml stacking gel solution was prepared by mixing 625 µl 4X stacking gel solution, 425 µl acrylamide solution (29:1 acrylamide: bisacrylamide), 1.425 ml deionized water, 38 µl APS (1 %), and 5 µl TEMED. The stacking gel solution was poured directly after mixing the ingredients onto the separating gel cast before. The gel casting combs of the appropriate number and sizes of the wells were then placed on top of the stacking gel solution poured before, and the apparatus was left at room temperature for 10 minutes for the formation of stacking gel.

When the aforementioned gels were being prepared, the protein lysates can be prepared for running on electrophoresis. The loading buffer was prepared by mixing the 4X laemli buffer with β-mercaptoethanol (10 % final concentration). 50 µg of protein lysates were brought to equal concentration by adding appropriate volumes of deionized water. The loading buffer was added to the protein samples at 1:4 and incubated at 95°C for 5 minutes for denaturation of the proteins. The lysates were then centrifuged briefly to collect the boiled samples from the walls of the Eppendorf tubes. The lysates were then placed on ice for at least 2 minutes prior to loading on the wells of the gel. The gel was then run for electrophoresis at 80-90 V until the front of the loading dye reaches the gel of the gel in a vertical running system for 3-4 hours at room temperature.

3.7.4. Method For Western Blotting

The protein transfer from gel to membrane was then conducted using a sandwich apparatus containing sponge, Whatman filter paper, gel, PVDF membrane, then again, a Whatman filter paper, and a sponge, in this order to tightly mount the sandwich apparatus for protein transfer. The Whatman filter papers were soaked in transfer buffer, and PVDF membrane cut to the approximate size of separating gel was soaked in methanol prior to making sandwich. The apparatus was then placed in a tank for transfer that was filled with transfer buffer and electric current was then supplied for overnight protein transfer from negative electrode to positive electrode (from gel to membrane) driven by transfer buffer at 4°C at 90 mA. The PVDF membrane was soaked in methanol before being placed in the apparatus.

After protein transfer, the membrane was taken out from the sandwich apparatus and immediately placed in a 5% milk solution in TBST (12 ml) for

blocking at room temperature on a shaking platform. After blocking the membrane, primary antibody solution prepared in 0.5% milk in TBST was added to the membrane followed by removing the blocking solution, and the membrane was incubated with primary antibody for 1 hour at room temperature (or overnight at 4 °C) on a shaking platform. The primary antibody solution (1:500 to 1:1000 final dilution) (12 ml) was removed and stored at -20 °C in falcon tube, and membrane was washing with TBST sequentially first for 15 minutes, followed by 3 times for 5 minutes at room temperature on a shaking platform. After washing the membrane to remove unbound primary antibody, the membrane was incubated with secondary antibody-conjugated with HRP solution (1:5000 to 1:20000 final dilution) prepared in 0.5 % milk in TBST (12 ml) for 1 hour at room temperature. After incubation, the membrane was washed with TBST sequentially first for 15 minutes, followed by 3 times for 5 minutes at room temperature on a shaking platform. After that, the ECL solution (Bio-Rad) was prepared from mixing solution A and solution B in equal amounts (total 1 ml) and poured onto membrane and membrane was placed in dark for 5 minutes. The excess ECL solution was removed using tissue paper gently. The membrane was placed between two acetate paper sheets, which was then placed in a cassette and dark room was closed. The red bulb in the corner of the room was turned on for sufficient light to observe the membrane and X-ray films in the dark. The X-ray film was taken out from the box and exposed to the acetate sheets containing the membrane and the chemiluminescent bands appearing on the membrane for different time periods. The exposed films were then developed using standard developer and fixer solution, where film was first placed in developer solution for two minutes with gentle shaking of the solution tray, followed by putting the film in fixer solution for at least two minutes. The films were then air dried and photographed for further analysis.

3.8. Immunofluorescence Microscopy

3.8.1. Materials

- Coverslips
- Cell culture dishes 3 cm^2 or 6-well plates
- Cell lines
- Cell Culture media

- Forceps
- Tissue papers
- Triton-X100
- Phosphate Buffered Saline (PBS)
- Methanol
- BSA (Thermofischer, USA)
- Ethanol
- Paraformaldehyde (Sigma, Germany)
- 0.25 μg/ml DAPI: 4,6-diamidino-2-phenylindole DAPI dilactate (Sigma- D9564, Germany) + % 30 glycerol (Sigma, Germany) + 70 % PBS solution
- Nocodazole (Sigma, Germany)
- Aphidicolin (Sigma, Germany)
- Control or siHN1 RNA (Santacruz Biotechnology)
- FUGENE HD (Promega, USA)
- Leica Immunofluorescence Microscope

3.8.2. Antibodies For Immunofluorescence

- Anti-Gamma Tubulin (produced in mouse) (sc-17787, Santacruz Biotechnology, USA)
- Anti-Gamma Tubulin (produced in goat) (sc-7396, Santacruz Biotechnology, USA)
- Anti-HN1 (produced in rabbit) (Cat #PA5-21779, Invitrogen, USA)
- Anti-beta Tubulin (produced in mouse) (Invitrogen, USA)
- Anti-CP110 (produced in mouse) (Santacruz Biotechnology, USA)
- Anti-Cyclin F (produced in mouse) (Santacruz Biotechnology, USA)
- Anti-Geminin (produced in mouse) (Invitrogen, USA)

3.8.3. Method

The coverslips placed in 70 % ethanol solution were taken out in the culture cabin and put on tissue paper and air-dried for 20-30 minutes prior to placing in wells of 6-well cell culture plates or 3 cm2 cell culture dishes. The cell culture media (2-3 ml) was then added on top of the coverslips in culture dishes prior to seeding counted cells after the cell passaging method of adherent cell cultures. The cells on coverslips were incubated for 24 priors at 37°C in a humidified cell culture incubator containing 5 % CO_2. The cells were then treated with the

experimental setup designed for immunofluorescence microscopy including DNA or siRNA transfections, chemical inhibitors including Aphidicolin, and Nocodazole among others accordingly for the appropriate time.

After completion of the experiment, the culture media was removed and replaced with PBS, which was also removed and cells were fixed with either ice-cold 1 ml 100 % methanol for a half-hour at -20°C or with 1 ml 4 % paraformaldehyde (in PBS) at room temperature for half-hour. After fixation, cells were washed with 1 ml PBS and treated with 0.2 % Triton X-100 (in PBS) for 5 minutes on a shaker at room temperature for cellular permeabilization. Cells were then washed with 1 ml PBS and blocked with 1 ml BSA (1 %) solution prepared in PBS and placed on a shaking platform for 5 minutes at room temperature. After blocking, 50 µl primary antibodies prepared in 1 ml BSA solution (1 % in PBS) were added to the coverslips, which were then covered with parafilm and incubated at 37°C for 1 hour. After incubation, the coverslips in culture dishes were washed with 1 ml PBS 4 times.

The secondary antibody solution (50 µl) prepared in 1 % BSA was added to coverslips, which were then covered with parafilm and incubated at 37°C for 20 minutes. After incubation, the coverslips were washed with 1 ml PBS 4 times to remove any unbound antibodies. The coverslips were then subjected to 1 ml 70 % ethanol (ice cold) solution and kept at room temperature for 1 minute. The 70 % ethanol solution was removed and 100 % ethanol solution (ice cold) was then added to the coverslips and kept at room temperature for at least one minute.

Coverslips were then removed from the culture dishes and placed on dry tissue papers for 10 minutes to dry off the ethanol. After drying, 10 µl DAPI solution (0.5 µg/ml) was dropped on the middle of the coverslips (on the side containing fixed cells) and placed on top of the microscope slide by inverting the DAPI containing side of the coverslip to spread the DAPI solution equally on the coverslips and glass slide to mount the cells on the microscope slide. The samples were then analyzed using Leica upright immunofluorescence microscope.

3.9. Lentivirus Production

3.9.1. Materials

- HEK293T cells
- Cell Culture Dishes
- Cell Culture Media
- Transporter™ 5 Transfection Reagent (PEI) (Polysciences, USA)
- Chloroquine Diphosphate (Sigma, Germany)
- Transfer plasmids: pCW57 (Vector), pCW57-HMHN1, pCW57-HN1-mVenus, pBOB-Fast-FUCCI
- 3rd generation lentiviral packaging plasmids: pMD2.G (Plasmid #12259), pMDLg/pRRE (Plasmid #12251), pRSV-Rev (Plasmid #12253) (Addgene)
- Membrane syringe filters (0.4 µm) (PES filters)
- Syringe injector
- Mini-centrifuge (Eppendorf, Germany)

3.9.2. Method

HEK293T cells were grown in DMEM F-12 media supplied with 5 % FBS and 1 % L-glutamine without adding antibiotics and 3 X 10^6 cells were seeded on 10 cm^2 cell culture dishes and maintained in standard cell culture conditions for 24 hours. Cell culture media was changed, and new media containing 25 µM chloroquine diphosphate was added to the cells 5 hours before transfection. The transfer plasmid (1.64 pmol), pMD2.G (0.72 pmol), pRS-Rev (1.3 pmol), and pMDLg/pRRE (1.3 pmol) were transfected in PEI as transfection reagent as 1:3 (DNA(µg): PEI(µl)). The DNA and PEI were separately diluted in 500 µl DMEM F-12 media and incubated at room temperature for 5 minutes, followed by adding PEI solution dropwise to DNA dilution. The mixture was incubated for 15-20 minutes at room temperature for the formation of DNA and transfection reagent complexes. The complexes were added to cells in a culture dish dropwise and carefully using a pipette tip. The transfected cells were incubated further in cell culture conditions for 18 hours, followed by a media change. 48-hour post-transfection, the cell culture media was taken using a sterile pipette and centrifuged at 4°C for 5 minutes. The supernatant was filtered through a 0.4 µm PES filter and distributed to Eppendorf tubes and centrifuged at 16000g for 18 hours at 4°C. The supernatant was removed and 100 µl PBS was added to the

pellet. The viral particles in the pellet were kept at 4°C for 24 hours for re-suspension and stored at -80°C prior to transduction. The fresh media was added to the cells for further collection of viruses for the second batch at 96-hours post-transfection.

3.10. Stable Cell Line Generation

3.10.1. Materials

- Polybrene (Sigma, Germany)
- Cell lines
- Cell Culture media
- Lentiviral particles
- Puromycin (Sigma, Germany)
- Cell culture dishes
- Sterile Pipettes
- Inverted Microscope (Leica, Germany)

3.10.2. Method

The PC-3 and LNCaP cells were grown in appropriate cell culture conditions and prior to transduction with lentiviral particles. The 6 cm^2 culture dishes were poured with appropriate media for cell type without antibiotics. Polybrene (10 μg/ml) was added to the media along with 100 μl of lentiviral particles, and cells were seeded in 6 cm^2 cell culture dishes at 2 X 10^5 density. After culturing the cells for 48 hours in viruses and Polybrene, the media was removed and cells were grown in normal culture media for 24 hours prior to antibiotic selection. 2 μg/ml Puromycin containing culture media was added to the cells. Cells were maintained at this concentration of Puromycin until all cells in the control group were killed in the presence of Puromycin. After Puromycin selection, the cells were propagated in normal culture media for further experimentation. The monoclonal populations of FUCCI-PC3 cells were obtained by seeding Puromycin-selected ½ cell per well of the 96-well culture plate and propagated for 2 weeks. The inverted fluorescence microscope was used to observe the positive single monoclonal population in a well.

3.11. Cell Cycle Synchronization Approaches

Centrosome Duplication Assay

PC-3 cells transfected with either control or HN1 specific siRNA or PC3-pCW57-HMHN1 cells were further treated with Aphidicolin (1.6 μg/ml) for 48 hours to stop the DNA replication while continuing centrosome duplication. The cells on cover slides were fixed in 100 % methanol and processed further for immunofluorescence microscopy.

Metaphase Cells For Immunofluorescence

DU-145 cells treated with either control or HN1 specific siRNA were further treated with Nocodazole (165 nM) for 18 hours and released into metaphase by removing Nocodazole containing media and replacing it with fresh media for 1 hour. Cells on covers slides were fixed with 100 % methanol and processed for immunofluorescence.

G1 Phase Synchronization

LNCaP, PC-3, and 104R2 cells were grown in normal cell culture and media prior to seeding for cell cycle synchronization. During the course of the experiment, cells were starved from serum and maintained in serum-free media for 48 hours, to enrich the cellular populations in G1, followed by processing for western blotting and flow cytometry.

S Phase Synchronization

LNCaP, PC-3, 104R2, and FUCCI-PC3 cells along with FUCCI-PC3 clones were synchronized at S-phase using double Thymidine blockage. Cells were treated with 2 mM Thymidine (Sigma, Germany) for 18 hours, followed by a release into fresh media after replacing old media, for 6-8 hours. After that, Thymidine (2 mM) containing media was added for another 18 hours to synchronize cells in the G1/S transition, and cells were released into the S phase for either 4 or 6-hour release from the double Thymidine block and processed for western blotting and flow cytometry. Furthermore, FUCCI-PC3 cells were synchronized in S-phase using Aphidicolin blockage as well.

G2 Phase Synchronization

LNCaP, PC-3, 104R2, and FUCCI-PC3 cells along with FUCCI-PC3 clones were treated with Nocodazole (165 nM) for 18 hours to synchronize the cells in the G2 phase by blocking the polymerization of microtubules. The cells were processed for either live or fixed cell flow cytometry or western blotting.

Mitotic Shake Off

LNCaP, PC-3, and 104R2 were synchronized at mitosis for western blotting by using the mitotic shake-off method. Cells were first synchronized at the G2 phase using Nocodazole block followed by release into mitosis for 1 hour. The mitotic cells were collected from the media after tapping the culture dishes gently. The procedure was repeated every 15 minutes four times to collect the cells. The collected cells in media were centrifuged and processed for western blotting or flow cytometry.

3.12. Apoptosis Assay And Live Cell Flow Cytometry

3.12.1. Materials

- Cell lines
- Cell Culture Dishes
- Cell Culture Media
- Falcon tubes
- Eppendorf tubes
- BD5 Acuri Flow Cytometer
- AG556 (Sigma Aldrich, Germany)
- Cytochalasin D3 (Sigma Aldrich, Germany)
- Sirtinol (Sigma Aldrich, Germany)
- Cyclohexamide (Sigma Aldrich, Germany)
- Actinomycin D (Sigma Aldrich, Germany)
- LYP294 (Sigma Aldrich, Germany)
- Trichostatin A (Sigma Aldrich, Germany)
- Flavopiridol (Sigma Aldrich, Germany)
- Etoposide (Sigma Aldrich, Germany)
- Camptothecin (Sigma Aldrich, Germany)
- Doxorubicin (Sigma Aldrich, Germany)
- FITC Annexin V (component no. 51-65874X, BD Biosciences)
- Propidium Iodide (PI) (component no. 51-66211E, BD Biosciences)
- Annexin V Binding Buffer (component no. 51-66121E, BD Biosciences)
- Ethanol
- PBS
- Doxycycline (Sigma, Germany)

3.12.2. Method

The PC3-pCW57-HMHN1 (either treated with Doxycycline or control untreated) cells treated with apoptosis-inducing chemical inhibitors were subjected to PI and Annexin V staining for measuring the rate of apoptosis and necrosis. The cells after completion of the experiment were washed with PBS and re-suspended in Binding buffer (diluted to 1X using deionized water). 1 X 10^6 cells were added to 1 ml of binding buffer. 100 µl cells were transferred to an Eppendorf tube where 2 µl FITC Annexin V solution was added along with 2 µl of the PI solution prior to vortexing and incubation for 15 minutes at room temperature in dark. The 4X (400 µl) binding buffer was added to cells and analyzed using flow cytometry. The appropriate unstained, only Annexin V and only PI stained cells were used as a control for gating the populations in flow cytometry.

FUCCI-PC3 cells either synchronized at different phases of the cell cycle or transfected with plasmid DNA (HM-Vec or HM-HN1) were subjected to live cell flow cytometry. Briefly, cells were trypsinized and washed with PBS and re-suspended in PBS prior to direct reading on flow cytometry.

3.13. Cell Migration And Invasion Assay

3.13.1. Materials

- Boyden Chamber (Merck Millipore, UK)
- Doxycycline (Sigma, Germany)
- Hemacytometer (Neubauer 0101050, Germany)
- Sterile pipette tip (200 µl)
- Cell lines
- Cell Culture media with 2 % FBS
- Cell Culture media with 10 % FBS
- Inverted microscope (Leica, Germany)

3.13.2. Method

The cell invasion assay was performed after growing the cells in Boyden Chamber (Merck Millipore, UK) with inserts containing lower serum levels (upper chamber) and lower chamber with higher serum levels to observe invaded cells from the chambers. The cells were plated in 2% FBS DMEM F/12 media on

the upper chamber (insert) with the lower chamber containing media with 10% FBS so that cells are incentivized for invasion through the porous membrane in the upper chamber. The procedure of the assay described by Guy et al in 2017 was utilized for Doxycycline-treated PC-3, PC3-pCW57, PC3-pCW57-HMHN1, and PC3-pCW57-Venus, and PC3-pCW57-HN1-Venus. The cells in the lower chamber that invaded through the upper chamber were photographed after 2 and 5 days after Doxycycline treatment. To determine the difference in the number of viable invaded cells, cells were counted by hemacytometer after cell harvesting from the lower chamber.

For the wound healing assay, the cells were plated in 6-well plates and allowed to reach confluency prior to generating a scratch (wound) by a sterile 200 µl pipette tip, followed by washing the cells in warm media and photographed from a specified marked position on the well. After generating the wound, cells were treated with Doxycycline and grown at normal cell culture conditions. The cells were then photographed at various time points to determine any wound healing effect through *HN1* expression.

4. RESULTS

4.1. *In Silico* Analysis On HN1

4.1.1. HN1 Is A Putative Disordered Protein

The structure of a protein is important in determining the function as it informs the basic domains required for forming the three-dimensional aspect of the protein. There are many different methods and tools available, which can be used to predict the structure of a protein-based on its amino acid sequence. In our study, we aim to characterize HN1 therefore HN1 protein sequence (154 amino acids) was used to predict its three-dimensional structure using different approaches such as iterative threading, comparative modeling, and *ab-initio* protein structure prediction. These methods when applied to the amino acid sequence of HN1 provide different conformations of HN1 without proper three-dimensional structure as shown in figure 4.1A. The iterative threading method using I-TASSER database and comparative modeling using the ROBETTA server, reveal two beta-sheets in the structure of HN1, while *ab initio* method applied by using the QUARK server shows that HN1 has two small alpha helices in its secondary structure. However, the overall protein domains are missing when the HN1 structure is predicted by *in silico* approaches.

The proteins with no known three-dimensional structure and functional domains are disordered proteins with flexible coiled-coil dynamics in their composition. After determining that HN1 lacks a clear three-dimensional domain, the amino acid sequence of HN1 was compared with a known disordered protein labeled as Disprot 3.4 in figure 4.1B. HN1 exhibits a similar pattern to Disprot 3.4 in terms of enrichment of the disorder-promoting residues. The amino acids with a similar pattern for a reduced abundance in HN1 and Disprot 3.4 are W, C, F, I, Y, V, L, H, M, and T. Meanwhile, the amino acids that promote the disordered conformation in Disprot 3.4 and are present in HN1 are G, P, and E.

Predictor of Natural Disordered Regions (PONDR) is a tool that predicts the disordered regions in a protein-based on the presence of certain amino acids. After showing a resemblance of the HN1 sequence with a known disordered protein, we calculated the PONDR score for HN1 using the PONDR database. A score of 0.5 and more implicates a presence of a predicted disordered region within a protein as shown in figure 4.1C. There are four disordered regions

predicted for HN1 and the largest region span the amino acid sequence range from 65th to 150th residue (86 amino acids) in the C-terminus with an average strength of prediction of 0.81 (figure 4.1E). The PONDR database also generates a graph of absolute mean net charge and mean scaled hydropathy, which is searched for HN1 and it is observed that HN1 sits right before the junction of disordered to order junction (figure 4.1D). The mathematical calculation of mean hydrophobicity and mean net charge can also help in the prediction of disorder in a protein and these values represent that HN1 is a potential disordered protein (figure 4.1E).

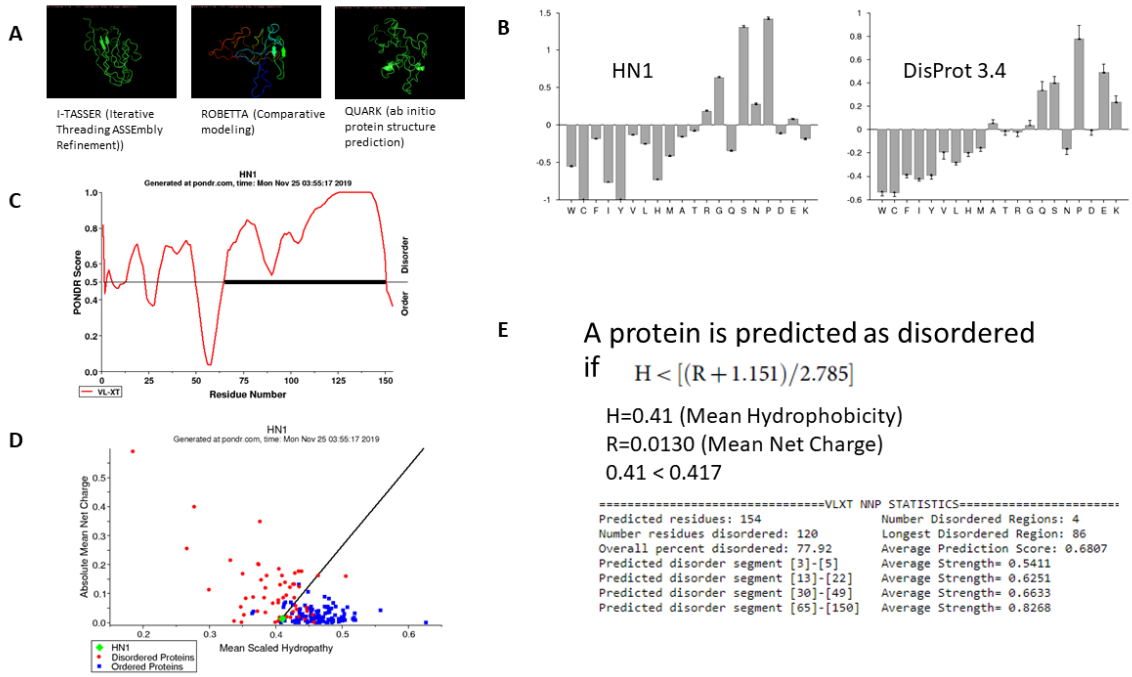

Figure 4.1: *In silico* approaches predict HN1 as a disordered protein (A) I-TASSER, ROBETTA, and QUARK methods show different HN1 protein structures as visualized in PyMol software. There are no prominent template sequences obtained in homology modeling and the tertiary structures constructed have no functionally relevant domains. (B) The enrichment of different amino acids in HN1 protein was compared with a known reference disordered protein (Disprot 3.4). Disorder-promoting amino acids are enriched in the HN1 protein sequence. (C) The PONDR plot shows the disordered regions in the HN1 protein sequence. The central and C-terminal region of HN1 is considered completely a disordered region according to the PONDR plot, with N-terminus also exhibiting disordered-ness. (D) Another measure of disorder-ness absolute mean net charge was measured for HN1 and plotted against the known disordered protein. HN1 lies at the boundary of ordered and disordered proteins and leans towards disordered proteins. (E) The mean hydrophobicity and mean net charge measures determine the disordered-ness of a protein and these measures for HN1 were measured and represented mathematically to determine that HN1 is a potential disordered protein.

4.1.2. *HN1* Co-Expression Network Identifies Its Potential Role In Cell Cycle And Centrosome Related Pathways

CoExpedia database when searched for *HN1* revealed 479 *HN1* co-expressed genes with significant log-likelihood score (LLS) extracted from Gene Expression Omnibus (GEO) database. 42 out of 479 genes are located on chromosome 17q in the human genome indicating the genetic linkage is involved in the co-expression mechanism. The co-expression network of *HN1* identified from GEO studies portrays a general network, which was further analyzed for enrichment analysis using Gene Ontology (GO) database in Funrich v3.13 software for CC, BP, and MF terms as described in figure 4.2A. Figure 4.2A1 shows enriched GO cellular component CC terms for *HN1* co-expression network as centrosome, midbody spindle, condensed chromosome, and kinetochore among others. The generic terms such as nucleus, nucleoplasm, and cytosol were removed from the analysis. Figure 4.2A2 illustrates the molecular function (MF) terms of the *HN1* co-expression network such as microtubule motor activity, single-stranded DNA binding, ATP-binding, microtubule-binding, and ATPase activity, kinase, RNA, and protein binding. For biological process (BP) analysis, the most significantly enriched terms include mitotic spindle organization, chromosome segregation, cell proliferation, DNA replication, mitotic sister chromatid segregation, APC/C dependent proteasomal degradation, and mitotic cell cycle, and cell division (figure 4.2A3).

To understand the function of HN1 specifically in Prostate cancer, the PRAD dataset from the TCGA database included in the GEPIA server was analyzed for *HN1*. 176 genes were observed as HN1 similar or co-expressed genes and used for defining the GO terms for CC, MF, and BP as described previously. The CC terms associated with the *HN1* co-expression network in Prostate cancer include microtubule, centrosome, spindle pole, centromere, and kinetochore (figure 4.2B1). The MF terms are Anaphase promoting complex binding, protein kinase binding, chromatin binding, ATPase activity, microtubule motor activity, ATP binding, and microtubule binding (4.2B2). The BP terms associated with the *HN1* co-expression network in the PRAD dataset include microtubule-based movement, mitotic metaphase plate congression, APC/C dependent proteasome degradation, mitotic spindle organization, cytokinesis, mitotic sister chromatid segregation, chromosome segregation, DNA replication,

mitotic cell cycle, and cell division (figure 4.2B3).

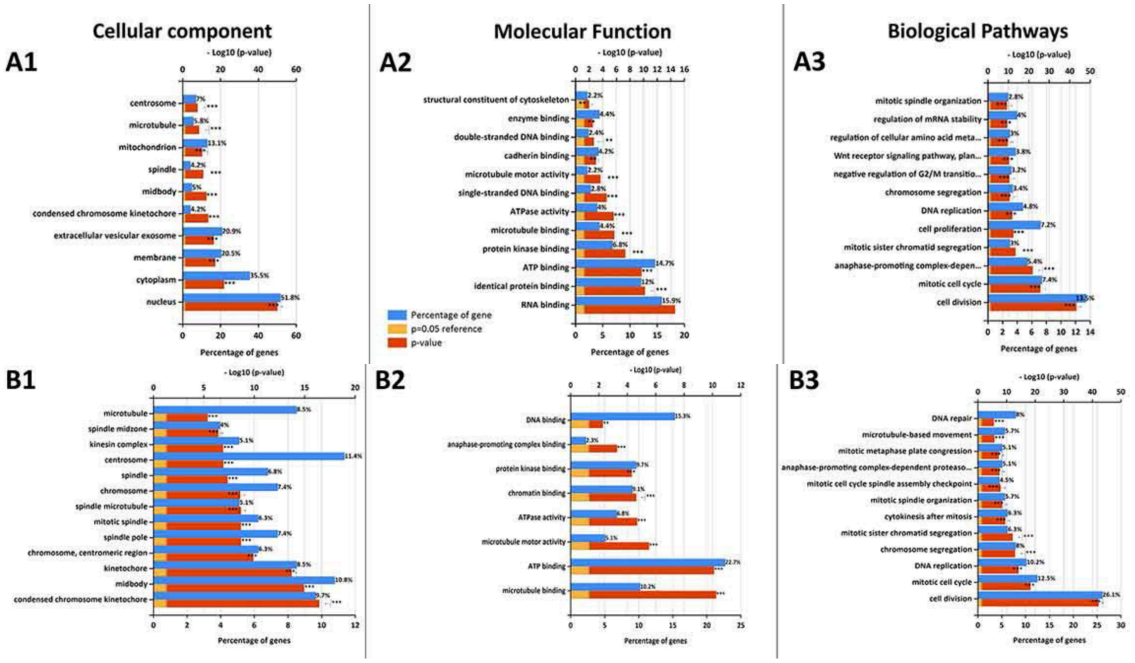

Figure 4.2: Enrichment of *HN1* co-expression network in CoExpedia database and PRAD dataset: (A) *HN1* co-expressed genes from CoExpedia uploaded to Funrich software provided significantly enriched GO terms for CC (A1), MF (A2) and BP (A3). The graphs were constructed from Bonferroni corrected *p-value* with cut of –log10 (*p-value*) as 7 and gene percetage as 4 for CC (excluded terms=nucleus, nucleoplasm, cytosol). The MF analysis resulted from Bonferroni corrected *p-value* with cut of –log10 (*p-value*) and gene percentage as 2 (excluded term=protein binding). The BP analysis resulted from Bonerroni corrected *p-value* with top 12 entries. (B) *HN1* co-expressed genes from PRAD dataset obtained from GEPIA database uploaded to Funrich software provided significantly enriched GO terms for CC (B1), MF (B2) and BP (B3). The graphs were constructed from Bonerroni corrected *p-value* with cut of –log10 (*p-value*) as 6 and gene percentage as 4 for CC (excluded terms=nucleus, nucleoplasm, cytosol). The MF analysis resulted from Bonferroni corrected *p-value* with cut of –log10 (*p-value*) and gene percentage as 2 (excluded term=protein binding). The BP analysis resulted from Bonferroni corrected *p-value* with top 12 entries.

The co-expression network in the context of Prostate cancer was further extracted for enriched pathways and it was observed that centrosomal, cell cycle-related, and kinesin family genes were the most significant. Important centrosomal genes associated within the network are mentioned in the table 4.1. The significant centrosomal genes in *HN1* co-expression network in PRAD include *AURA, AURB, PLK1, BUB1, NEK2, and STMN1,* which function collectively in centrosome duplication, maturation and separation. Moreover, cell cycle pathway genes associated with *HN1* is Prostate cancer are detailed in table

4.2. The prominent cell cycle genes in *HN1* co-expression network in PRAD include *CDC20, CDC25C, CCNB1, CDT1, ORC1, CCNA2, and CDC7,* which collectively function in regulating G2/M, M/G1, and G1/S transition. Furthermore, the enriched kinesin family members in *HN1* co-expression network in PRAD include *KIF4A, KIF2C, KIFC1, and KIF14* among others, as mentioned in table 4.3.

Gene ID	**Description**	**Function**	**PCC**
TROAP	Tastin	During mitosis, regulates centrosome integrity and bipolar spindle assembly	0.67
SPAG5	Sperm-associated antigen 5	Organization of spindle apparatus and segregation of chromosomes	0.67
BIRC5	Survivin	Microtubule nucleation and dynamics	0.66
PLK1	Polo-like kinase 1	Phosphorylates proteins on centrosomes, kinetochores, spindle, and midbody	0.66
TPX2	Microtubule Nucleation Factor	Microtubule organization, centrosome separation and maturation	0.66
AURKB	Aurora kinase B	Chromosomal segregation	0.65
AURKA	Aurora Kinase A	Centrosome separation and maturation	0.65
POC1A	Centriolar protein A	Spindle organization and Centrosome localization	0.65
OIP5	Opa Interacting Protein 5	Recruitment of CENP-A and Centrosome localization	0.65
E2F1	E2F Transcription Factor 1	Centrosome integrity	0.65
AUNIP	Aurora Kinase A And Ninein Interacting Protein	Mitotic entry and bipolar spindle assembly	0.63
BUB1	BUB1 Mitotic Checkpoint Serine/Threonine Kinase	Mitotic and spindle checkpoint	0.63
ASPM	Assembly Factor For Spindle Microtubules	Mitotic spindle regulation	0.62
PRC1	Protein Regulator Of Cytokinesis 1	Mitotic spindle midzone maintenance	0.61
TACC3	Transforming Acidic Coiled-Coil Containing Protein 3	Centrosome and Nucleus coupling by microtubules	0.6
SGO1	Shugoshin 1	Cohesion of centrioles	0.56
NEK2	Serine/Threonine-Protein Kinase Nek2	Phosphorylating centrosomal proteins and Centrosome separation	0.56
STMN1	Stathmin 1	Microtubule destabilization	0.54

Table 4.1: TCGA PRAD dataset contains *HN1* co-expressed centrosomal genes with PCC association greater than 0.5 ($p < 0.05$ *).

Gene ID	Description	Function	PCC
CDC20	Cell Division Cycle 20	Spindle assembly checkpoint (SAC)	0.65
CDKN3	Cyclin Dependent Kinase Inhibitor 3	Centrosome number maintenance	0.63
CDCA2	Cell Division Cycle Associated 2	Chromosome structure and mitotic regulation	0.62
CDC25C	Cell Division Cycle 25 C	Dephosphorylating CDK1 and triggering entry into mitosis	0.62
CDCA8	Cell Division Cycle Associated 8	Microtubule stabilization via chromatin	0.62
CDCA3	Cell Division Cycle Associated 3	Degradation of WEE1 kinase at G2/M	0.61
CBX2	Cell Division Cycle Associated 6	Polycomb multiprotein complex	0.6
Cdca5	Cell Division Cycle Associated 5, soronin	Centrosomal declustering and sister chromatid cohesion	0.59
CCNB1	G2/Mitotic-Specific Cyclin-B1	Spindle checkpoint assembly and G2/M transition	0.59
CDT1	Chromatin Licensing And DNA Replication Factor 1	DNA replication via pre-replication complex	0.55
ORC1	Origin Recognition Complex Subunit 1	DNA replication initiation	0.55
CDKN2D	Cyclin Dependent Kinase Inhibitor 2D	CDK kinase inhibition	0.54
Cdc45	Cell Division Cycle 45	DNA replication initiation	0.53
CCNA2	Cyclin A2	G1/S and G2/M transition	0.53
Cdc7	Cell division cycle 7	Origin firing	0.51

Table 4.2: TCGA PRAD dataset contains *HN1* co-expressed cell cycle genes with PCC association greater than 0.5 ($p < 0.05$ *).

Gene ID	Description	Function	PCC
KIF4A	Kinesin Family Member 4A	Microtubule organization	0.7
KIF2C	Kinesin Family Member 2A	Depolymerizes of the microtubules	0.67
KIF20A	Kinesin Family Member 20A	Chromosome passenger complex (CPC)-mediated cytokinesis	0.66
KIF18B	Kinesin Family Member 18B	Destabilization of the astral MTs	0.61
KIFC1	Kinesin Family Member C1	Centrosome clustering	0.61
KIF23	Kinesin Family Member 23	Transport of organelles and chromosomes	0.58
KIF14	Kinesin Family Member 14	Chromosome segregation, mitotic spindle formation, and cytokinesis	0.58
KIF18A	Kinesin Family Member 18A	Chromosome congression and suppression of chromosome movements	0.53

Table 4.3: TCGA PRAD dataset contains *HN1* co-expressed kinesin family genes with PCC association greater than 0.5 ($p < 0.05$ *).

4.1.3. STRING Interaction Network For *HN1* Co-Expressed Genes In PRAD

HN1 co-expressed genes were downloaded from TCGA PRAD dataset. The co-expression network of HN1 in the context of Prostate Cancer can provide an initial functional pathway for the activity of HN1 protein in Prostate cancer cells. As shown in the figure 4.3, there is a dense network of the protein-protein interaction in the middle of the map. The central core of the network consists of the cell cycle and mitotic regulators such as Cdc20 and Cyclin B1 along with Aurora and BUB kinases. The central core of mitotic regulators is connected to another cluster of proteins (upper right) that regulation and G1 and S phases of the cell cycle such as Cdt1, ORC1 and MCM10. The kinesin family members, regulate the microtubule activity, are also condensed in central core and in other parts connected within the map. Therefore, it can be assumed that HN1 resides as a functional unit in this map as a function of co-expression to play a role in cell cycle and centrosome related activities.

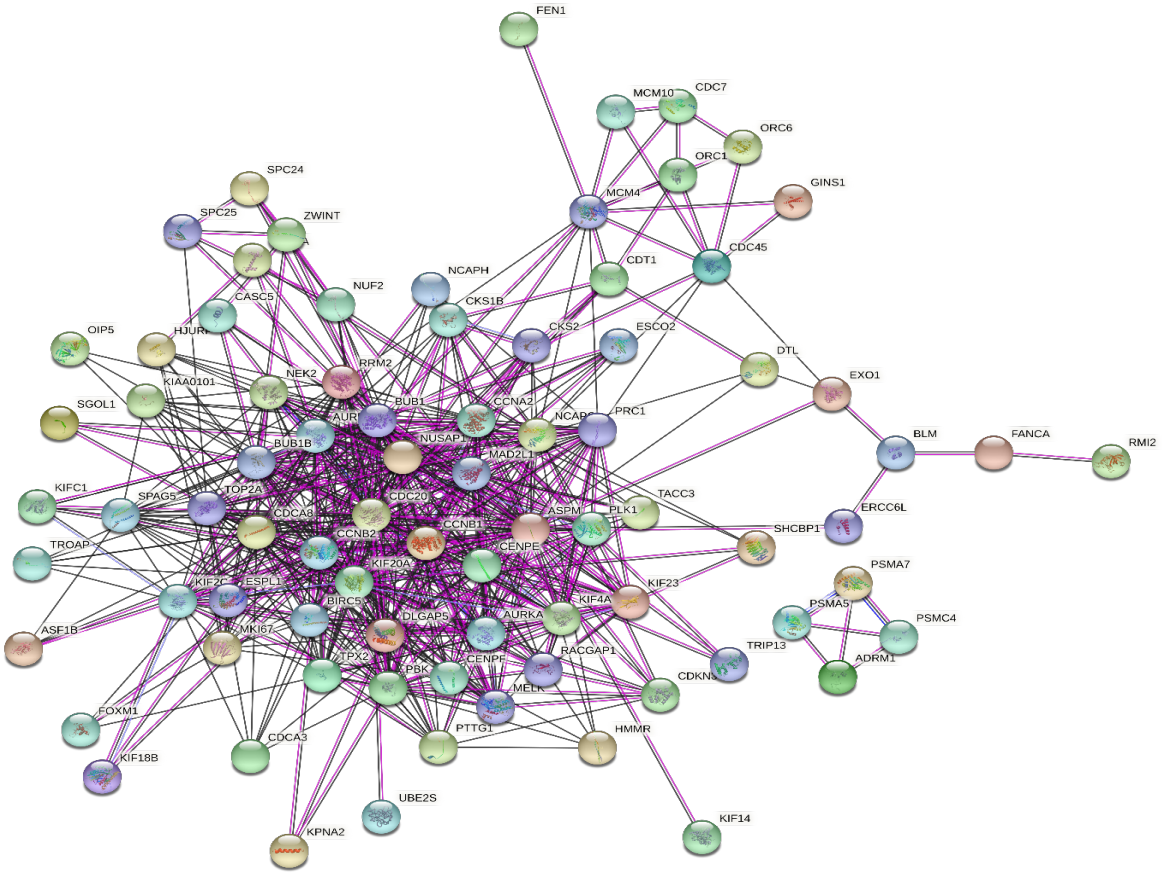

Figure 4.3: Protein-protein interaction map of *HN1* co-expressed genes in PRAD. STRING database searched for multiple proteins list was used. The gene products (proteins) of HN1 co-expressed genes (176) were added as one list of protein with a confidence score of 0.9 to get the core map of the interaction network.

4.1.4. *HN1* Is Overexpressed In Prostate Cancer

The survival analysis for prognosis of Prostate cancer based on the expression of HN1 dictates that *HN1* overexpression separates the survival time for the Prostate cancer patients in a worse manner as shown in figure 4.4A. The disease free survival plot was generated from a *p(HR)* (Hazard Ratio) significantly describing the association of *HN1* overexpression to poor prognosis. There are 5 studies available in c-Bioportal database that contain datasets with more than 100 patients of Prostate cancer and more than 1 % of the patients with amplification of *HN1* as a primary mutation for *HN1* (4.4B). This data indicates that *HN1* is amplified specifically in Prostate cancer patients, implying that HN1 functions in promoting tumorigenesis. The HN1 mRNA (transcript) levels are significantly

higher in Prostate cancer samples as compared to normal Prostate tissues as shown in figure 4.4C.

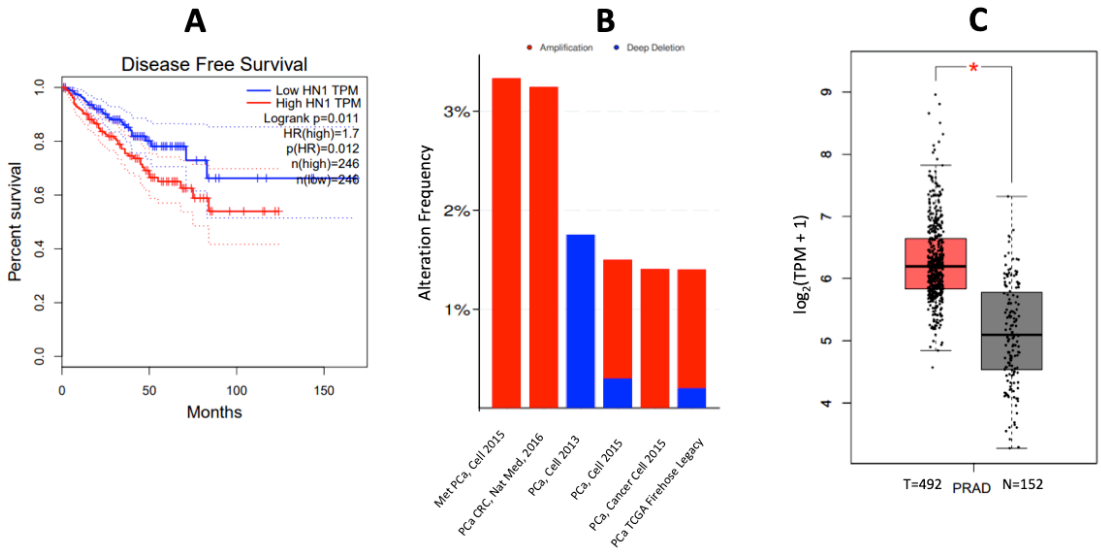

Figure 4.4: *HN1* is overexpressed in Prostate cancer. (A) HN1 overexpression (red line) decreases the survival time from the Prostate cancer as compared to low expression (blue line) of HN1. (B) The studies in c-Bioportal describing HN1 mutations (red=amplification, blue=deep deletion) based on the threshold of mutation rate of 1 % and minimum number of cases of 100. (C) HN1 transcript levels in normal (grey=N=152) and tumor samples of PRAD (red=T=492) with $\log_2$(TPM + 1) for log scale, jitter size at 0.04, *p-value* cut-off as 0.01 (*), and |Log_2FC| Cutoff as 1.

4.2. Plasmid DNA And siRNA Transfections In Prostate Cell Lines

4.2.1. Effect Of Altered HN1 Expression On Proliferation

The normal Prostate epithelial RWPE-1 cells, when depleted with HN1 after siRNA transfection resulted in no difference of viable cell count as compared to untreated and control RNA-treated cells. However, *HN1* overexpression led to a reduced rate of proliferation in these cells as shown in figure 4.5A. The Lymph node metastasized Cancer of the Prostate (LNCaP) cells is an androgen sensitive Prostate cancer cell line and show early tumorigenesis phenotype. LNCaP cells showed reduced proliferation in HN1 depleted and overexpressed cells as shown in figure 4.5B. PC-3 cells are bone metastasized androgen insensitive Prostate cancer cells and are more aggressive as compared to LNCaP cells and portray advanced phenotype of the Prostate cancer. HN1 depleted PC-3 cells by siRNA transfection showed reduced viable cell count as compared to the control cells, implying that HN1 is involved in regulating cellular growth in these cells. Moreover, HN1 overexpression by plasmid DNA transfection led to increase in

viable cell count, implicating that HN1 is involved in boosting the growth of these advanced cancer cells as shown in figure 4.5C.

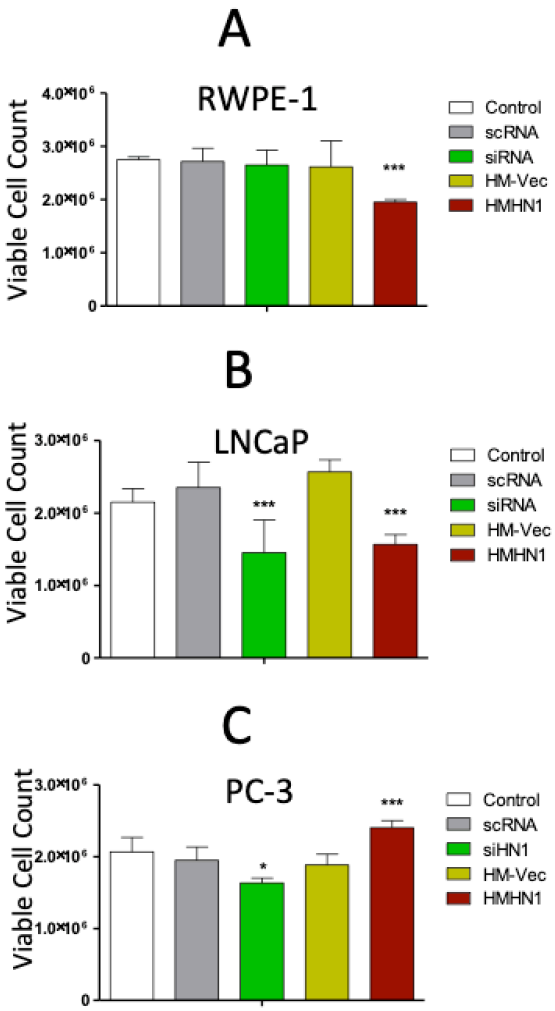

Figure 4.5: Effect of HN1 alteration on proliferation of Prostate cell lines: (A) RWPE-1 cells transfected with HM-HN1 (red) showed a decrease in number of viable cells as compared to control cells (white) (***). (B) In LNCaP cells, HN1 depletion by siRNA (green) and HN1 overexpression by HM-HN1 (red) leads to decreased number of viable cells as compared to control cells (white) (***). (C) In PC-3 cells, HN1 depletion (green) reduced viable cell count (**), while overexpression (red) increased the proliferation (*). The *p-value* less than 0.05 is indicated with * sign.

4.2.2. Effect Of Altered HN1 Expression On Cell Cycle Distribution

The PI staining on ethanol fixed cells was used for measuring the DNA content of HN1 depleted and HN1 overexpressed RWPE-1, LNCaP, and PC-3 cells to determine the cell cycle distribution. Figure 4.6 illustrates the differences among the samples analyzed for PI staining and the data obtained from flowjo v10 software. In LNCaP and PC-3 cells HN1 silencing resulted in a decrease of G1 populations from 62.5 ± 1.6 to 70.8 ± 0.5, and 45.2 ± 0.8 to 54.75 ± 0.7,

respectively. However, HN1 depletion in RWPE-1 showed no change in G1 population as compared to control cells. In PC-3 cells, polyploidy cells increased from 1.38 ± 0.2 to 6.00 ± 0.4 when HN1 was depleted. G1 populations increased in all RWPE-1, LNCaP, and PC-3 cells from 59.2 ± 0.81 to 33.605 ± 0.65, 61.3 ± 1.7 to 54.49 ± 1.02, and 44.87 ± 0.62 to 41.64 ± 0.36, respectively. On the other hand, HN1 overexpression increased S-phase cells in RWPE-1, LNCaP, and PC-3 from 21.64 ± 0.64 to 31.88 ± 0.52, 22.14 ± 0.54 to 27.27 ± 0.97, and 23.62 ± 2.37 to 35.69 ± 0.59, respectively.

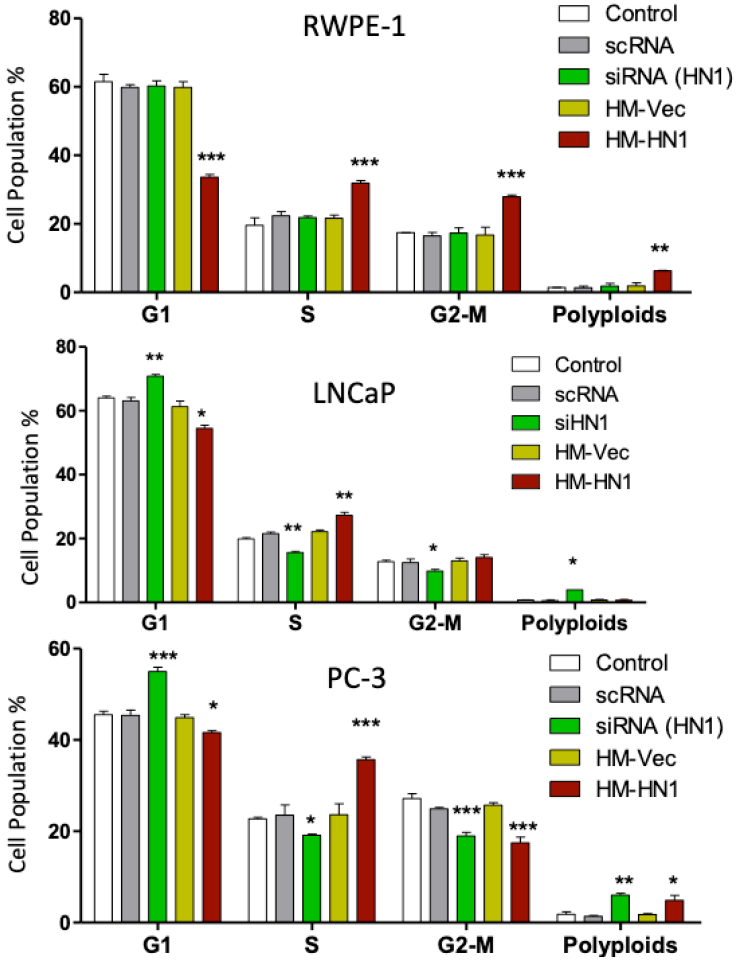

Figure 4.6: Cell Cycle Distribution Analysis of altered HN1 levels in Prostate cells. RWPE-1, LNCaP, and PC-3 cells transfected with scrRNA control (grey), siHN1 (green), HM-Vec (brown), and HM-HN1 (red) were subjected to PI staining and flow cytometry to determine cellular populations in different phases of cell cycle including G1, S, G2, and polyploidy. The differences among samples were significant if *p-value* was less than 0.05 (*), 0.01 (**), and 0.001 (***).

It can be inferred that *HN1* overexpressed cells were arrested in RWPE-1 with reduced proliferation rate, and increased S, G2, and polyploidy populations (1.88 ± 0.63 to 6.31 ± 0.1). Moreover, in LNCaP cells, *HN1* overexpression

arrested cells in S-phase and reduced proliferation with no change in G2-M population. In PC-3 cells, *HN1* overexpression showed higher S-phase population, increased polyploidy and higher proliferation rate, implying that HN1 controls cell cycle transition and in aggressive cancer cells shorten the cell cycle. Taken together, these results indicate that HN1 behaves differently in different cell lines, which constitute different stages of the tumorigenesis in Prostate cancer.

4.2.3. HN1 Depletion And Overexpression In DU-145 Cells

DU-145 cells were also transfected with control and siHN1 RNAs along with HM-Vec and HM-HN1 plasmids to observe the effects of HN1 depletion and overexpression on cell proliferation and cell cycle distribution. HN1 depletion and overexpression both led to decrease in cell proliferation as indicated by viable cell count after performing trypan blue exclusion assay 48 hours post-transfection as shown in figure 4.8. Interestingly HN1 silencing resulted in increase of G1 and polyploidy cells and decrease in S and G2-M populations in DU-145 cells. Meanwhile, *HN1* overexpression caused a decrease in G1 population only and increased only S-phase populations. These results indicate a pivotal role of HN1 in regulating cell cycle as HN1 depletion led to G1 arrest in all Prostate cancer cell lines, while HN1 overexpression caused S-phase populations to enrich in all Prostate cells including normal epithelial RWPE-1 and cancer LNCaP, DU-145, and PC-3 cells.

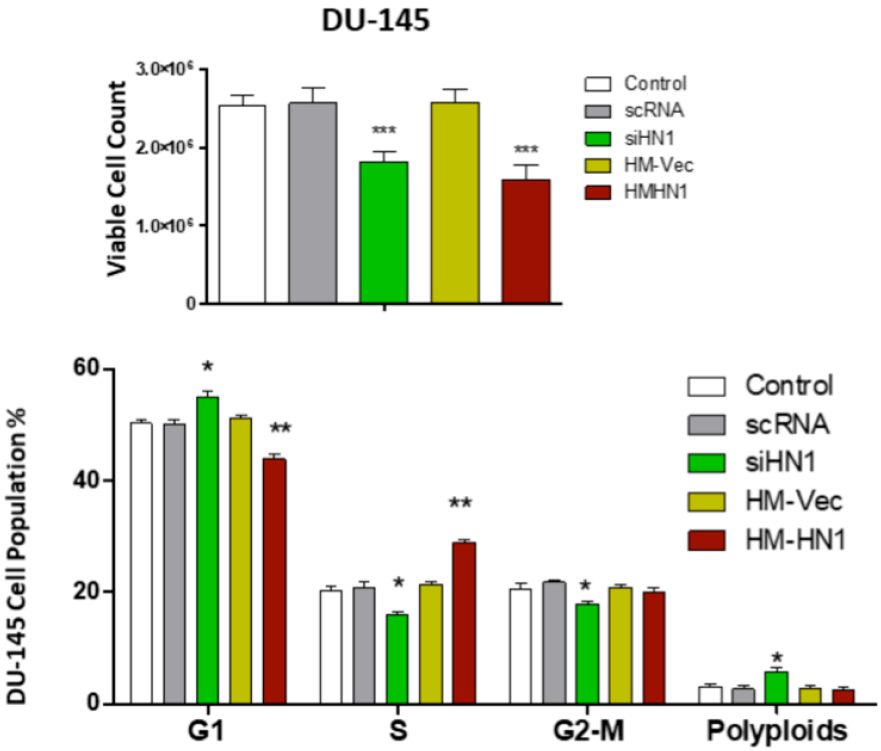

Figure 4.7: Effect of altered HN1 expression on proliferation and cell cycle distribution of DU-145 cells. In upper panel, the result of cell proliferation assay is provided, where HN1 depletion (green) showed lower viable cell count as compared to control RNA transfected cells (grey) (*** shows p-value less than 0.001) and HN1 overexpression (red) also showed reduced viable cell count as compared to vector transfected cells (brown). In lower panel, the effect of altered HN1 expression on cell cycle distribution of HN1 is displayed.

4.2.4. HN1 Depletion In DU-145 Leads To Disruption Of γ-Tubulin

The *in silico* analysis of *HN1* showed that HN1 is a component of cell cycle and centrosome pathways. Therefore, the impact of HN1 depletion by siRNA transfection on γ-tubulin was measured in an immunofluorescence assay. 2 X 10^5 cells were seeded on a cover glass in 3 cm^2 cell culture dishes containing culture media for cell growth. 24 hours post-seeding, cells were treated with Aphidicolin (1.6 μg/ml) and transfected with control (scrambled) RNA or siHN1 RNA and propagated for further 48 hours to trigger the centrosome duplication, and hence centrosome duplication assay. The cells were immunostained with primary antibodies against HN1 and γ-tubulin produced in rabbit and mouse, respectively. After incubating with secondary antibodies and DAPI counterstaining, cells were imaged in an immunofluorescence microscope. The γ-tubulin core in control cells showed partial co-localization with HN1 as shown in a magnified merged image in figure 4.8. In HN1 depleted cells showing negligible

HN1 staining, γ-tubulin cores multiplied, leading to a state of phenotype similar to supernumerary centrosomes.

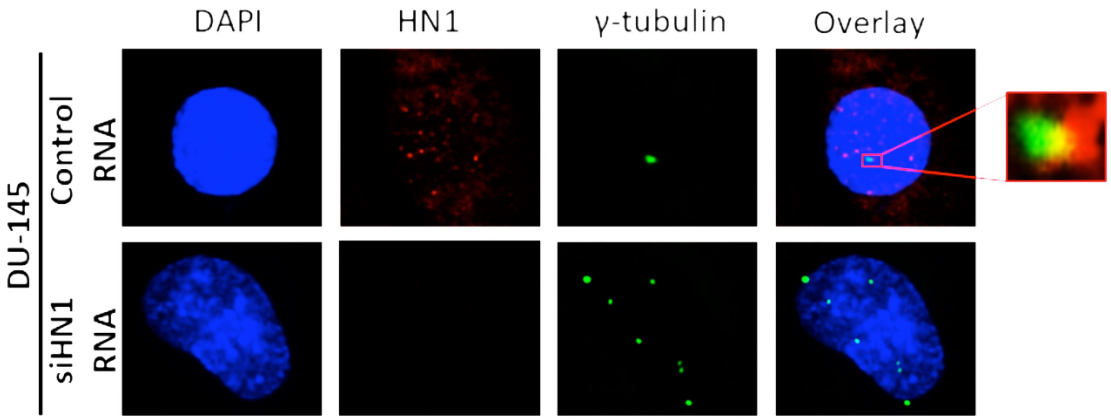

Figure 4.8: HN1 depletion in DU-145 cells causes disruption of γ-tubulin by siRNA transfection. Control RNA and siHN1 treated cells were stained with primary HN1 and γ-tubulin antibodies prior to secondary-Alexa fluor-594 against rabbit and Alexa-fluor-488 against mouse antibodies and cells were counterstained with DAPI. HN1 (red) partially localized with γ-tubulin (green) is shown in a magnified image from overlay of two images from different fluorescence colors in control RNA treated cells. siRNA treated cells depleted HN1 with no staining for red fluorescence, and displayed amplified γ-tubulin cores.

The metaphase cells are characterized by spindle assembly and can be observed by cells released for one hour from Nocodazole block for cell cycle synchronization in G2 phase. In DU-145 cells, HN1 was depleted by siHN1 and prior to cell fixation by methanol; cells were synchronized in G2 by Nocodazole treatment (165 nM) for 18 hours, and released into mitosis by washing Nocodazole and adding fresh culture media for one hour. Fixed cells on cover slips were subjected to immunofluorescence after staining with primary γ-tubulin (produced in goat) and β-tubulin (produced in mouse) antibodies prior to secondary Alexa fluor-488 goat and Alexa fluor-594 mouse antibodies. The cells were counterstained with DAPI and mounted on glass slides for imaging under an immunofluorescence microscope. The metaphase cells were observed in both samples. However, the metaphase plates in siHN1 treated cells showed mono-polarity and pseudo-polarity as compared to control cells as shown in figure 4.9.

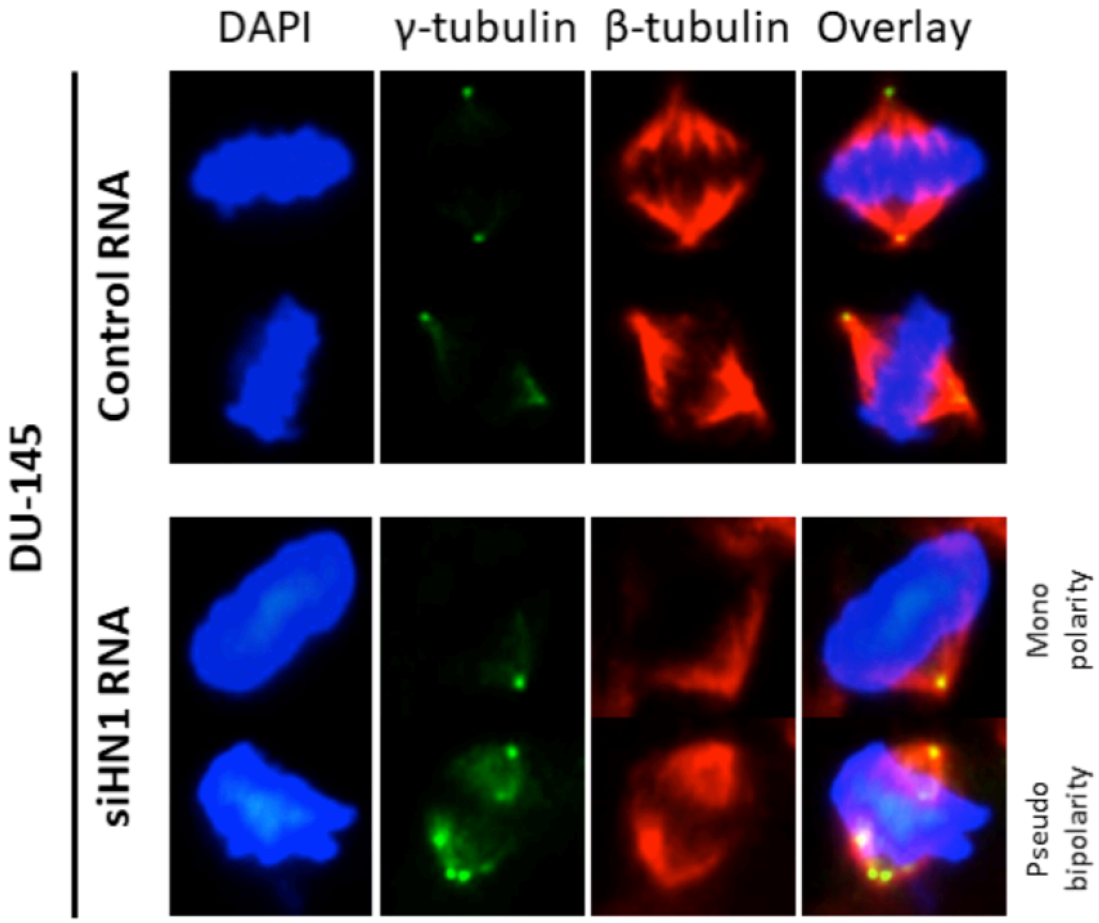

Figure 4.9: HN1 depletion in metaphase DU-145 cells, result in dysregulation of spindle assembly. Immunofluorescence microscopy of control RNA and siHN1 RNA treated cells revealed that HN1 depletion leads to catastrophic phenotypes of monopolarity or pseudo bipolarity (with multiple γ-tubulin cores).

4.2.5. Effect Of *HN1* Overexpression On Cell Cycle Related Proteins

HN1 was overexpressed in RWPE-1, LNCaP, and PC-3 cells to determine any impact on cell cycle related proteins. Cells cultured in 6 cm^2 culture dishes were transfected with either HM-Vec or HM-HN1 using FUGENE HD transfection reagent. After 48 hours of transfection, cells were harvested by washing with PBS, and scraped from the surface of the dish using a sterile plastic cell scraper. The cells were then pelleted and lysed with RIPA modified buffer containing appropriate protease and phosphatase inhibitors. After protein isolation, protein quantification was performed using BCA kit. Equal concentration and volume of total protein lysates (50 µg) was run on a 12 % SDS-gel using constant voltage. After running the gel, proteins were transferred to a PVDF membrane in a wet transfer system, which was validated by coomassie blue staining of the gel. The membrane was then blocked and stained for anti-

HN1 antibody to validate the transfection by observing an ectopic band of HN1 resulting from His-Max tag on the N-terminal of the protein as shown in figure 4.10.

Interestingly, the native protein levels of HN1 are observed to be low in normal Prostate epithelial (RWPE-1) cells as compared to LNCaP and PC-3 cells. This data is in compliance to a previous observation that normal Prostate tissues exhibit lower levels of HN1 as compared to tumor tissues of the Prostate. Furthermore, the impact of *HN1* overexpression on different cyclins was determined in the same experiment. It is shown that in RWPE-1 and LNCaP cells, HN1 ectopic expression is positively correlated with cyclin E levels, and negatively correlated in PC-3 cells. *HN1* overexpression also increased cyclin A in RWPE-1 cells, but decreased it in PC-3 cells, showing that HN1 impacts cell cycle differentially in different Prostate cells. Cyclin B was increased in RWPE-1 and LNCaP cells, but decreased in PC-3 cells upon HN1 overexpression. Moreover, the CDK1 protein levels in RWPE-1 and PC-3 cells remained unchanged, while decreased in LNCaP cells. CDK2 levels however increased in RWPE-1 and PC-3 cells, and reduced in LNCaP cells. PLK1 levels significantly increased in RWPE-1 cells and decreased in PC-3 cells, implying a different role of HN1 based on cellular profile. CDC20 was observed as higher in HN1 overexpressed RWPE-1 cells as compared to controls, however reduced in HN1 overexpressed PC-3 cells as compared to PC-3 control cells and HM-Vec transfected PC-3 cells.

CDT1, the replication control protein showed a faint band in HN1 overexpressed RWPE-1 cells as compared to no expression in control RWPE-1 cells. CDT1 was reduced in LNCaP cells and increased in PC-3 cells as compared to their control counterparts, further implying that HN1 could have a significant role in regulating replication as observed in S-phase enrichment of HN1 overexpressed cells in cell cycle distribution analysis. CDH1 a co-factor of APC/C also showed a higher protein level in RWPE-1, while reduction in LNCaP and PC-3 cells as observed in HN1 overexpressed samples. The mitotic marker $pH3^{S10}$ was not expressed in RWPE-1 cells at all, however showed an increased expression in LNCaP and reduced expression in PC-3 cells. The detailed western blot experiment is shown in figure 4.10.

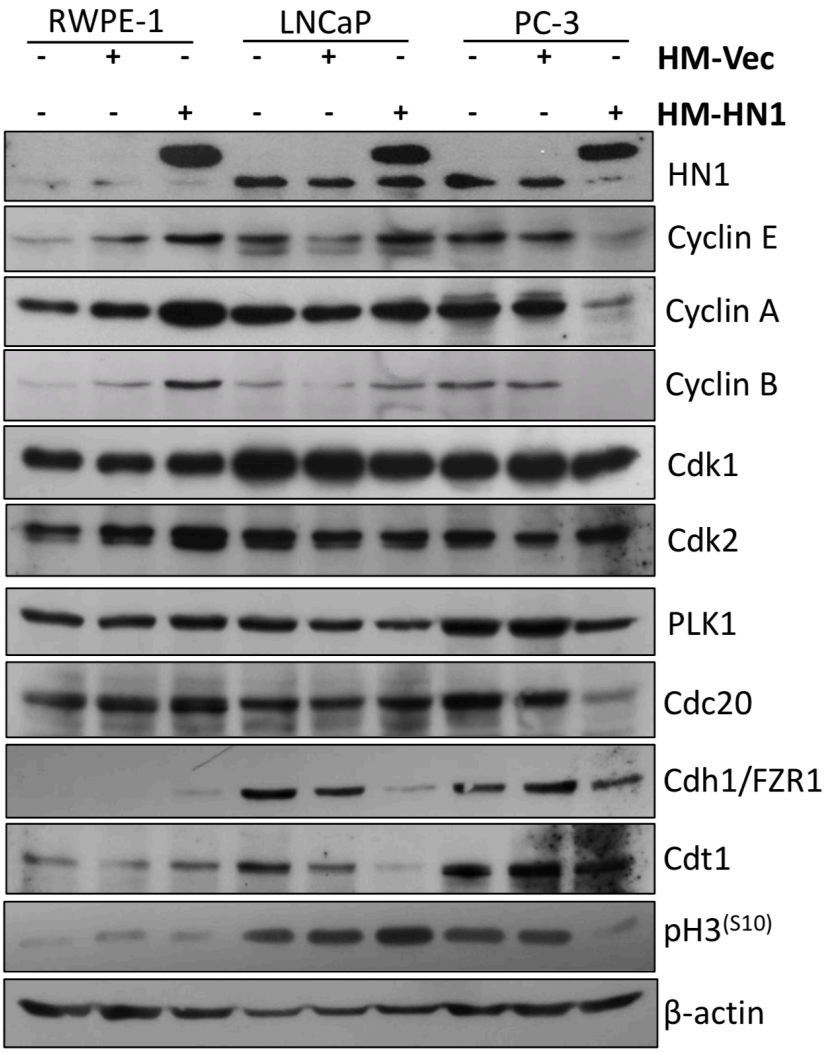

Figure 4.10: Effect of altered HN1 expression on different cell cycle related proteins. HN1 was overexpressed in RWPE-1, LNCap, and PC-3 cells. The isolated proteins from these cells were separated on a 12 % SDS-gel and subsequent immunoblots were prepared using anti-HN1, anti-cyclin E, anti-cyclin B, anti-cyclin A, anti-CDK1, anti-CDK2, anti-PLK1, anti-CDC20, anti-Cdh1, anti-CDT1, and anti-pH3^{S10}. Anti-β-actin was stained as a loading control of the experiment.

4.3. Analyzing Native HN1 Protein In Prostate Cancer Cells

4.3.1. Cyclohexamide (Chx) Chase Assay

Prostate cancer cell lines including LNCaP, 104R2, DU-145, and PC-3 were grown in their appropriate culture media. 4 X 10^5 cells from each cell line were seeded on 6 cm^2 cell culture dishes and grown for 2 days. 100 μg/ml cycloheximide (CHX) dissolved in ethanol was used to inhibit the transcriptional machinery of the cells, and to determine the impact on native HN1 protein levels. Cells were treated for up to 8 hours with cycloheximide and harvested by cell scraping as described previously. After isolating proteins, total protein lysate (μg)

was loaded on a 12 % SDS-Gel for the separation of proteins. After electrophoresis, the proteins were transferred to a PVDF membrane for subsequent immunoblotting. The anti-HN1 antibody and anti-β-actin antibodies were used. HN1 levels remained high in LNCaP cells even after 8 hours of cycloheximide treatment. In LNCaP-104R2 cells, HN1 levels initiate to go down after 4 hours and remained low at 8 hours of CHX exposure. In DU-145 cells, HN1 protein levels varied among different hours, however eventually went down in 8 hours of CHX treatment. Interestingly, HN1 native protein levels significantly reduce from 1 to 2 hours and almost completely disappear at 8 hour time period of CHX exposure. This data indicates that HN1 is a relatively short-lived protein in PC-3 cells as compared to other Prostate cancer cell lines as shown in figure 4.11.

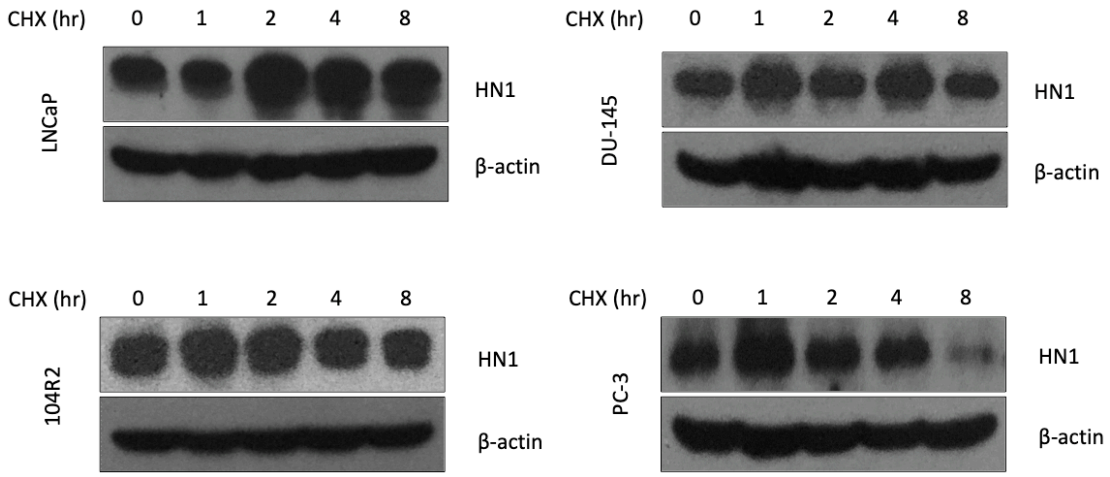

Figure 4.11: Cyclohexamide (CHX) chase assay for HN1 in different Prostate cancer cell lines shows that HN1 stays in stabilized form for longer in LNCaP, 104R2, and DU-145 cells as compared to PC-3 cells. β-actin was stained as control for western blot.

4.3.2. HN1 Protein Levels In Cell Cycle Synchronized Prostate Cancer Cells

Cell cycle synchronization approaches provide a valuable tool to study the cell cycle in a temporal fashion. PC-3 cells grown in culture media were seeded on 6 cm^2 cell culture dishes and after one day, serum starvation for 48 hours was conducted to synchronize cells in G1 phase. Simultaneously, Thymidine double block was performed to synchronize cells in G1/S boundary. Moreover, after double Thymidine block, cells were released in to fresh culture media for 6 hours after washing the Thymidine with PBS, to synchronize cells in S phase. Cells were treated with 165 nM Nocodazole, for 18 hours to synchronize cells in G2

phase (Nocodazole blockage). Lastly, the mitotic cells were harvested by applying mitotic shake-off technique. Mitotic shake-off implies that the cells after Nocodazole block are released into mitosis by washing the cells with PBS and adding fresh media and incubation of one hour, followed by the tapping of the culture dish gently to suspend the loosely attached mitotic cells in culture media, which can be collected.

The western blot analysis of cell cycle synchronized cells showed that HN1 levels remained low in G1 phase, started to manifest in G1/S transition, and were the highest during the S-phase. In G2-phase, the native HN1 protein levels start to go down and remained low in mitosis with an extra distinct band higher than normal HN1 position on the PVDF membrane stained with anti-HN1 antibody. The cell cycle synchronization approaches were validated by immunoblotting of cell cycle related proteins such as cyclin B1, PLK1, and $pH3^{S10}$. β-actin was used a loading control of the experiment (figure 4.12). The cyclin B levels start to come up in S phase and remained high in G2 and M phases. The $pH3^{S10}$ levels show the mitotic populations, which are clearly higher in mitotic shake-off synchronization approach. PLK1 levels also remained high in G2 and M phases of the cell cycle, showing that the cell cycle synchronization approaches worked. Moreover, a portion of the cellular populations was subjected to PI staining and subsequent flow cytometry to evaluate the synchronization approaches and the relevant peaks of different phases are shown above the samples in figure 4.12.

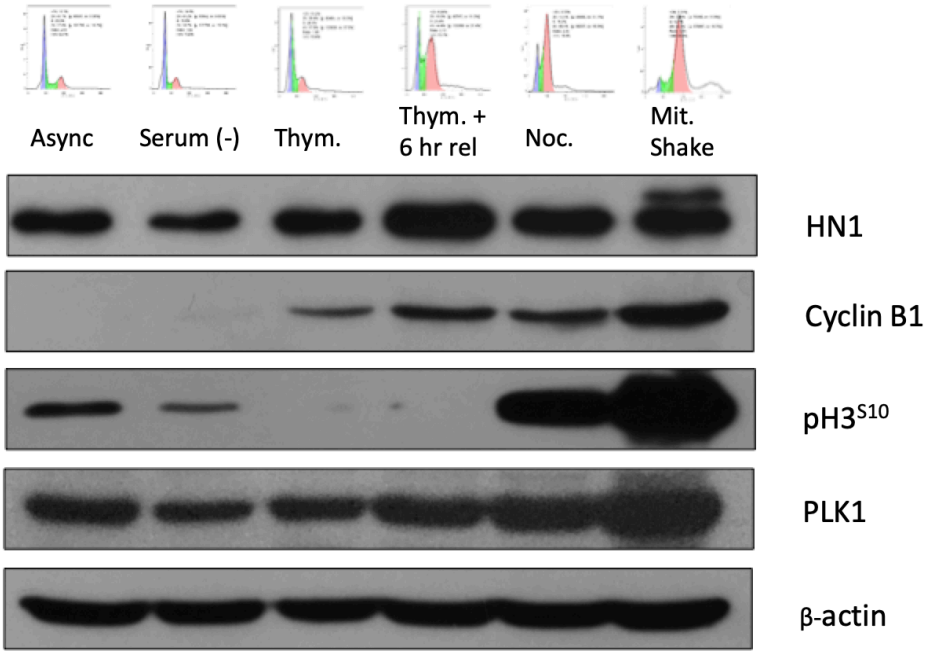

Figure 4.12: Cell cycle synchronization approaches show that HN1 levels fluctuate in cell cycle in PC-3 cells. HN1 levels were enriched in S-phase of the cell cycle and dropped in G2 and remained low until G1. Cyclin B1, $pH3^{S10}$, and PLK1 levels also change during the cell cycle. β-actin was used as a loading control.

The same experiment was repeated in other cell lines such as LNCaP, and 104R2, along with PC-3 cells. The similar profile as shown in figure 4.12 was observed in LNCaP and 104R2 cells. In this experiment, to enrich cells in early S phase, the cells were released from double Thymidine block for 2 hours instead of 6 hours as shown in figure 4.13. In LNCaP cells, serum starved G1 cells (or quiescent G_0 cells) show significantly reduced protein levels of HN1 as compared to asynchronized control cells. The G1/S cells enriched by double Thymidine block exhibited similar HN1 levels as control cells but higher than serum-starved cells. The early S cells derived by 2 hour release double Thymidine block displayed highest HN1 expression, implying that HN1 function in regulation of S-phase of the cell cycle. In G2 enriched populations, HN1 levels started to diminish and almost completely disappeared in mitotic populations in LNCaP cells (figure 4.13). In 104R2 cells, slightly different results were obtained. HN1 was expressed in G1 and remained higher in G1/S cells, and went down in S phase, and exhibited an extra (phospho) band in G2 cells which stayed in mitotic populations as well. In PC-3 cells, again, HN1 was enriched in G1/S, and S phase and went down in G2 and mitosis (figure 4.13).

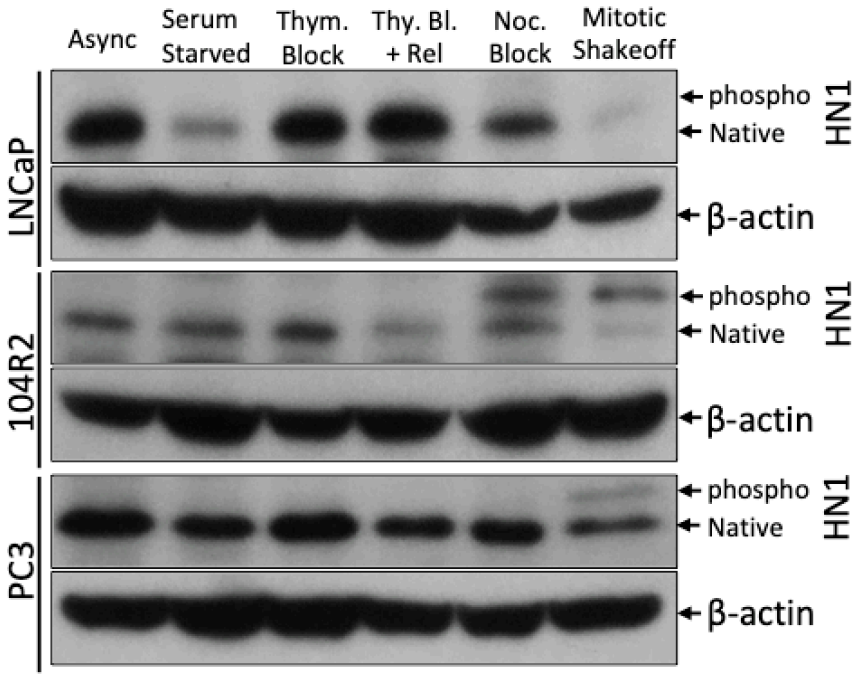

Figure 4.13: LNCaP, DU-145, and PC-3 cells have HN1 levels fluctuating throughout the cell cycle. HN1 native protein levels remain higher in S-phase populations in LNCaP and PC-3 cells with a slight variation in 104R2 cells. Therefore, it can be safely assumed that HN1 levels oscillate during cell cycle, implicating that HN1 is a cell cycle regulated protein. β-actin was used as a loading control.

4.4. HN1 Inducible Tet-ON System

4.4.1. *HN1* Cloning In Tet-ON Inducible Expression System

To construct an inducible expression system containing the HN1 ORF sequence, plasmid vector pCW57.1 from Addgene.org was obtained from a collaborator from IBG. Plasmid pCW57.1 was digested with Nhe1 and Sal1 enzymes and run on 1 % agarose gel electrophoresis. After gel excision and purification of the larger fragment, T4 DNA polymerase with dNTPs was used to make blunt ends in the DNA vector. The plasmid DNA was then self-ligated to form a circular plasmid with the ccdB fragment deleted. The ligation reaction was transformed into chemically competent DHFα bacterial cells, which were grown from a single clone and lysed to obtain a circular plasmid by the alkaline lysis method. The HM-HN1 plasmid containing the HisMax tag at the N-terminus of the HN1 ORF was used to obtain the insert by sequentially digesting first with Sma1 and then with EcoRV. These enzymes already produce blunt ends, so the insert fragment was cut and purified from agarose gel and was ligated with pCW57.1 (ccdB deleted linearized with SalI) using T4 DNA ligase. After transformation, the resulting colonies were checked by colony PCR using LNCX

forward primer and HN1 reverse primer. Positive clones were propagated in LB (Ampicillin containing) medium and used for plasmid isolation by alkaline lysis (miniprep method). Correct clones were validated by cutting plasmid DNA with enzymes Xho1 and Xba1. Next, a clone for midiprep (Hispeed midi kit) was used to obtain high purity DNA and confirmed by restriction diagnostic testing with HindIII (figure 4.14).

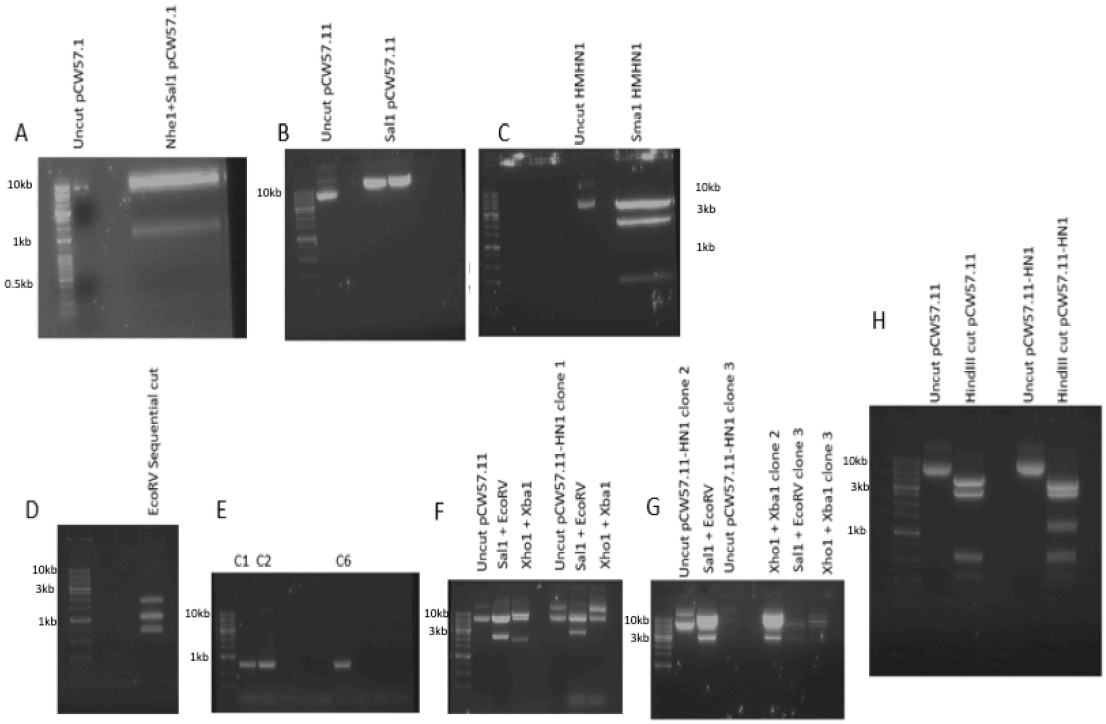

Figure 4.14: *HN1* was cloned into pCW57.1 expression plasmid. (A) pCW57.1 cut with Nhe1 and Sal1. (B) pCW57.11 (ccdB deleted circularized) cut with Sal1 to obtained vector DNA. (C) HM-HN1 plasmid digested with Sma1. (D) Sma1 digested HM-HN1, further sequentially digested with EcoRV to obtain the fragment containing His-Max-HN1 only. (E) Colony PCR from colonies obtained from transformation of ligation reaction with LNCX forward and HN1 reverse primers using Taq polymerase (C1, C2, and C6 are positive clones). (F,G) Three clones of pCW57-HMHN1 were validated by miniprep and using Sal1 + EcoRV double digestion, and Xho1 + Xba1 double digestion. (H) Clone 2 was selected for isolation from Hi-Speed midi prep and validated by using HindIII digestion.

4.4.2. Validating HN1 Inducible System By Western Blotting

After constructing the *HN1* inducible plasmid based on Tet operator and tetracycline activator system, the pCW57-HMHN1 plasmid DNA was transfected into PC-3 cells using FUGENE HD transfection reagent. To determine whether *HN1* ectopic expression is inducible upon Doxycycline treatment, cells were transfected for 24 and 48 hours, and treated afterwards with Doxycycline for 24 or

48 hours. Cells were washed and pelleted for protein isolation. After protein quantification, 50 µg total protein lysate was loaded for protein separation for SDS-PAGE and subsequent western blotting. The anti-HN1 antibody stained the HN1 ectopic bands only in the presence of Doxycycline, validating the success of cloning and induction of Tet-ON system for HN1-induction as shown in figure 4.15.

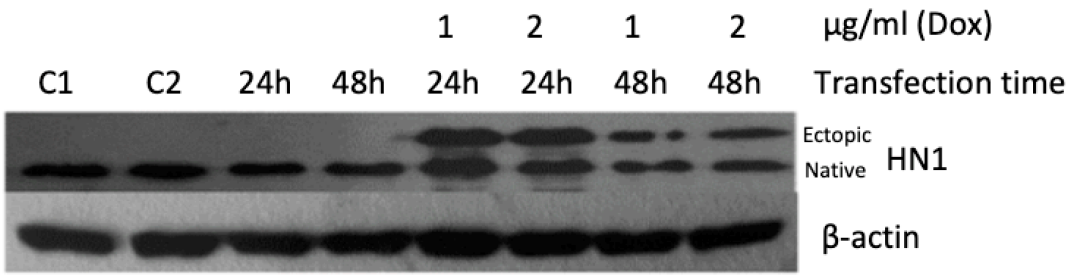

Figure 4.15: HN1 induction upon Doxycycline treatment in PC3-pCW57-HMHN1 cells was validated. Western blotting was performed on pCW57-HMHN1 transfected cells treated with different concentrations of Doxycycline. C1 and C2 are two untreated controls. Two samples containing 24 and 48-hour transfection period without Doxycycline treatment, showed only native HN1 band without exhibiting ectopic expression. The Doxycycline treated samples for 24 and 48 hours, showed ectopic expression, regardless of the transfection period and Doxycycline concentration. β-actin was stained as a loading control for the experiment.

4.4.3. Effect Of HN1-Induction By Doxycycline In HN1-Inducible Stable Prostate Cancer Cell Lines

After validating the HN1-induction specifically in Tet-ON system, lentiviruses were generated using HEK-293T cells. Hek293T cells were transfected with either pCW57 control or pCW57-HMHN1 transfer plasmids along with the 3rd generation lentiviral packaging plasmids such as pMD2.G, pRSV-Rev, and pMDgL/pRRE obtained from Addgene. The resultant viruses were collected 48 to 96 hour post-transfection. The LNCaP and PC-3 cells were transduced with either pCW57 control and pCW57-HMHN1 lenti-viruses using polybrene transduction reagent. After a 2-day transduction period, cells were washed and propagated in normal media prior to puromycin selection for enriching transgene-carrying cells. Transduced cells were incubated in puromycin (2 µg/ml) for 6 days until all un-transduced control cells were dead. After puromycin selection, stable cell lines were propagated further and plated for cell proliferation assay using trypan blue exclusion method as shown in figure 4.16. LNCaP and PC-3 transduced cells were propagated in the presence of

Doxycycline (1 µg/ml) for 6 days with media changes after every 2 days. PC-3-pCW57-HMHN1 cells grew more as compared to PC3-pCW57 control cells, showing a higher proliferation capacity when HN1 was induced. However, LNCaP cells carrying HM-HN1 transgene under the influence of tet-O sequences inducible upon Doxycycline treatment, showed lowered proliferation rate as compared to control pCW57 with no HM-HN1 as a transgene. Therefore, HN1 overexpression in HN1-inducible stable cell lines showed a higher proliferation capacity in PC-3 cells and decreased it in LNCaP cells (figure 4.16).

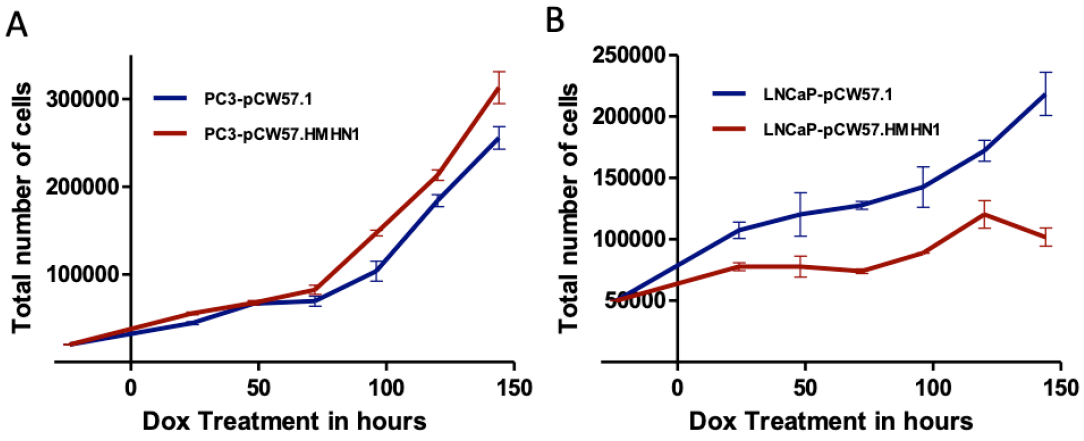

Figure 4.16. HN1 inducible PC-3 and LNCaP cells show differential response to HN1 induction for cell proliferation. (A) PC-3 cells transduced and stabilized for pCW57 control (blue) were compared for proliferation rate as a measure of Doxycycline induction (1 µg/ml) with pCW57-HMHN1 (red) cells. PC-3 HN1-inducible cells showed higher proliferation capacity as compared to control cells. (B) LNCaP cells transduced and stabilized for pCW57 control (blue) were compared for proliferation rate as a measure of Doxycycline induction with pCW57-HMHN1 (red) cells. LNCaP HN1-inducible cells showed reduced proliferation capacity as compared to control cells.

4.4.4. HN1 Rescue After Depletion By siRNA In HN1-Inducible PC-3 Cells

The centrosome duplication assay used to determine the impact of a protein of interest on centrosome duplication pathway was utilized in HN1-inducible PC-3 cells. The experimental design contained the application of Aphidicolin (1.6 µg/ml) together with transfection of either control or HN1 targeting siRNA for 48 hours. To rescue the expression of HN1 from the effects of HN1 depletion by siRNA, Doxycycline was applied for 48 hours after 2-day siRNA transfection period (figure 4.17).

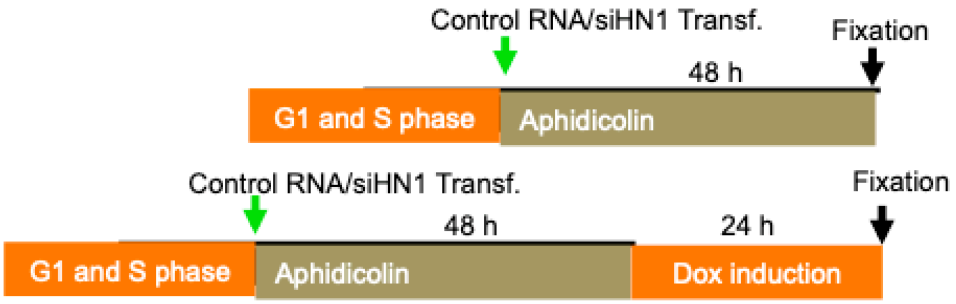

Figure 4.17: Schematic representation of HN1 rescue experiment in HN1-inducible PC-3 cells shows induction of HN1 in a centrosome duplication assay. Cells were fixed after siRNA treatments in non-induced cells, while cell fixation was carried out after HN1-induction by Doxycycline (1 µg/ml) for 24 hours in HN1-rescue sample.

The PC-3 cells inducible for HN1 by applying Doxycycline were plated on cover glass in 6-well plates. The centrosome duplication experiment was performed as detailed previously for DU-145 cells in transfection-based setting. Here, HN1 expression was rescued after depletion by applying 1 µg/ml Doxycycline. After cell fixation by 100 % cold methanol for half an hour, cells were permeabilized and stained for HN1 and γ-tubulin using primary anti-HN1 (produced in rabbit) and primary anti- γ-tubulin (produced in mouse). The alexa-fluor 594 anti-rabbit and alexa-fluore 488 anti-rabbit secondary antibodies were used for targeting primary antibodies in an indirect immunofluorescence assay. The HN1 (red fluorescence) was co-localized with γ-tubulin (green fluorescence), as seen in control RNA, and control RNA and Doxycycline treated PC3-pCW57-HMHN1 cells (figure 4.18). The HN1-depeleted cells by siHN1 led to disruption of γ-tubulin cores and there are multiple γ-tubulin foci observed. The HN1 rescue sample consisting of HN1-induced by Doxycycline after HN1 depletion by siRNA, showed γ-tubulin cores clustered together instead of dispersing throughout as observed in HN1 depleted cells (figure 4.18). The HN1 induced sample with control RNA and Doxycycline treatment, exhibited HN1 overexpression and its impact on γ-tubulin, which showed γ-tubulin foci to be clustered near the nuclear boundary in an interphase cell. Therefore, t can be assumed that HN1 overexpression leads to clustering of γ-tubulin foci together and HN1 is a potential centrosome clustering protein in Prostate cancer cells.

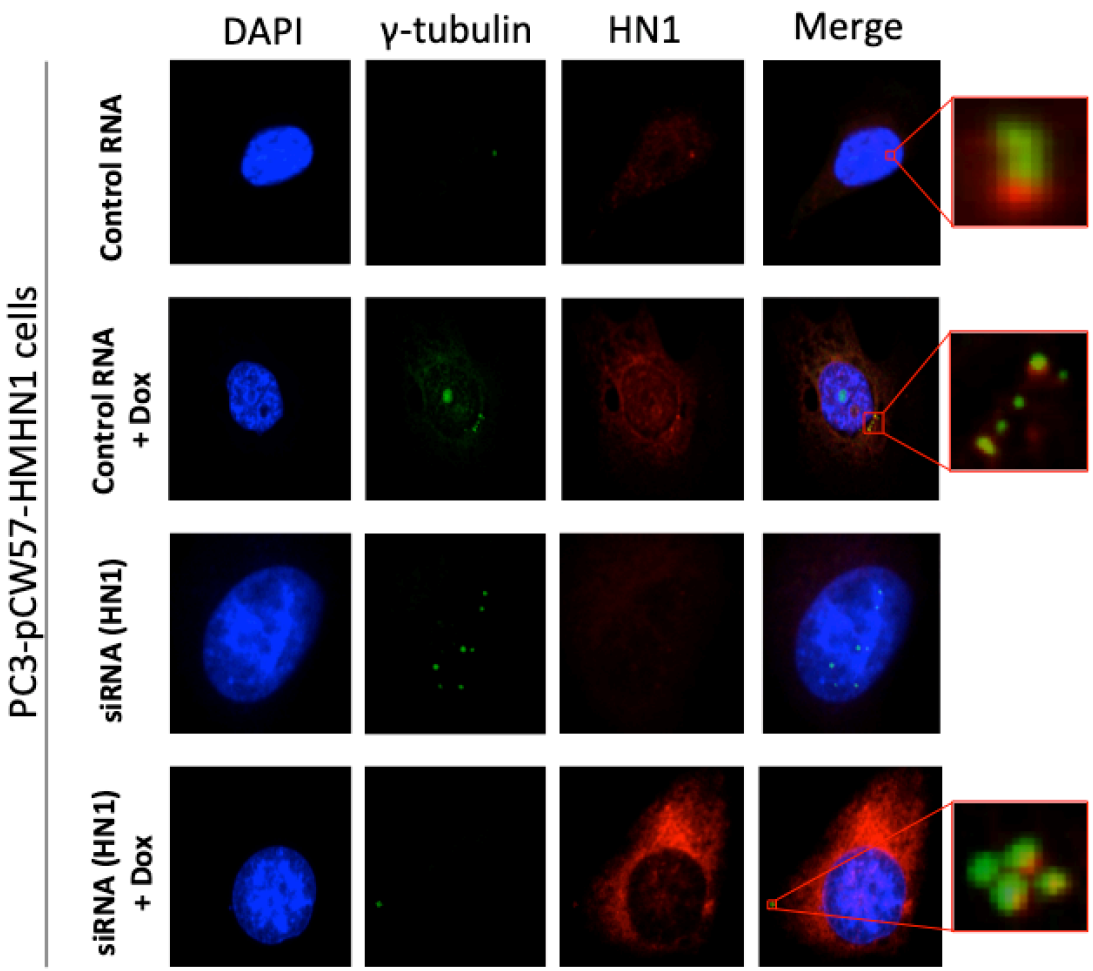

Figure 4.18: HN1 rescue causes centrosome clustering like phenotype in PC-3 cells. PC3-pCW57-HMHN1 cells plated on cover glass were immune-stained with anti-HN1 and anti- γ-tubulin primary antibodies, along with relative secondary anti-rabbit and anti-mouse alexa-fluor 594 and alexa-fluore-488 antibodies. DAPI was used for counterstaining the nucleus. HN1 (red) colocalized with γ-tubulin foci (green) as shown in magnified images with HN1 stained cells. HN1 depletion after siRNA transfection showed significantly reduced staining of HN1 in immunofluorescence. HN1 rescue led to γ-tubulin foci being clustered together in HN1-inducible PC-3 cells.

The nuclear morphology as observed in DAPI staining showed some abnormalities in HN1 rescue experiment. The *HN1* overexpressed cells showed abnormal nucleus with clustered γ-tubulin foci, HN1 depleted cells exhibited degraded nuclear boundaries and HN1 rescued cells showed the formation of micronuclei, as shown in figure 4.19. These results indicate that HN1 has a function in regulating the nuclear morphology as well, which can be disturbed upon increasing or decreasing the native HN1 protein levels.

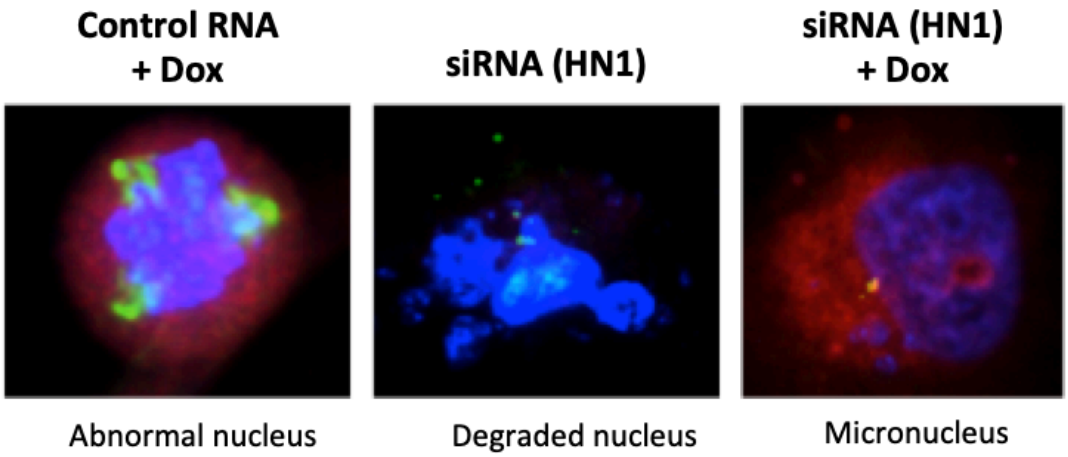

Figure 4.19: HN1 alteration or rescue causes nuclear abnormalities. HN1 overexpressed cells identified with higher red fluorescence showed abnormal nuclear morphology along with to γ-tubulin foci defects (green fluorescence). HN1 depleted cells showed nuclear boundary degradation, and HN1 rescued cells, exhibited micronuclei formation.

The centrosome duplication assay employing the approach of HN1 rescue in HN1-inducible PC-3 cells showed irregular number of to γ-tubulin foci, which can be identified as numerical defects of centrosomes. The statistical calculations were performed on 300 cells from each sample of the rescue experiment and γ-tubulin foci were counted. The control RNA treated cells showed 16.75 ± 1.04% γ-tubulin ≥ 3 populations, which increased to 26.88 ± 1.0% in HN1 overexpressed cells. This data indicates that HN1 controls the numerical fidelity of γ-tubulin cores in Prostate cancer cells. Moreover, HN1 depleted cells exhibited 29.71 ± 1.4% of γ-tubulin ≥ 3 populations, which is also higher than control cells. The HN1 rescued cells after depletion showed 34.14 ± 1.03% γ-tubulin ≥ 3 populations, further implicating that HN1 alteration leads to centrosomal defects in Prostate cancer PC-3 cells (figure 4.20). The numerical defects of centrosomes recognized by amplification of γ-tubulin ≥ 3 populations, in HN1 rescue attempt, dictates that HN1 is involved in spatial regulation of centrosomes and is a player in centrosome duplication pathway as well.

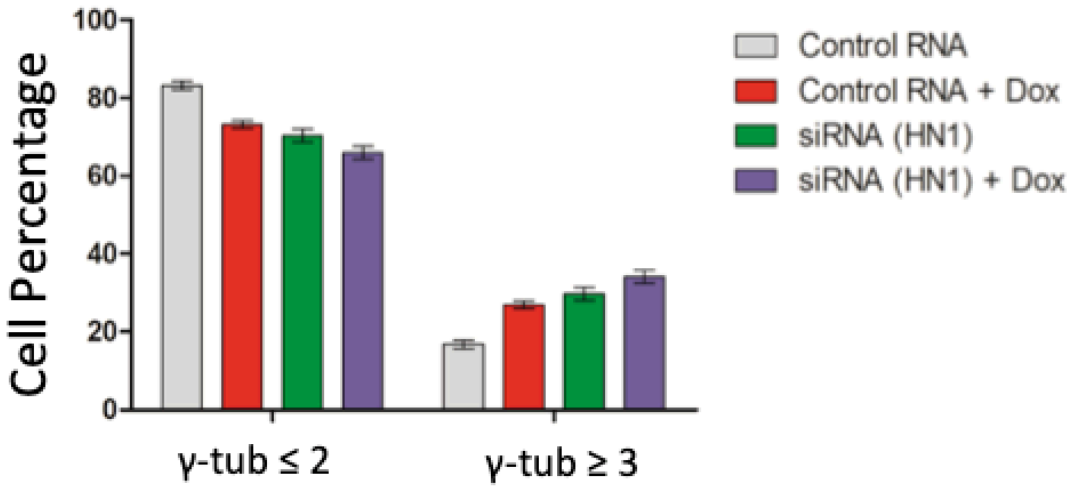

Figure 4.20: HN1 rescue did not rescue the centrosomal defects in PC-3 cells. The number of cells counted in sample was n ≥ 100 from three independent regions of the samples. The normal cells are indicated as γ- tubulin ≤ 2, whereas multiplied γ- tubulin foci are shown as γ- tubulin ≥ 3 populations. HN1 overexpressed cells (red) showed an increase in γ- tubulin ≥ 3 populations as compared to control cells (grey). HN1 depleted cells (green) and HN1 rescued cells (purple) also showed a higher percentage of γ- tubulin ≥ 3 populations.

4.4.5 Effect Of *HN1* Overexpression On Cyclin B1 In HN1-Inducible PC-3 Cells

The Tet-ON system provides a temporal response of induction of gene of interest. Therefore, HN1 expression was induced temporally for up to 24 hours using 1 µg/ml Doxycycline in PC3-pCW57-HMHN1 cells. The ectopic expression of HN1 increased temporally in HN1-inducible cells (figure 4.21). The western blotting performed on these samples showed that HN1-overexpression temporally decreased the levels of cyclin B1 in PC-3 cells, which is in compliance to previous results shown in figure 4.10. The ectopic expression of HN1 manifests in 2 hours of 1 µg/ml Doxycycline and reaches to the levels of native HN1 in 4 hours of Doxycycline induction and exceeds the native levels in 8 hours of induction. This data shows the usability of inducible expression system for temporally investigating the function of a protein of interest. The decrease in cyclin B1 protein levels upon HN1 induction revealed that HN1 protein directly inhibits the cyclin B1 protein perhaps by inducing the ubiquitination based degradation of cyclin B1, which has been investigated in another study (Varisli et al., 2010).

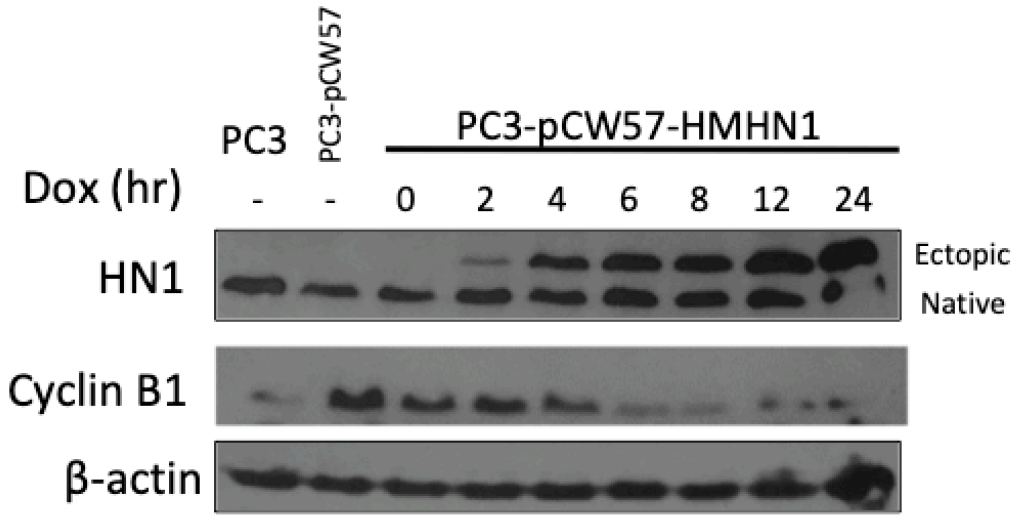

Figure 4.21: HN1 induction in HN1-inducible PC-3 cells show reduction in cyclin B1 levels. Untreated parental PC-3 cells and stabilized PC3-pCW57 control cells were used as controls for the experiment. 1 µg/ml Doxycycline was used for inducing HN1 expression for 2, 4, 6, 8, 12, and 24 hours. The anti-HN1, anti-cyclin B1, and anti-β-actin (loading control) were used for immunostaining.

4.4.6. HN1 Induced PC-3 Cells Are Protective Against Apoptotic Inducers

HN1 overexpression by Doxycycline induction was also explored in determining whether HN1 induces any other negative phenotype such as apoptosis in PC-3 cells. The cells were treated with Doxycycline for 24 hours and then treated with apoptosis inducing 11 chemical inhibitors. Protein lysates were prepared from these samples, and western blotting was performed to observe any changes in HN1 and Bax (an apoptosis regulator) (figure 4.22).

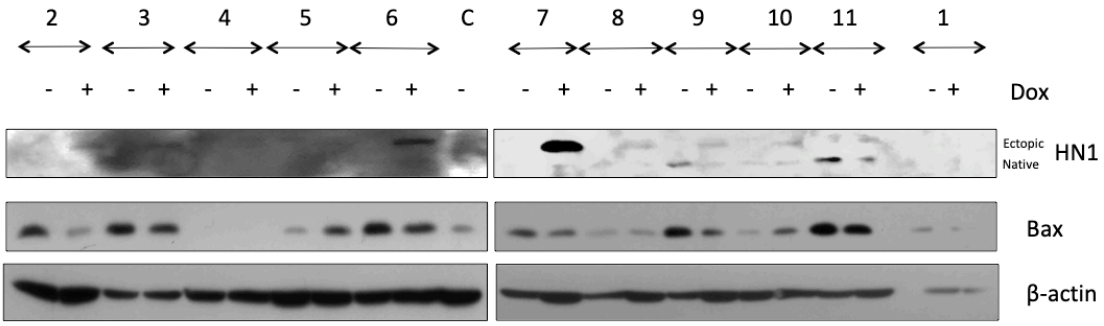

Figure 4.22: The effect of *HN1* overexpression on apoptotic inducing factor Bax. The HN1 inducible PC3-pCW57-HMHN1 cells were treated with 11 chemical inhibitors. These are 1= AG556 100 uM (EGFRi), 2= Cytochalasin D 5 uM (prevents actin polymerization), 3= Sirtinol 33 uM (sirtinol class III histone deacetylases inh.), 4= Cyclohexamide 100 uM (inhibit protein synthesis), 5= Actinomycin D 100 ng/ml (transcription inhibition), 6= LYP294 50 uM (PI3Ki), 7= Trichostatin A 2 ug/ml

(class I and class II histone deacetylases inh), 8= Flavopiridol 600 ng/ml (CDKi), 9= Etoposide 25 ug/ml (topoisomerase inh), 10= Camptothecin 1 ug/ml (topoisomerase inh), and 11= Doxorubicin 1 nM (topoisomerase II inh). The untreated control cells are indicated as 'C', Dox indicates 1 ug/ml Doxycycline, '-' indicates cells treated with inhibitors only and '+' shows cells treated with Doxycycline prior to treatment with inhibitors. HN1 and Bax were stained with anti-HN1 and anti-Bax antibodies for western blotting. Anti-β-actin was used as loading control of the experiment.

The *HN1* ectopic expression was stabilized in Trichostatin A (TCA) treated cells, which indicates that histone deacetylase inhibition stabilizes HN1; therefore HN1 might transcriptionally be controlled by histone deacetylases. HN1 overexpression significantly reduced the expression of pro-apoptotic Bax protein in Cytochalasin D, PI3Ki, TCA, Etoposide, and Doxorubicin as compared to control HN1-uninduced cells. Therefore, this data indicated that HN1 could be cell survival protein, which attempts to protect the cells from the apoptotic effects of aforementioned chemical inhibitors.

The cells collected from the experiment were subjected to apoptosis assay using Annexin-V and PI staining and read on flow cytometer. *HN1* overexpressed cells, when treated with various inhibitors as shown figure 4.22, showed a decreased rate of apoptosis or necrosis as compared to uninduced PC3-pCW57-HMHN1 cells. There were less necrotic cells in HN1-induced and Cytochalasin D treated cells; implicating that *HN1* overexpression provided a protective response to these cells. Moreover, necrotic populations also decreased in Sirtinol and TCA treated but HN1 overexpressed cells as compared to only inhibitor treated cells. The apoptotic populations also decreased in HN1 overexpressed and Camptothecin, Flavopiridol, TCA, PI3Ki, and Actinomycin D treated cells as compared to only inhibitor treated cells (figure 4.23).

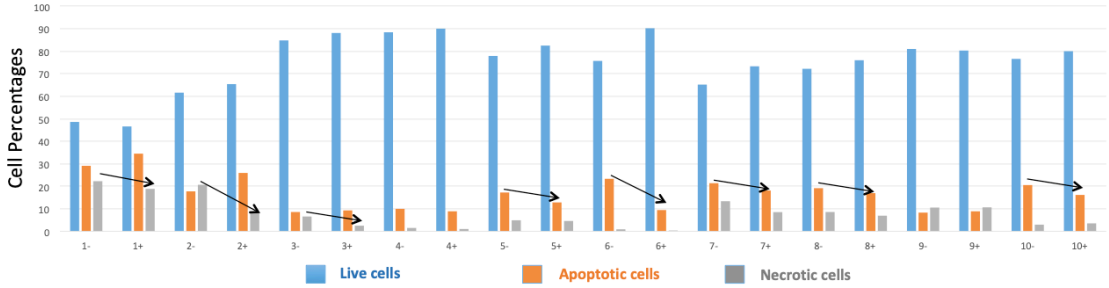

Figure 4.23: The *HN1* overexpressed PC-3 cells are protective against apoptotic inducers. The pCW57-HMHN1 cells treated induced with Doxycycline (+) and chemical inhibitors showed reduced necrotic (grey) or apoptotic (orange) populations as compared to cells not treated with Doxycycline (-). The ten chemical inhibitors are: 1= AG556 100 uM (EGFRi), 2= Cytochalasin D 5 uM (prevents actin polymerization), 3= Sirtinol 33 uM (sirtinol class III histone deacetylases inh.), 4=

Cyclohexamide 100 uM (inhibit protein synthesis), 5= Actinomycin D 100 ng/ml (transcription inhibition), 6= LYP294 50 uM (PI3Ki), 7= Trichostatin A 2 ug/ml (class I and class II histone deacetylases inh), 8= Flavopiridol 600 ng/ml (CDKi), 9= Etoposide 25 ug/ml (topoisomerase inh), and 10= Camptothecin 1 ug/ml (topoisomerase inh). The annexin-V staining showed apoptotic cells, while PI only and annexin-V + PI stained cells showed necrotic populations. The live cells were gated as showing no staining for PI or annexin-V. Untreated cells were used as negative control for the experiment.

4.4.7. *HN1* Overexpression After G2 Induces An Early Exit From Mitosis

The temporal regulation of *HN1* ectopic expression in PC3-pCW57-HMHN1 cells provide a unique tool to determine the impact of HN1 overexpression on individual cell cycle phase transitions. Therefore, the PC3-pCW57-HMHN1 cells were synchronized in G2 cells by Nocodazole treatment and released into G1 for up to 6 hours in normal media. The experimental design is provided in figure 4.24A, where cells were treated with Doxycycline for 6 hours in Nocodazole treated cells. The cells were subjected to cell cycle distribution analysis and western blotting. The cells not treated with Doxycycline were control cells without ectopic expression of HN1. The western blotting conducted on these cells with anti-HN1 antibody, showed that HN1 has an ectopic band displaying the induction of HN1 by Doxycycline treatment (figure 4.24B). The mitotic marker ($pH3^{S10}$) showed the mitotic populations and is not present mostly in asynchronized cells. The HN1 induction in G2 cells released into G1 after Nocodazole block, the mitotic marker is reduced at 6 hour release as compared to control cells, indicating an early exit from mitosis as a function of *HN1* overexpression. The PLK1 protein levels however were lower in asynchronized HN1 overexpressed cells as compared to control cells, which is consistent with the previous data provided in figure 4.10, where *HN1* overexpression by plasmid DNA transfection resulted in a decrease in PLK1 expression.

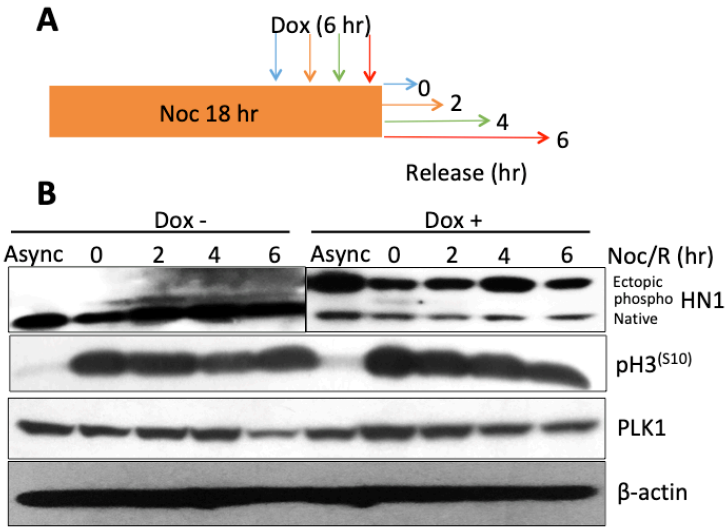

Figure 4.24: The *HN1* overexpression in G2 synchronized cells show early exit from mitosis. (A) The experimental design showing that HN1 induction period was 6 hours in all samples with 1 ug/ml Doxycycline. PC3pCW57-HMHN1 cells were treated with Nocodazole (165 nM) for 18 hours and released into G1 for up to 6 hours (0, 2, 4, 6 hours). (B) The immuno-blotting was performed for determining the protein levels of HN1 and mitotic marker ($pH3^{S10}$). β-actin was used a loading control for the experiment.

The cell cycle distribution analysis of the samples mentioned in figure 4.24A by cell fixation and subsequent PI staining was performed. HN1 overexpression for 6 hours in PC3-pCW57-HMHN1 cells compared with cells not treated with Doxycycline, showed a decrease in G1, and an increase in S-phase populations (Async cells) (figure 4.25). This data is consistent with the result of HN1 overexpression by plasmid DNA transfection shown in figure 4.6. The HN1-inducible cells synchronized at G2 by treatment with 165 nM Nocodazole, when treated with 1 µg/ml Doxycycline for last 6 hours of synchronization (during Nocodazole block), showed an increased S-phase population as compared to cells not treated with Doxycycline. After 2-hour release from Nocodazole block, S-phase populations remained higher, however, G2 cells started to decrease in HN1 overexpressed cells as compared to cells not treated with Doxycycline. After 4-hour release from Nocodazole block, G1-phase populations remained higher, however, G2 cells remained lower in *HN1* overexpressed cells as compared to cells not treated with Doxycycline. After 6-hour release from Nocodazole block, G1 populations remained similar, S-phase populations remained higher, and G2 cells remained lower in HN1 overexpressed cells as compared to cells not treated with Doxycycline (figure 4.25).

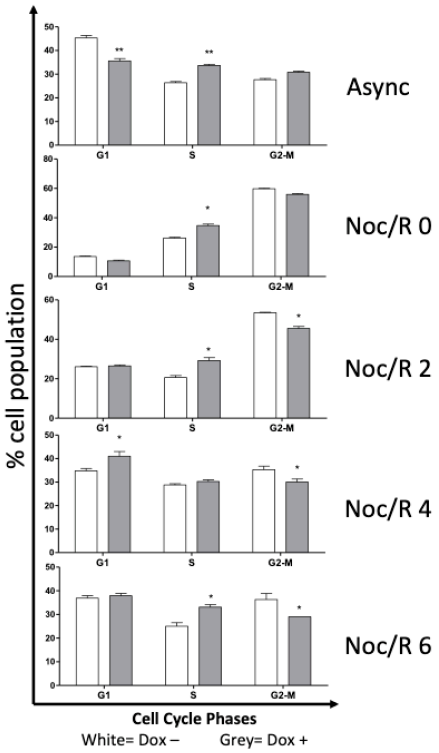

Figure 4.25: Cell cycle distribution analysis for cells released into G1 after G2 synchronization. The PC3-pCW57-HMHN1 cells treated with Doxycycline for 6 hours (grey) were compared with untreated cells (white), and subjected to PI staining after fixation with ethanol. Async cells (not synchronized) showed lower G1 (**) and higher S-phase populations (**). The cells synchronized in G2 by Nocodazole (165 nM) for 18 hours, when induced for HN1 for last 6 hours of synchronization, showed that cells did not reach G2 and remained higher in S phase (*). The 2-hour released cells (from G2 block by replacing Nocodazole containing media with normal media for 2 hours), showed reduced G2-M (*) and higher S-phase populations (*). G1 populations increased (*) in 4-hour released samples in Doxycycline treated cells as compared to untreated cells. Lastly, at 6-hour release from G2 (Nocodazole), S-phase populations increased (*) in HN1 overexpressed cells with a reduction in G2-M population (*). The * sign indicate statistically different populations based on t-test applied for individual cell cycle with *p-value* less than 0.05.

4.4.8. Wound Healing Assay In HN1 Inducible PC-3 Cells

The wound-healing assay was performed to determine the impact of *HN1* overexpression on migration capability of HN1 inducible PC-3 cells. The cells were plated in 6-well plates and allowed to reach confluency prior to generating a scratch (wound) by a sterile 200 µl pipette tip, followed by washing the cells in warm media and photographed from a specified marked position on the well. After generating the wound, cells were treated with Doxycycline and grown at normal cell culture conditions. The cells were then photographed at various time points to determine any wound healing effect through HN1 expression. Figure 4.26A shows that when HN1 is overexpressed in PC-3 by Doxycycline induction,

the wound healing capability of PC-3 cells is increased as compared to control cells. The rate of migration and wound closure increased in *HN1* overexpressed cells as compared to control pCW57 cells treated with Doxycycline (Figure 4.26B).

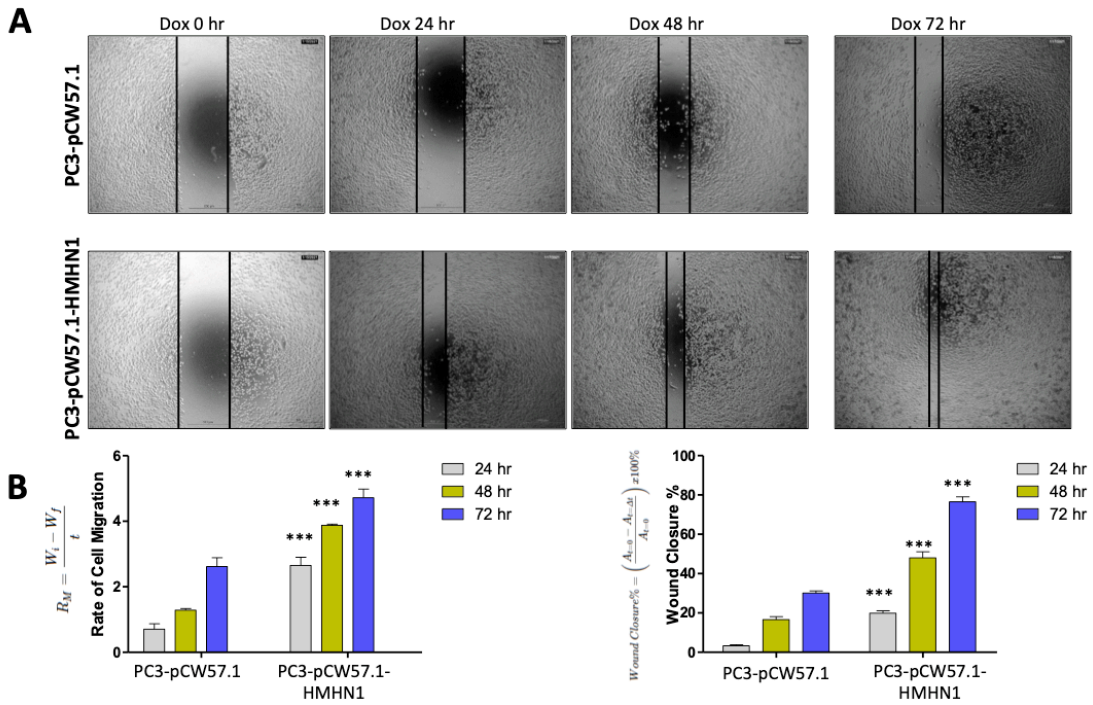

Figure 4.26: Effect of *HN1* overexpression on the migration of PC3 cells: (A) PC3 cells stabilized with either mock or HMHN1 containing Doxycycline-inducible pCW57 lentiviral particles, were cultured in 6-well plates followed by scratch assay to determine the effect of HN1 overexpression on the wound healing effect of HN1. Doxycycline (1µg/ml) was applied to cells for indicated periods of time after establishing a scratch using a 200 µl pipette tip when cells reached equal confluency in all wells of the 6-well plate. Wound healing effect in indicated periods was measured after taking photographs under an inverted microscope. (B) The rate of cell migration as a function of time was measured by the given formula (The images were processed by using the ImageJ software package). The wound closure percentage was measured by scaling the range of the area closed in indicated periods for Doxycycline treatment from the images by using the ImageJ software package (*p-values* less than 0.05 are denoted by *).

4.5. *HN1* Overexpression In FUCCI Cells

4.5.1. Generating And Validating FUCCI-PC3 Cells

The FUCCI plasmid (pBOB-Fast-FUCCI) obtained from Addgene was used as a transfer plasmid for generating FUCCI lentiviral particles. The FUCCI and other plasmids were validated from restriction enzyme digestions, and subsequent agarose gel electrophoresis as shown in figure 4.27. The FUCCI viral

particles were generated as mentioned for pCW57 virus particles previously. The transfer plasmid (pBOB-Fast-FUCCI) was co-transfected with other packaging plasmids (pRSV-Rev, pMD2.G, and pMDLg/pRRE) to HEK293T cells. The lentivirus particles were collected from media 48 hours post-transfection and used for transducing PC-3 cells with polybrene as transduction reagent.

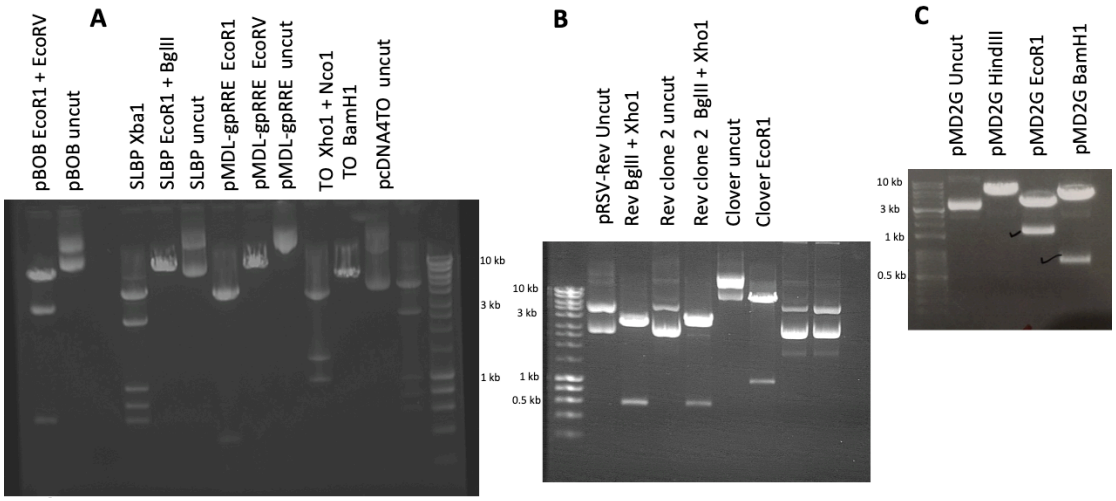

Figure 4.27: Validating FUCCI and lentiviral packaging plasmids by restriction digestion. (A) pBOB-Fast-FUCCI plasmid was digested with EcoR1 and EcoRV. SLBP (Another FUCCI plasmid with different fluorescence protein encoding construct) was digested with Xba1, and also with EcoR1 and BglII for validation. pMDL-gpRRE was digested with EcoR1, and also with EcoRV for validation. Another plasmid containing Tet-operator (with mVenus) was validated by digestion with BamH1, and also with Xho1 and Nco1. (B) pRSV-Rev was validated by digestion with BglII and Xho1. pRSV-Rev (labelled as Rev clone 2) was digested with BglII and Xho1. Clover (another FUCCI plasmid with different fluorescence protein encoding construct) was digested with EcoR1 for validation. (C) pMD2.G plasmid was validated by digestion with HindIII alone, EcoR1 alone, and BamH1 alone, separately.

The pBOB-FUCCI-PC3 cells (labeled as FUCCI-PC3) were further validated using immunofluorescence and flow cytometry. The FUCCI-PC3 cells were plated on cover glass in 3 cm^2 cell culture dishes and treated with Nocodazole for 18 hours for synchronizing cells in G2 phase of the cell cycle. Since FUCCI cells contain two specific probes including mKO2 (fused with degron of Cdt1) and mAG (fused with degron of Geminin), the levels of these fluorescence tags fluctuate during different phases of the cell cycle. The mKO2 (orange) tag appears only in G1 phase and mAG (green) tag appears only in S/G2/M phases. Therefore, cells synchronized in G2 showed a higher percentage of enrichment of mAG (greem) fluorescence tag expressing cells as shown in

figure 4.28. The fluorescence tags contain the minimal degron sequence recognized by E3 ubiquitin ligases for the degradation of these tags and consequently the fluorescence tagged proteins. In control cells, not treated with any cell cycle synchronization reagent, both tags appeared in different cells with a predominant mKO2 tag in most cells showing G1 phase. However, in G2 synchronized cells using Nocodazole blockage, cellular population exhibiting green fluorescence (mAG) appeared to be enriched (figure 4.28).

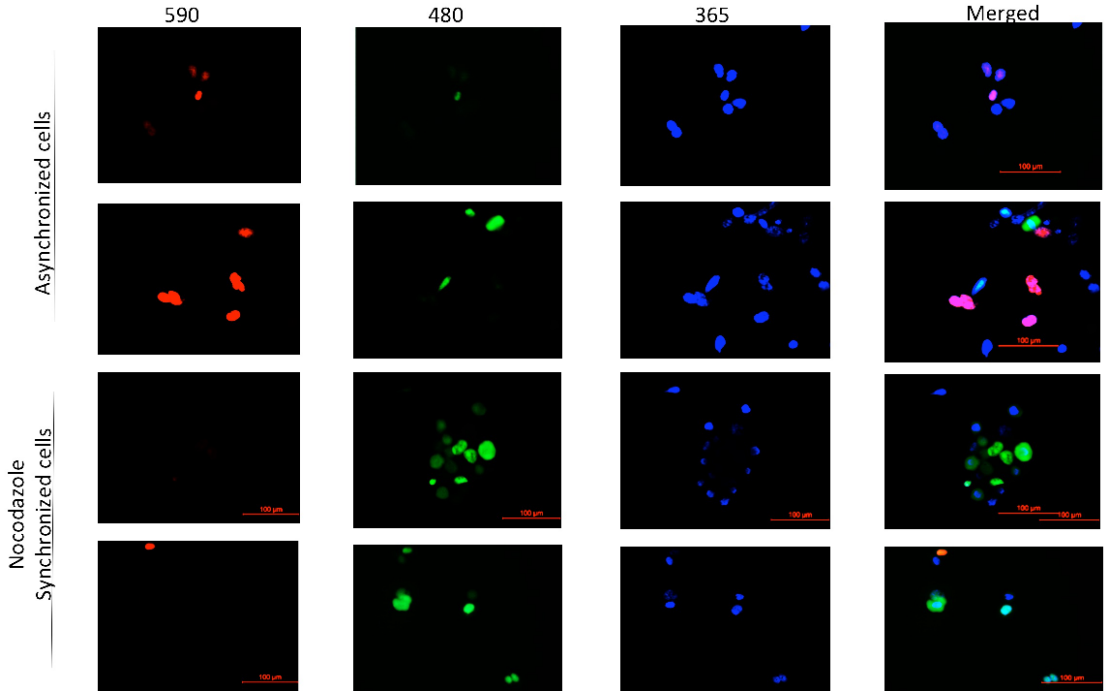

Figure 4.28: Validation of FUCCI-PC3 cells using Nocodazole treatment and immunofluorescence microscopy. FUCCI-PC3 cells plated on cover glass were fixed with 4 % paraformaldehyde and subsequently counterstained with DAPI. The asynchronized control cells showed appearance of both red fluorescence (mKO2) (590 channel), and green fluorescence (mAG) (480 channel). However, FUCCI-PC3 cells synchronized in G2 phase with Nocodazole block, showed the enrichment of green fluorescence (mAG) (green channel) carrying cells. The DAPI is shown in blue color staining (365 channel). The merged images show the overlay of both red and green channels.

The FUCCI-PC3 cells were further validated using flow cytometry on live and fixed cells. Live cell flow cytometry involved the washing of cells in culture with PBS, subsequent trypsinization, followed by another washing with PBS and re-suspension of cells in PBS prior to reading on flow cytometry. The negative control used for flow cytometry was parental PC-3 cells for gating out the auto-fluorescence. The dot plot of control cells showed two distinct populations when

FL2A channel (red) was set at y-axis and FL1A channel (green) was set at x-axis simultaneously. The FL1A leaning population was increased in Aphidicolin and Nocodazole treated cells as shown in figure 4.29. The mAG tag containing FUCCI probe exhibits Geminin degron expression, and is supposed to be increased in S, and G2 cells, therefore, the live cell flow cytometry provided a unique tool to decipher the distinct populations of FUCCI-PC3 cells. The cell cycle synchronization approaches (Aphidicolin and Nocodazole treatment), were further validated as cells were fixed in ethanol, followed by PI staining to observe the cell cycle distribution (figure 4.29).

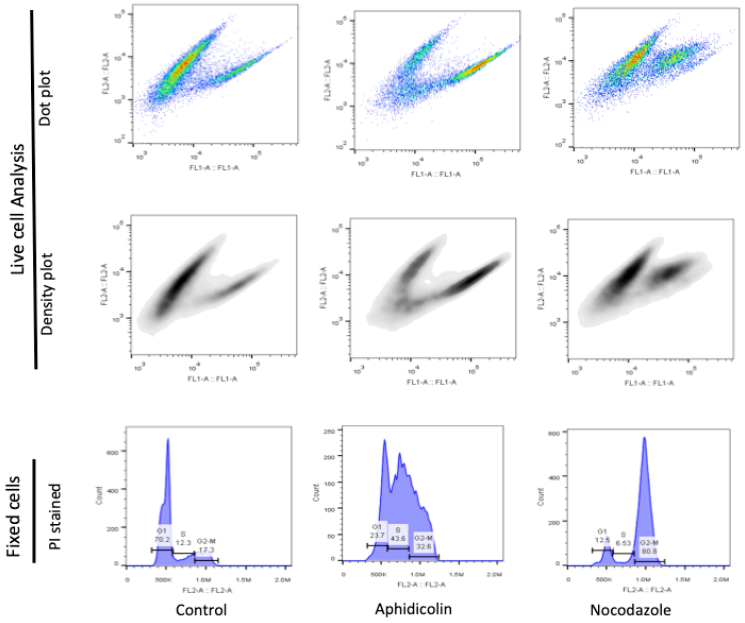

Figure 4.29: FUCCI- PC3s were validated using flow cytometry. The live cell cytometry with parental PC-3 cells as auto-fluorescence gating control yielded two distinct populations on Dot plot when y-axis was set as FL2A channel and x-axis as FL1A channel. The distinct populations were validated by density plot. The FUCCI-PC3 cells treated with Aphidicolin (1.6 ug/ml) showed an increase in FL1A population showing green fluorescence. The Nocodazole (165 nM) treatment also validated the increase in FL1A leaning population. The cell cycle synchronization was validated by PI staining and subsequent flow cytometry on fixed cells showing distinct phases of the cell cycle.

4.5.2. Deciphering APC/C Activity Using Live FUCCI Cells

The FUCCI-PC3 cells were plated on a 96-well plate as ½ cell per well to obtain the monoclonal populations of FUCCI-PC3 cells. After 3 weeks of culturing, three monoclonal populations were obtained and were named as F3, E12, and H7 clones of FUCCI-PC3. It has been reported that APC/C activity

fluctuates during cell cycle as observed in the oscillation of the substrate of APC/C Geminin, which is degraded during G1 phase of the cell cycle, and therefore its degron can be utilized as a probe in FUCCI reporter. Moreover, the activity of APC/C can be monitored in live cells displaying FUCCI probes at different levels in different phases of the cell cycle. For example, the presence of Geminin (and its degron fused with mAG) shows that APC/C is inactive as if it was active, the Geminin degron recognized by APC/C^{CDH1} would have been degraded. Furthermore, the presence of Cdt1 (alongside its degron) dictates that APC/C is active as Cdt1 itself inhibits Geminin and presence of Cdt1 corresponds to the absence of Geminin, displaying an active APC/C complex. The early S phase is supposed to exhibit both mKO2 and mAG fluorescence in FUCCI cells, however, if the median fluorescence intensity of the sample is taken from a sample, it masks the measures of dual probe carrying cells. Therefore, FUCCI-PC3 clones (F3, E12, and H7) were propagated and synchronized in different phases of the cell cycle using serum starvation, double Thymidine block, and Nocodazole blockage. The PI staining showed the validation of cell cycle synchronization as shown in figure 4.30A.

The live cell flow cytometry on different FUCCI-PC3 clones showed that the median fluorescence intensity ratios of mKO2:mAG is different in different phases of the cell cycle. The median fluorescence intensity ratio (mFI mKO2 / mFI mAG) directly corresponds to the APC/C activity as shown in figure 4.30B. In G1 enriched cells (serum starved), the indirect measure of APC/C activity was highest, and went down in early S enriched cells (double Thymidine block), and went further down in G2 enriched cells (Nocodazole blockage). The different clones of FUCCI-PC3 showed similar results, further implicating the accuracy of the measure of APC/C activity in live FUCCI cells.

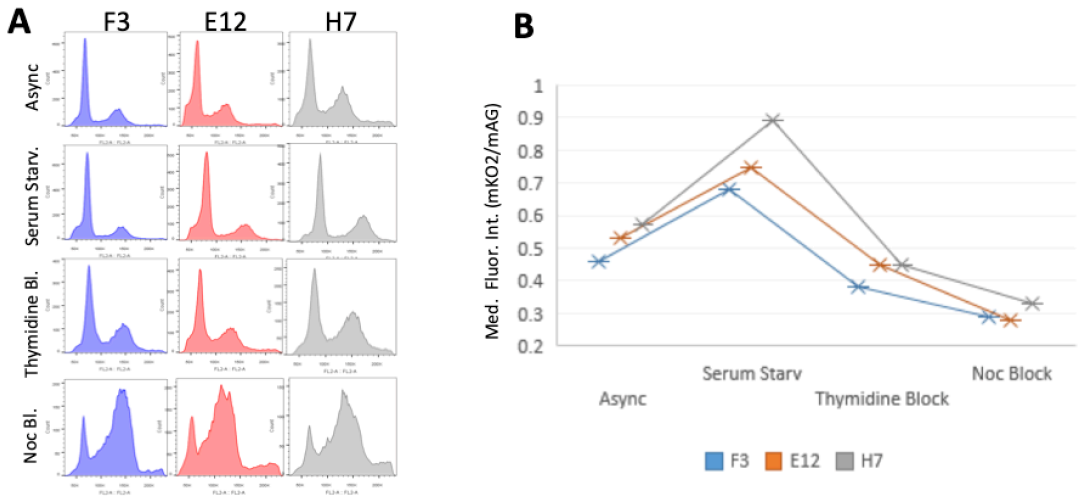

Figure 4.30: FUCCI cells can be used for deciphering APC/C activity. (A) Different clones of FUCCI-PC3 (F3, E12, and H7) were synchronized in different phases of the cell cycle using serum starvation, double Thymidine block, and Nocodazole blockage and fixed with ethanol and stained with PI for measuring cell cycle distribution using flow cytometry. (B) The same cells from (A) were subjected to live cell flow cytometry and median fluorescence intensity for mKO2 (FL2A channel) and mAG (FL1A channel) of the samples was measured. The indirect measure of APC/C activity as median fluorescence intensity (mKO2)/median fluorescence intensity(mAG) was calculated and plotted for control cells, serum starved cells, double Thymidine blocked cells, and Nocodazole treated cells.

4.5.3. Effect Of *HN1* Overexpression On Fucci-PC3 Cells

The FUCCI-PC3 clones validated previously, were transfected with HM-Vec and HM-HN1 plasmids to determine the impact of *HN1* overexpression on the measure of APC/C activity. It was shown that HN1 overexpression resulted in the increase of APC/C activity as shown in figure (4.31). Different FUCCI-PC3 clones (F3, E12, and H7) showed an increase in mFI-mKO2/mFI-mAG displaying the indirect measure of APC/C activity.

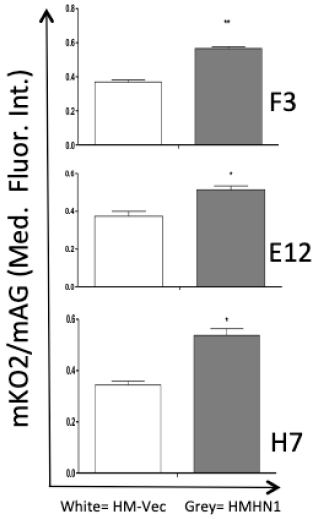

Figure 4.31: *HN1* overexpression leads to stabilization of an indirect measure of APC/C activity. FUCCI-PC3 clones (F3, E12, and H7) were transfected with control HM-Vec (white) and HM-HN1 (grey) plasmids using FUGENE HD transfection reagent. FUCCI clones transfected with HM-HN1 showed increased ratio of median fluorescence intensity ratio of mKO2/mAG as compared to control. The *p-value* less than 0.05 is denoted by * sign.

The FUCCI-PC3-F3 clone was transduced with pCW57-HMHN1 lentiviral particles to incorporate the HN1 inducible expression system in the cells stably expressing FUCCI reporters. The double transduced cells were synchronized in G2 phase of the cell cycle using Nocodazole blockage. HN1 expression was induced during or after Nocodazole block for 6 hours to understand the impact of *HN1* overexpression on the FUCCI probes using live cell flow cytometry. The cellular populations obtained as a result of live cell flow cytometry were gated according to the enrichment of FUCCI probes as mKO2 enriched populations showing orange fluorescence were labelled as mKO2+, mAG expressing cells were labelled as mAG+ and the cells falling in between the two gates were given a separate category as mKO2+ mAG+. Theoretically, mKO2+ cells should be considered G1 cells, mKO2+ mAG+ cells should be considered early S cells, and mAG+ cells should be considered S/G2/M cells. The effect of *HN1* overexpression was measured for FUCCI probes in FUCCI-PC3-F3-pCW57-HMHN1 cells upon Doxycycline treatment in Nocodazole synchronized G2 cells as shown in figure 4.32A. The western blotting with anti-HN1 and anti-β-actin, validated the HN1 induction (figure 4.32B). The live cell flow cytometry of the experimental design, illustrated that HN1 induction resulted in early release from mitosis in cells induced for HN1 expression after G2 phase

arrest in Nocodazole (figure 4.32C). The mKO2+ population significantly increased in cells released from G2 block for 6 hours, carrying HN1 induced expression after G2 blockage.

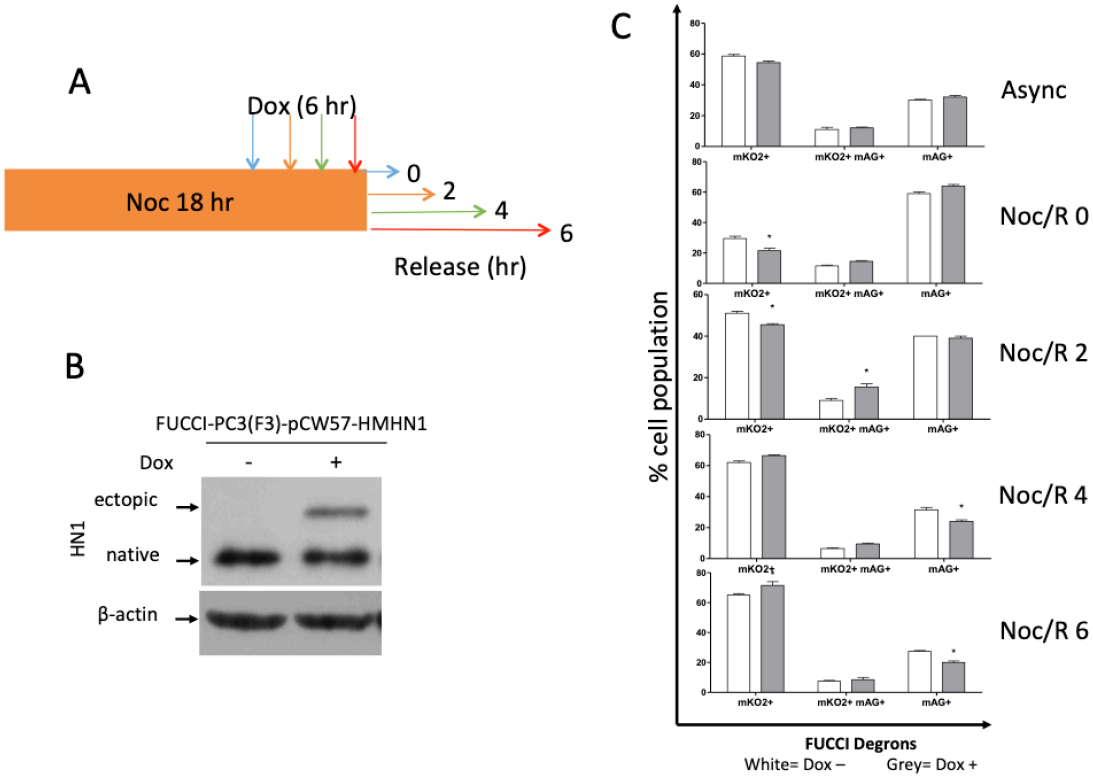

Figure 4.32: HN1 induction after G2 using Tet-ON system in FUCCI-PC3 cells showed early exit from mitosis. (A) The experimental design showing the HN1 induction using Doxycycline for total 6 hours during the Nocodazole blockage and after it, until 6 hour release from the blockage into G1. (B) The HN1 induction in FUCCI-PC3-pCW57-HMHN1 cells (double transduced) stable cells was validated as HN1 ectopic band appeared in only Doxycycline treated cells. β-actin was used as loading control for the experiment. (C) FUCCI-PC3-pCW57-HMHN1 cells were induced for HN1 using Doxycycline (total 6 hours) and synchronized in G2 using Nocodazole blockage according to the experimental design of (A). The cellular populations were gated as mKO2+ (FL2A), mKO2+ mAG+ (both FL1A and FL1A), and mAG (FL1A). There was no siginifant difference among control (dox -, white) cells and HN1 overexpressed (dox+, grey) in asynchronized group of the experiment. In G2 synchronized cells, mKO2+ population decreased in HN1 overexpressed cells (*). At 2 hour release from G2, mKO2+ population decreased (*), and mKO2+ mAG+ population increased (*) in HN1 overexpressed cells as compared to control cells. At 4 hour release from G2, only mAG population decreased (*) as compared to control cells. At 6 hour release from G2, mAG+ population decreased (*) and mKO2 population increased (*) in HN1 overexpressed cells as compared to control cells. P-value less than 0.05 is denoted with * sign.

4.6. HN1-Venus Induction Using Tet-ON Inducible Expression System

4.6.1. Constructing And Validating pCW57-HN1-Venus Transgene Plasmid System

HN1 ORF was amplified using Not1 and EcoR1 sites containing flanking primers with 3'end having no stop codon sequence. The amplified fragments along with the pcDNA4-TO-Venus plasmid containing Venus ORF were then digested with Not1 and EcoR1 restriction enzymes. The vector and insert were then ligated and transformed into DHFα chemical competent cells. The resulting colonies were then screened using the primers used for amplifying *HN1*. After screening, 3 clones were propagated and lysed using alkaline lysis method for isolation of plasmid DNA, which was validated by digesting with Not1 and EcoR1. One of the clones was propagated further and purified DNA was isolated using Hi-speed midi kit and transfected into PC-3 cells to observe the localization of HN1 fused with Venus fluorescence tag (figure 4.33). The HN1-venus localized in a perinuclear region and diffused into the cytoplasm of PC-3 cells as compared to control pcDNA4-TO-Venus transfected cells showing venus localization, which was found bot in nucleus and cytoplasm.

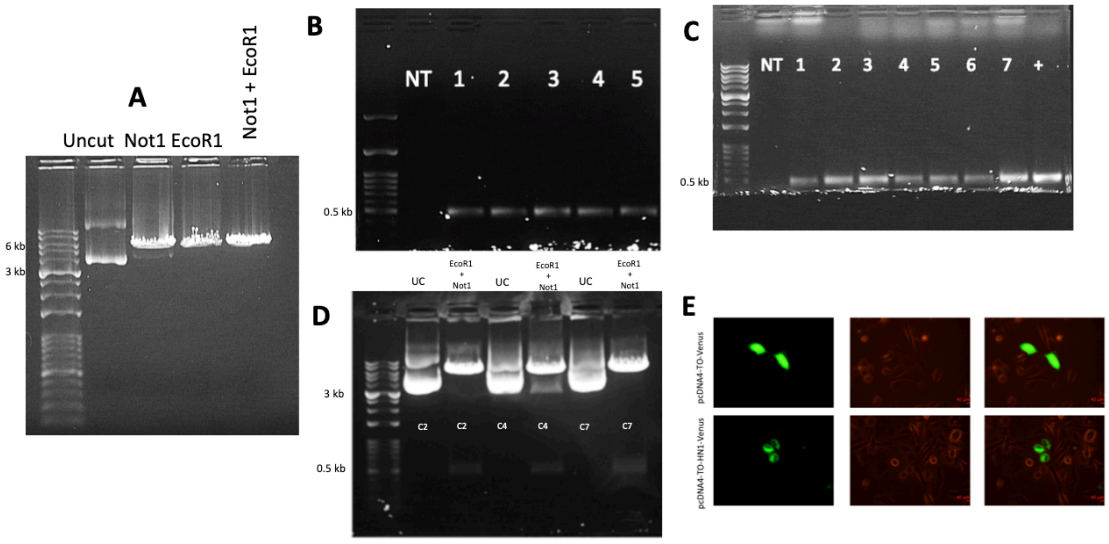

Figure 4.33: *HN1* insertion in pcDNA4-TO-Venus by PCR and restriction cloning. (A) Vector was prepared by digesting pcDNA4TO-Venus with Not1 and EcoR1. (B) HN1 amplification by primers flanking HN1 ORF with Not1 and EcoR1 sites using HM-HN1 plasmid as template DNA. NT is no template sample, 1-5 represent different PCR reactions in separate tubes (C) Colony PCR on colonies appeared after transformation of ligation reaction. NT is no template control. 1-7 represents 7 different clones. HN1 forward and HN1 reverse primers were used. (D) 3 clones (2, 4, 7) were propagated for plasmid DNA isolation using mini-prep method and digested with Not1 and EcoR1 to validate the insertion of HN1 fragment in pcDNA4-TO-Venus. (E) pcDNA4-TO-HN1-Venus and pcDNA4-TO-Venus

plasmids were transfected to PC-3 cells and observed under inverted microscope in green fluorescence filter and imaged using Leica inverted microscope and camera.

The pcDNA4-HN1-Venus plasmid was further digested with Mme1 and Xba1 first to obtain a fragment, which when digested with EcoR1 provided HN1-Venus fragment. HN1-Venus fragment was ligated with vector used for inserting HM-HN1 in pCW57 plasmid. The ligation reaction was transformed into DHFα cells and resultant colonies were screened using LNCX forward from vector backbone and HN1 reverse primers. The correct clone was then further propagated and validated using BamH1 restriction digestion. The pCW57-HN1-Venus plasmid was then transfected as a transfer plasmid along with lentiviral packaging plasmids to HEK293T cells for generating lentiviral particles. The pCW57-HN1-Venus particles were transduced to PC-3, LNCaP, and MDA-MB231 cells and validated by microscopy (LNCaP and MDA-MB231 cells) and western blotting (MDA-MB231 cells) (figure 4.34).

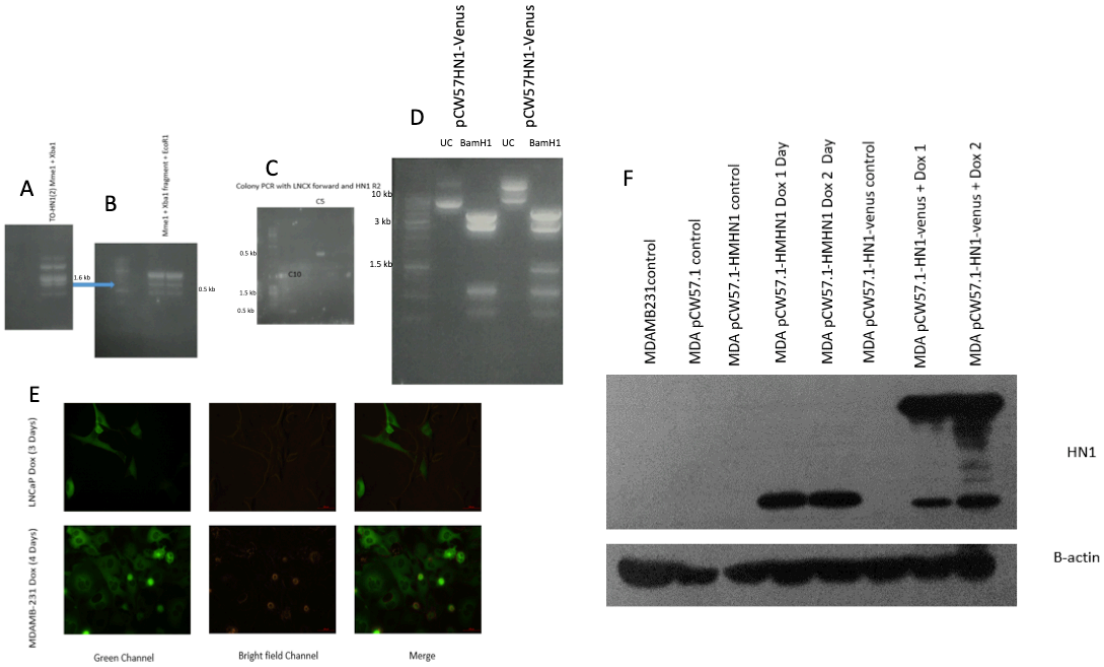

Figure 4.34: HN1-Venus insertion in pCW57 vector and validation by microscopy and western blotting. (A) pcDNA4-HN1-Venus was digested sequentially, first with Mme1 and Xba1, and (B) then with EcoR1 to obtain a 1.5 kb insert. (C) The colony PCR was performed with LNCX forward and HN1 reverse primers after ligation reaction containing the insert from (B) and vector used for preparing pCW57-HMHN1, was transformed into chemically competent bacteria. (D) The correct clone was then validated by propagating and isolating followed by restriction digestion with BamH1. (E) The LNCaP and MDA-MB231 cells transduced with pCW57-HN1-Venus lentiviral particles were observed under inverted microscope upon Doxycycline treatment. (E) The western blotting confirmed the HN1-Venus band as

observed in the size difference between HM-HN1 and HN1-Venus. β-actin was used a loading control for the experiment.

4.6.2. Effect Of *HN1* Overexpression Using pCW57-HN1-mVenus

The pCW57-mVenus control and pCW57-HN1-mVenus lentiviral particles were produced in HEK293T as described previously for pCW57-HMHN1 particles. Later, the mock control and HN1-mVenus containing particles were transduced into PC-3 cells to generate stable cell lines after selecting the transgene containing cells via puromycin selection procedure. The effect of HN1 localization and gain of function (overexpression) on CP110, cyclin F, and Geminin was determined using immunofluorescence assay. The control mVenus and HN1-mVenus under the influence of *tet O* were monitored upon Doxycycline induction (1 μg/ml). For CP110, cyclin F, and Geminin localization assay, PC3-pCW57-HN1-mVenus cells were plated on cover slides and were grown for 24 hours with or without Doxycycline. Upon completion of the treatment, cells were fixed with 4 % paraformaldehyde and subjected to cell permebilization and immunostaining. The primary antibodies against CP110, cyclin F, and Geminin were staining with secondary anti-mouse alexa fluor-594 antibodies. DAPI was used for nuclear staining. HN1-mVenus expression was induced in Doxycycline treated cells only. The cells stained with CP110 showed that, HN1-mVenus exhibiting cells stabilized CP110 with more polarized cells as compared to control cells with no HN1-mVenus (figure 4.35, upper panel). Furthermore, HN1-mVenus labeled cells illustrated a nuclear accumulation of cyclin F as compared to control cells without Doxycycline, where cyclin F is present in cytoplasm and nucleus (Figure 4.35, lower panel). Moreover, the HN1 overexpression marked through appearance of HN1-mVenus showed that ectopic HN1 containing cells showed reduced expression of Geminin in nucleus. The control cells without HN1-mVenus expressing cells had different populations of cells containing both high and low Geminin immunostained with anti-Geminin antibody. However, the PC3-pCW57-HN1-mVenus cells treated with Doxycycline, displayed two types of cellular populations, one with high HN1-mVenus and the other with low HN1-mVenus. It is clearly apparent that high HN1-mVenus exhibiting cells had lower Geminin levels as compared to low HN1-mVenus displaying cells, which showed higher Geminin intensity (figure 4.36).

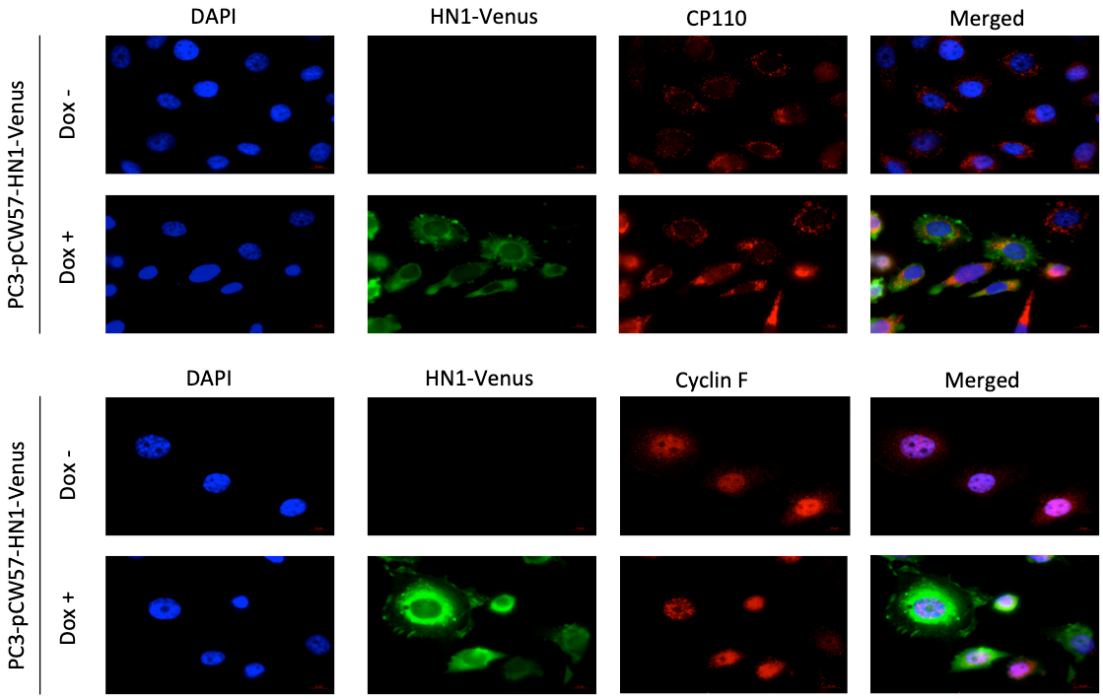

Figure 4.35: Effect of HN1-mVenus on CP110 and cyclin F using Doxycycline in Tet-inducible system. Immunofluorescence assay was performed to determine if HN1-mVenus alters the fluorescence intensity or localization of CP110 and cyclin F. The PC3-pCW57-HN1-mVenus cells were either treated with Doxycycline containing media (Dox +) or normal culture media (Dox -). The anti-CP110 and anti-cyclin F antibodies (produced in mouse) were used for immunostaining prior to secondary antibody (anti-mouse alexa fluor-594). Nuclei were staining using DAPI. The 480-channel shows the green fluorescent m-Venus fused at C-terminus of HN1.

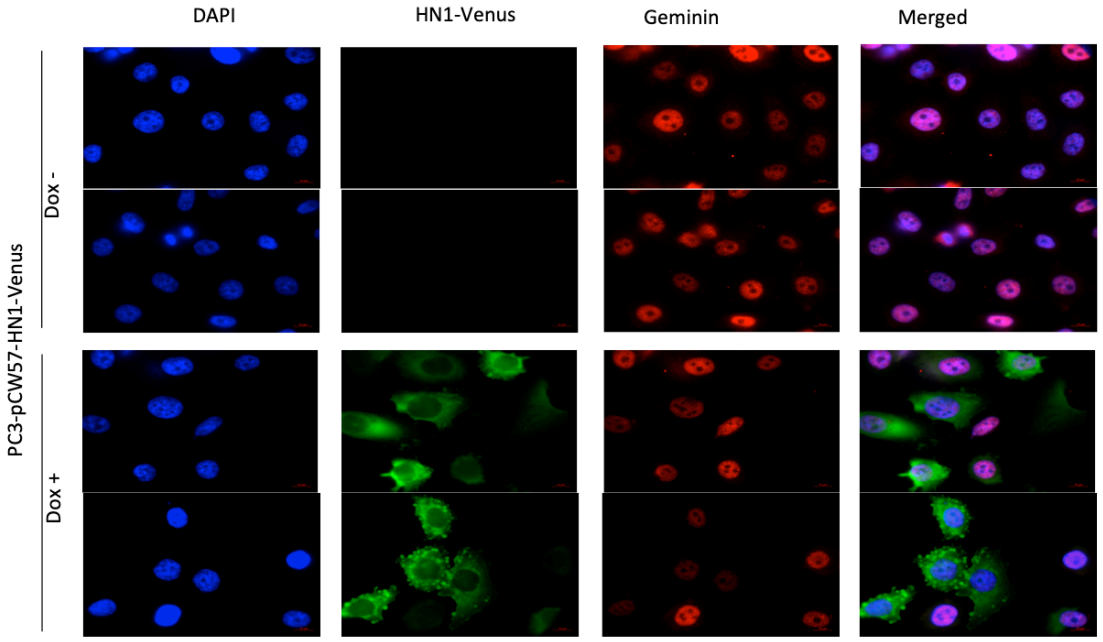

Figure 4.36: Effect of HN1-mVenus on Geminin using Doxycycline in Tet-inducible system. Immunofluorescence assay was performed to determine if HN1-mVenus alters the fluorescence intensity or localization of Geminin. The PC3-pCW57-HN1-mVenus cells were either treated with Doxycycline containing media (Dox +) or normal

culture media (Dox -). The anti-Geminin antibody (produced in mouse) was used for immunostaining prior to secondary antibody (anti-mouse alexa fluor-594). Nuclei were staining using DAPI. The 480-channel shows the green fluorescent m-Venus fused at C-terminus of HN1.

The invasion capability of *HN1* overexpressing cells was compared with control cells lacking ectopic HN1. HN1 expression was induced in PC3 cells by Doxycycline treatment. Control mock (empty vector particles) was used as a negative control. The impact of *HN1* overexpression on the invasiveness of PC3 cells was investigated by using a cell invasion assay in Boyden chambers. The cells were seeded on the upper chamber with 2% serum condition and the lower chamber contained higher 10% serum levels in the media to facilitate the invasion of cancer cells. The Doxycycline was treated for up to 5 days with media changes after 2 days. The cells invaded through the upper chamber were collected in the lower chamber and photographed after 48 hours and 120 hours of Doxycycline treatment for continuous overexpression of *HN1*. Figure 4.37 shows that HN1 overexpressed cells were higher in amount as compared to all the control cells included in the experimental design. The three controls of the experiment include parental PC3, PC3-pCW57 (mock control with empty lentiviral particles), and pCW57-Venus (only Venus expressing cells upon Doxycycline induction), showing significantly reduced cell invasion properties as compared to *HN1* overexpressed samples of PC3-pCW57-HMHN1 and PC3-pCW57-HN1-Venus. This leads to the conclusion that *HN1* overexpression in PC3 cells increases their invasive potential.

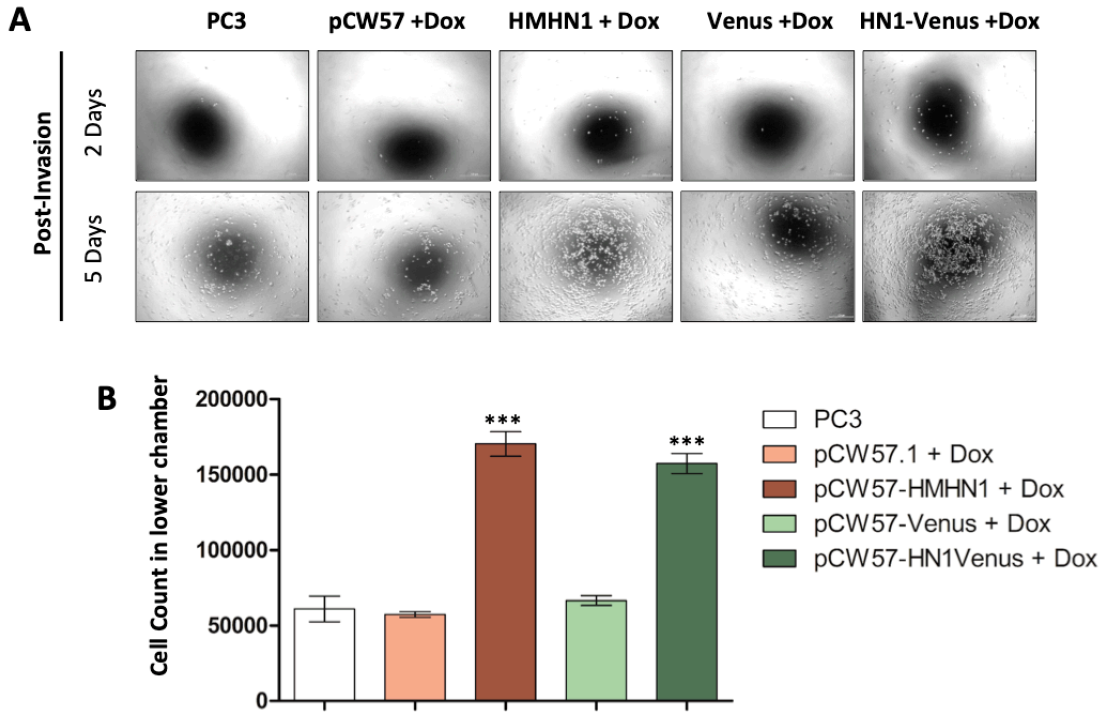

Figure 4.37: Effect of *HN1* overexpression on Invasion capability of PC3 cells was measured using cell invasion assay (A) HN1 inducible PC3 cells with either His-Max or Venus tag with appropriate mock controls were seeded on Boyden Chamber with 2% FBS in the upper chamber and 10% FBS in the lower chamber. Cells were cultured for indicated periods and photographed under an inverted microscope. (B) After 120 hours of culture in Boyden Chamber, cells in the lower chamber were trypsinized and counted to determine the change in viable cell count difference between mock controls and *HN1* overexpressed cells.

5. DISCUSSION

Prostate cancer is characterized by irregularities in genetic and epigenetic factors leading to uncontrolled growth of normal cells, which acquire the metastatic potential to cause damage to the body and even become lethal in many cases. The evolution of Prostate cancer results from changing paradigms of genomes and transcriptomes, providing survival advantage and genetic heterogeneity to promote tumorigenesis (Ren et al., 2018). There are many genes that are overexpressed in Prostate cancer and act as proto-oncogenes, which play vital roles in promoting the growth and metastasis of cancer. The major mechanisms controlled due to overexpression of function of such genes include the centrosome and cell cycle regulation, which are intricately intertwined with each other (Lin et al., 2022). The entry from G1 to the S phase marks the centriole duplication, which leads to centrosome pairs maturing and moving to opposite poles during the G2 and M-phase of the cell cycle. The equal distribution of chromosomes in daughter cells is ensured then by the spindle assembly in metaphase, and segregation of chromosomes in anaphase (Pancione et al., 2021). In many cancers including Prostate cancer, the centrosome errors have been linked to the genomic instability arising from aneuploidy and genomic catastrophes (Schatten & Ripple, 2018). Therefore, the cell cycle and centrosome components remain central to cancer biology research. There have been many factors explored in this area of research; however, there are still many unexplored factors that remain. Hematological and Neurological Expressed 1 (HN1) is a protein that was previously explored in Prostate cancer cell lines and found as a regulatory element of the Androgen receptor (Varisli et al., 2012). HN1 is also considered a tumorigenesis-promoting factor for other cancers. In Prostate cancer cell lines, HN1 further regulates the stability of the β-catenin-E-cadherin complex along with the Akt-mediated GSK3β signaling (Varisli et al., 2011; Varisli et al., 2015). In this study, we explored *in silico* and *in vitro* approaches to determine the role of HN1 in the cell cycle and centrosome in Prostate cancer.

5.1. HN1 Is A Disordered Protein Expressed Highly In Prostate Cancer

The lack of three-dimensional structure and any functional domain demonstrate the qualities of disordered proteins, which show a higher degree of post-translational modifications and are involved in various cell-signaling

pathways (Wright & Dyson, 2015). The protein sequence information of HN1 was used to determine the structure-related attributes, and it was observed that HN1 could be predicted as one of the intrinsically disordered proteins. The amino acid residues promoting disordered-ness were enriched in the HN1 protein sequence. It has been reported that intrinsically disordered proteins are involved in cell cycle regulation (Yoon et al., 2012). The structural flexibility of HN1 could be involved in determining the multi-functionality of HN1 as observed throughout this study. The high-throughput expression data that is available in online databases from various experiments can help determine the unknown factors in specific biological conditions (Rhodes et al., 2007). The *HN1* mRNA levels were increased in Prostate cancer samples, as compared to normal Prostate samples derived from the TCGA PRAD dataset. The overexpression of *HN1* could be due to the amplification mutations shown in different datasets of Prostate cancer available in the c-Bioportal database. Furthermore, *HN1* overexpression was correlated with a worse prognosis of Prostate cancer, implicating that HN1 functions in promoting the survival of Prostate cancer cells. The HN1 protein levels in normal Prostate epithelial cells (RWPE-1) were significantly lower as compared to cancerous LNCaP and PC-3 cells, as observed on western blots. Therefore, the *in silico* data showcasing the correlation of *HN1* expression with Prostate cancer was validated in *in vitro* models of Prostate cancer.

5.2. HN1 Is Involved In Regulating Centrosomes In Prostate Cancer

Cellular polarization and microtubule nucleation are well-established functions of centrosomes (Zyss & Gergely, 2009). The cellular stress responses along with the cytokinesis and cell cycle control are also some of the roles of centrosomes, which when become impaired lead to mitotic abnormalities (Fukasawa, 2011). The centrosome structural elements form the spatial organization of centrosomes through various protein binding regions and reside on centrosomes temporally in response to cell cycle-related changes (Blanco-Ameijeiras et al, 2022). The CoExpedia database covering hundreds of GEO datasets was explored to collect *HN1* co-expressed genes (Yang et al., 2017). The general co-expression network of *HN1* was enriched for centrosome, microtubule, spindle, midbody, and kinetochore as cellular compartments. The Prostate cancer-specific co-expression network further narrowed down the cellular components to

centrosomes and midbody along with kinetochore. The immunofluorescence assays determined that HN1 was co-localized with γ-tubulin in Prostate cancer cell lines such as DU-145 and PC-3. Therefore, HN1 is a partial centrosomal protein, which is physically associated with γ-tubulin, found at the core of centrosomes, as determined previously (Varisli, 2012). The biological processes of the *HN1* co-expression network in Prostate cancer were spindle organization, chromatid separation, APC/C processes, and mitotic cell division. HN1 depletion in DU-145 showed mitotic defects such as pseudo-bipolarity and mono-polar spindles. The centrosome duplication assay indicated that γ-tubulin foci multiplied and got scattered in HN1 depleted DU-145 cells, further implicating that HN1 regulates cell division by controlling the functions of centrosomes in Prostate cancer cells.

Centrosome abnormalities including numerical errors such as centrosome amplification are present in various cancers including Prostate cancer (Mittal et al., 2021). The tumorigenesis profile indicated from the increase in the proliferation rate of PC-3 cells upon *HN1* overexpression dictates that HN1 is involved in promoting the progression of cancer phenotype and the survival mechanisms of the cells. Cancer cells with amplified centrosomes tend to cluster the centrosomes to bypass the catastrophic effects of mitotic death or genomic instability beyond repair (Schatten & Ripple, 2018). HN1 depletion in PC-3 cells showcased the deregulated centrosomes indicated via γ-tubulin foci multiplication in the centrosome duplication assay. The *HN1* expression is therefore considered essential for centrosome integrity in Prostate cancer cells and HN1 rescue illustrated a different phenotype of clustered centrosomes. The microtubule nucleation and organization functions of centrosomes were also impaired as observed in HN1-altered cells suggesting that *HN1* promotes Prostate cancer as a function of its higher expression and spatially regulating centrosomes.

The HN1 co-expression network in Prostate cancer encompasses multiple centrosome pathway-related genes including surviving, *PLK1, AURKA, AURKB, BUB1, NEK2,* and *STMN1*. In this study, *HN1* overexpression resulted in increased PLK1 protein levels in normal RWPE-1 cells as opposed to decreased PLK1 in cancerous LNCaP and PC-3 cells. Furthermore, the impact of HN1 depletion on microtubule organization could be due to its interaction with microtubule depolymerization protein stathmin 1 (Pan et al., 2021), which is also

observed in *HN1* co-expression and interaction work from the Prostate cancer dataset. Therefore, HN1 functions in promoting Prostate cancer by deregulating PLK1 in advanced Prostate cancer cells. The stabilization of PLK1 in normal Prostate epithelial cells and destabilization in cancerous cells upon *HN1* overexpression could be due to differential activators present in different cells. The normal cells have active tumor suppressors such as p53, which are not functional in cancer cells, thereby might regulate HN1 function in different cells. Moreover, there is another family of genes enriched in the *HN1* co-expression network in Prostate cancer known as the kinesin family of genes. The kinesin family regulates the microtubule motor activity and is involved in various microtubule-related functions (Yu & Feng, 2010). Microtubule motors provide the driving force for clustering amplified centrosomes and therefore based on the observation that *HN1* co-expressed with these genes, it can be hypothesized that HN1 clusters centrosomes in Prostate cancer cells, by regulating the microtubule motor proteins such as KIFC1 and KIF14.

HN1 level alterations also had differential impacts on cell cycle distribution for other phases in different Prostate cell lines. *HN1* overexpression reduced G1 and increased G2-M and polyploidy cells in RWPE-1 cells. The lower expression of HN1 in RWPE-1 makes these cells an efficient candidate to study the impact of *HN1* overexpression. Furthermore, HN1 silencing arrested LNCaP, DU-145, and PC-3 cells in G1 and showed higher polyploidy than control cells. An increase in polyploidy revealed that HN1 is involved in regulating the genomic integrity of these cells. Polyploidy is known to result from centrosomal errors (Duensing & Duensing, 2010). Therefore, the evidence of the involvement of HN1 in centrosome and polyploidy mechanisms is apparent from this study. Moreover, CP110 is known to control the polyploidization as the suppression of CP110 phosphorylations have been reported to increase polyploidy (Chen et al., 2002). *HN1* overexpression using inducible expression system, demonstrated that an increase in stability of CP110, thereby showing that HN1 silencing and subsequent increase in polyploidy could be due to HN1 regulation of CP110. CP110 is regulated via cyclin F mediated ubiquitination and subsequent degradation by $SCF^{Cyclin\ F}$. Cyclin F is localized to cytoplasm and centrosomes in G2 phase and functions in degradaing CP110, however in G1 and S phase, cyclin F localizes to nucleus and remains unavailable on centrosomes to degrade CP110

(D'Angiolella et al., 2010; D'Angiolella et al., 2013). *HN1* overexpression leads to increased accumulation of cyclin F in nucleus, and therefore increased the stability of CP110, which is required for centrosome duplication and maturation, providing a potential mechanism for the regulation of centrosomes.

Previously, it has been demonstrated that increased phosphorylation of AKT^{S473} results from HN1 depletion which has been associated with chromosomal instability, and centrosome reduplication due to the activation of PI3K/AKT pathway (Varisli et al., 2011; Nam et al., 2010). Mono-polar spindles form due to misalignment of spindle caused by GSK3-β inhibition via AKT pathway (Wakefield et al., 2003). HN1 depletion caused similar phenotypes in metaphase DU-145 cells. GSK3-β mediated degradation of β-catenin is also known to irregularities in microtubule nucleation from γ-tubulin (Bahmanyar et al., 2010; Vora et al., 2020). A previous study also showed that HN1 depletion can result in stabilized β-catenin which could be the reason for nucleation-deficient centrosomes as observed in mono-polar spindle in DU-145 cells in this study. Moreover, the HN1 co-expressed PLK1 and NEK2 protein, as observed in *HN1* co-expression network could function as upstream kinases for HN1 to regulate the centrosome-related pathways. Thee mechanisms should be studied in detail in future.

5.3. HN1 Is A Cell Cycle Regulatory Protein In Prostate Cancer Cells

Cell cycle regulation is a mechanism, which is at the center of carcinogenesis as the cell cycle checkpoints are overhauled in cancers (Icard et al., 2019). During the progression of Prostate cancer, the cell cycle pathways are altered in a way that provides the proliferative advantage of Prostate cells, and even after chemotherapy Prostate cancer cells become independent of AR signaling for growth (Balk & Knudsen, 2008). There were many cell cycle-related genes in the *HN1* co-expression network in Prostate cancer including *CDC20, CCNB1, CDT1, ORC1,* and *CDC7* among others. The cell cycle synchronization approaches indicated that HN1 levels were enriched in S-phase and decreased in G2, and M phases, and remained lower in the G1 phase as well in LNCaP, LNCaP-104R2, and PC-3 cells. The overexpression of *HN1* also led to enriched S-phase populations in RWPE-1, LNCaP, DU-145, and PC-3 cells. This data

implies that HN1 functions specifically in the S phase and its levels fluctuate in the cell cycle.

The *HN1* overexpression, even though resulted in enriching S-phase populations in all Prostate cell lines, showed a differential response in altering the cell cycle-related proteins. In RWPE-1 and LNCaP cells, *HN1* overexpression positively correlates with cyclin E levels, and negatively correlated in PC-3 cells. It also increased cyclin A in RWPE-1 cells, but decreased it in PC-3 cells, showing that HN1 impacts the cell cycle differentially in different Prostate cells. Cyclin B was increased in RWPE-1 and LNCaP cells and decreased in PC-3 cells upon *HN1* overexpression. The CDK1 protein levels in RWPE-1 and PC-3 cells remained unchanged, while decreased in LNCaP cells. CDK2 levels increased in RWPE-1 and PC-3 cells and reduced in LNCaP cells. CDC20 was higher in *HN1* overexpressed RWPE-1 cells as compared to reduction in *HN1* overexpressed PC-3 cells, implying that HN1 regulates the cell cycle differentially in these cells. The replication control protein CDT1 was increased in *HN1* overexpressed RWPE-1 and PC-3 cells and reduced in LNCaP cells, further implying that HN1 could have a significant role in regulating replication as observed in S-phase enrichment of *HN1* overexpressed cells in cell cycle distribution analysis. An APC/C cofactor CDH1 also showed a higher protein level in RWPE-1 and was reduced in LNCaP and PC-3 cells when *HN1* was overexpressed. The mitotic marker $pH3^{S10}$ showed an increased expression in *HN1* overexpressed LNCaP and was reduced in PC-3 cells. HN1 exhibits a separate phosphorylated band in mitosis, which is absent in other phases of the cell cycle (Varisli et al., 2012). Therefore, HN1 is considered a novel cell cycle regulatory protein, which manifests significantly in S-phase and goes down in G2 and modified in mitosis, and remains lower in G1. The temporal reduction or degradation of HN1 protein coincides with the activity of APC/C at mitosis and therefore, the impact of HN1 on APC/C activity was then measured.

The APC/C^{CDC20} becomes active during mitosis and after cofactor exchange during metaphase to anaphase transition; APC/C^{CDH1} remains active throughout mitosis and G1 until the start of the S-phase. Therefore, the cell fate decisions of division and growth are preliminarily dependent on APC/C activity (Schrock et al., 2020). The APC/C activity can be derived for live cells using FUCCI technology, based on the APC/C^{CDH1} degron levels (Cappell et al., 2016). In our study, we also utilized FUCCI particles and generated stable FUCCI-PC3

cells and transfected them with *HN1* containing plasmid or lentiviral particles. It was observed that the indirect measure of APC/C activity remained higher in *HN1* overexpressing cells, implying that HN1 has a role in maintaining APC/C activity either directly or indirectly in Prostate cancer cells. Since HN1 native levels go down in G2 and M phases of the cell cycle, the tet-ON system was utilized to specifically induce HN1 in G2 phase. It was deduced that *HN1* overexpression before G2, results in S-phase enrichment, and HN1 induction after G2 using Nocodazole block, leads to an early exit from mitosis. The same experiment conducted in FUCCI-PC3 indicated that Cdt1 degron (G1 marker) bearing cells increased when *HN1* was overexpressed after G2. This data indicates that HN1 is a player in cell cycle regulation, which needs to be degraded in a temporal manner to delay the mitosis. HN1 phosphorylation and its impact on HN1 stability is yet to be explored, and can provide a mechanism for HN1 regulation in mitosis.

The control of DNA replication and genomic fidelity are regulated by different molecular pathways, which ensure the licensing of replication once per cell cycle (Diffley, 2010). One such mechanism involves the Geminin-Cdt1 complex, which functions as a switch for the regulation of the cell cycle. This molecular switch disables or enables the origin of replication to fire, for initiating DNA replication (Caillat & Perrakis, 2012). *HN1* overexpression in Tet-inducible HN1-mVenus exhibiting cells showed a decrease in Geminin levels. This data indicates another level of HN1 regulation of the cell cycle. It has long been known that Geminin suppression especially in the absence of p53 results in re-replication of DNA (Melixetian et al., 2004), therefore HN1 could be at the barrier between p53 and Geminin for regulating the cell cycle as p53 exhibiting cells such as RWPE-1 lack HN1 and p53 deficient cells such as PC-3 show higher levels of HN1. This further implies that *HN1* overexpressed p53 deficient cells, showcasing suppressed Geminin levels, might lead to polyploidy as evidenced by the cell cycle distribution analysis of HN1 altered cells. This mechanism needs to be explored further by mechanistic studies.

5.4. *HN1* Overexpression Promotes Tumorigenic Profile Of PC-3 Cells

The proliferation rate indicates the normal rate of cell division and multiplication of cells in cell culture conditions and can be used to determine the impact of exogenous agents on the cellular metabolism and overall health of the

cells. The HN1 level alterations led to differential responses in different Prostate cells. The HN1 silencing using siRNA technology did not alter the proliferation rate of normal Prostate RWPE-1 cells. It could due to the fact that these cells exhibit very lower levels of native HN1 protein levels. However, *HN1* overexpression in normal cells of the Prostate reduced the proliferation rate. In androgen insensitive LNCaP cells, both HN1 depletion and *HN1* overexpression reduced the proliferation rate of the cells, showcasing that HN1 is tightly controlled in these cells, and it has been proposed previously that HN1 is involved in the proteasomal degradation of AR (Varisli et al., 2012). However, in androgen insensitive Prostate cancer cells, HN1 depletion led to reduced proliferation and this effect was the opposite in HN1 overexpressed cells. This data indicates that HN1 is influenced by the activity of AR and the cellular profiles, further validated by differences in native protein levels of HN1 in these cell lines. HN1 native protein levels are shown as stabilized in LNCaP- LNCaP-104R2, and DU-145 for a longer duration as compared to PC-3 cells, where the half-life of HN1 is significantly lower. The *HN1* overexpression in HN1-inducible Tet-ON system also showed similar results, where *HN1* overexpressed cells showed reduced proliferation rate in LNCaP cells, which was increased in PC-3 cells along with the reduction of Cyclin B1 levels in PC-3 cells.

The evasion of apoptosis has long been termed a central hallmark of cancer, and in Prostate cancer, the signaling pathways leading to programmed-cell death are also significantly altered (Campbell & Leung, 2021). In this study, various apoptosis inducing chemical inhibitors targeting different cellular mechanisms were utilized to kill PC-3 cells and compared the apoptosis and necrosis rate of *HN1*-overexpressing and control cells. HN1 induction reduced the apoptotic populations in Actinomycin D, PI3K inhibitor, Trichostatin A, Flavopiridol, and Camptothecin treated cells. Furthermore, HN1 induced also reduced necrotic populations in EGFR inhibitor, Cytochalasin D, Sirtinol, and Trichostatin A (TCA) treated cells. The inhibition of Histone Deacetylase via Trichostatin A showcased a dramatically stabilized HN1 protein levels, implicating that HN1 could be transcriptionally regulated by Histone Deacetylases. Moreover, the pro-apoptotic Bax was reduced in *HN1* overexpressing cells treated with apoptotic inducers such as Doxorubicin, Etoposide, TCA, PI3Ki, and Cytochalasin D. Therefore, it can be deduced that

HN1 plays a survival promoting role in PC-3 cells against cell death. *HN1* overexpression Prostate tissues along with this data demonstrate that HN1 promotes Prostate cancer via apoptosis evading mechanisms.

The progression of Prostate cancer is also correlated with the metastasis originating from increased epithelial to mesenchymal transition, cell motility, invasion, migration, and other key biological events regulating these mechanisms (Datta et al., 2016). The Tet-inducible system also illustrated that *HN1* overexpression upon Doxycycline induction increases the migration and invasion capabilities of PC-3 cells. Therefore, *HN1* being a proto-oncogene by virtue to its overexpression in Prostate cancer, provide the tools of increased evasion from apoptosis, higher migration and invasion capability for the progression of Prostate cancer. The increased proliferative advantage in androgen insensitive cells along with the altered cell cycle pathways and centrosome clustering are also correlated with the *HN1* overexpression.

6. CONCLUSION AND FUTURE RECOMMENDATIONS

Here, we attempted to showcase the role of *HN1* in the development of Prostate cancer by using different Prostate cell lines. We also utilized *HN1* co-expression networks obtained from transcriptomics databases to evaluate the function of *HN1* in the context of Prostate cancer. The *in silico* studies showed that HN1 is a putative disordered protein that could be localized to the centrosome and have a role in regulating cell cycle and centrosome-related pathways. The *HN1* overexpression and silencing by DNA transfections resulted in a differential response for cellular proliferation and cell cycle distribution in Prostate epithelial cells (RWPE1), androgen-sensitive Prostate cancer cells (LNCaP), and androgen insensitive Prostate cancer cells (DU-145 and PC-3). *HN1* overexpression enriched S-phase populations in all Prostate cells. *HN1* overexpression increased the cyclin E, cyclin A, and cyclin B in normal RWPE1 cells, however, the protein levels of these cyclins decreased when *HN1* was overexpressed in aggressive Prostate cancer PC-3 cells. Therefore, it can be deduced that HN1 is a cell cycle regulatory protein. Moreover, native HN1 expression is considerably higher in cancer cells as compared to normal epithelial cells further demonstrating that HN1 is a cancer-related protein.

Our findings suggest that *HN1* silencing leads to centrosome multiplication defects as observed in amplified γ-tubulin foci in DU-145 and PC-3 cells. The native HN1 protein levels also fluctuate during the cell cycle with the highest protein levels observed in S-phase. The Tet-ON inducible *HN1* expression system was applied to determine the impact of HN1 rescue after silencing in PC-3 cells. HN1 rescue experiment illustrated that HN1 could be a centrosome clustering protein, a mechanism, utilized by cancer cells to survive the lethal effects of centrosome amplification. This study also reported that *HN1* promotes the survival of cancer cells by reducing the expression of pro-apoptotic Bax protein as indicated in samples treated with apoptosis-inducing reagents. *HN1* overexpression after the G2 phase exhibited an early exit from mitosis observed in Fluorescent Ubiquitination Cell Cycle Indicator (FUCCI) carrying FUCCI-PC3 cells. Moreover, *HN1* ORF was fused with Venus fluorescent protein in the Tet-ON system to study the HN1 localization and HN1 seems to occupy the perinuclear boundary and is diffused in the cytoplasm. *HN1* overexpression resulted in

increased migration and invasion in PC-3 cells, implicating the oncogenic effects of *HN1*. *HN1* overexpression provided survival-promoting phenotypes to Prostate cancer cells such as increased proliferation rate, centrosome clustering, evasion from apoptosis, and increased invasion and migration. In summation, our study placed *HN1* as a Prostate cancer-specific gene being overexpressed in Prostate cancer, which potentially functions in S-phase and is responsible for genomic and mitotic fidelity.

In the future, HN1 interactions with major cell cycle and centrosome pathway regulating complexes including APC/C components using immunoprecipitations must be explored for the mechanistic role of HN1. HN1 degradation in the cell cycle using transfections, cell cycle synchronization, and ubiquitination analysis can be performed for further characterization of HN1. HN1 is a carcinogenic protein that manifests in cancer cells therefore; the role of HN1 in the context of p53 should also be monitored. This study mostly reported the gain of function effects of HN1 in the context of the cell cycle. HN1 loss of function effects using shRNA particles targeting coding sequence of *HN1* mRNA or untranslated regions of *HN1* mRNA, and *HN1 mutants* can be utilized for exploring the centrosome and cell cycle-related role of HN1 further.

REFERENCES

Abida, W., Armenia, J., Gopalan, A., Brennan, R., Walsh, M., Barron, D., ... & Scher, H. I. 2017. Prospective genomic profiling of Prostate cancer across disease states reveals germline and somatic alterations that may affect clinical decision making. *JCO precision oncology*, *1*, 1-16.

Adams, E. J., Karthaus, W. R., Hoover, E., Liu, D., Gruet, A., Zhang, Z., ... & Sawyers, C. L. 2019. FOXA1 mutations alter pioneering activity, differentiation and Prostate cancer phenotypes. *Nature*, *571*(7765), 408-412.

Agircan, F. G., Schiebel, E., & Mardin, B. R. 2014. Separate to operate: control of centrosome positioning and separation. *Philosophical Transactions of the Royal Society B: Biological Sciences*, *369*(1650), 20130461.

Alberts, B., Johnson, A., Lewis, J., Raff, M., Roberts, K., & Walter, P. 2002. An overview of the cell cycle. *Molecular Biology of the Cell. 4th edition*.

Antonarakis, E. S., Armstrong, A. J., Dehm, S. M., & Luo, J. 2016. Androgen receptor variant-driven Prostate cancer: clinical implications and therapeutic targeting. *Prostate cancer and prostatic diseases*, *19*(3), 231-241.

Arias, E. E., & Walter, J. C. 2007. Strength in numbers: preventing rereplication via multiple mechanisms in eukaryotic cells. *Genes & development*, *21*(5), 497-518.

Armenia, J., Wankowicz, S. A., Liu, D., Gao, J., Kundra, R., Reznik, E., ... & Van Allen, E. M. 2018. The long tail of oncogenic drivers in Prostate cancer. *Nature genetics*, *50*(5), 645-651.

Arquint, C., & Nigg, E. A. 2016. The PLK4–STIL–SAS-6 module at the core of centriole duplication. *Biochemical Society Transactions*, *44*(5), 1253-1263.

Asghar, U., Witkiewicz, A. K., Turner, N. C., & Knudsen, E. S. 2015. The history and future of targeting cyclin-dependent kinases in cancer therapy. *Nature reviews Drug discovery*, *14*(2), 130-146.

Bahmanyar, S., Guiney, E. L., Hatch, E. M., Nelson, W. J., & Barth, A. I. 2010. Formation of extra centrosomal structures is dependent on β-catenin. *Journal of cell science*, *123*(18), 3125-3135.

Balk, S. P., & Knudsen, K. E. 2008. AR, the cell cycle, and Prostate cancer. *Nuclear receptor signaling*, *6*(1), nrs-06001.

Banerjee, P. P., Banerjee, S., Brown, T. R., & Zirkin, B. R. 2018. Androgen action in Prostate function and disease. *American journal of clinical and experimental urology*, *6*(2), 62.

Banterle, N., & Gönczy, P. 2017. Centriole biogenesis: from identifying the characters to understanding the plot. *Annual review of cell and developmental biology*, *33*, 23-49.

Barford, D. 2011. Structure, function and mechanism of the anaphase promoting complex (APC/C). *Quarterly reviews of biophysics*, *44*(2), 153-190.

Barger, C. J., Zhang, W., Hillman, J., Stablewski, A. B., Higgins, M. J., Vanderhyden, B. C., ... & Karpf, A. R. 2015. Genetic determinants of FOXM1 overexpression in epithelial ovarian cancer and functional contribution to cell cycle progression. *Oncotarget*, *6*(29), 27613.

Barsouk, A., Padala, S. A., Vakiti, A., Mohammed, A., Saginala, K., Thandra, K. C., ... & Barsouk, A. 2020. Epidemiology, staging and management of Prostate cancer. *Medical Sciences*, *8*(3), 28.

Bashir, T., Dorrello, N. V., Amador, V., Guardavaccaro, D., & Pagano, M. 2004. Control of the SCFSkp2–Cks1 ubiquitin ligase by the APC/CCdh1 ubiquitin ligase. *Nature*, *428*(6979), 190-193.

Bashir, T., Dorrello, N. V., Amador, V., Guardavaccaro, D., & Pagano, M. 2004. Control of the SCFSkp2–Cks1 ubiquitin ligase by the APC/CCdh1 ubiquitin ligase. *Nature*, *428*(6979), 190-193.

Bateman, N. W., Teng, P. N., Hope, E., Hood, B. L., Oliver, J., Ao, W., ... & Conrads, T. P. 2020. Jupiter microtubule‐associated homolog 1 (JPT1): A predictive and pharmacodynamic biomarker of metformin response in endometrial cancers. *Cancer medicine*, *9*(3), 1092-1103.

Baugh, E. H., Lyskov, S., Weitzner, B. D., & Gray, J. J. 2011. Real-time PyMOL visualization for Rosetta and PyRosetta. *PloS one*, *6*(8), e21931.

Beltran, H., Rickman, D. S., Park, K., Chae, S. S., Sboner, A., MacDonald, T. Y., ... & Rubin, M. A. 2011. Molecular characterization of neuroendocrine Prostate cancer and identification of new drug targets. *Cancer discovery*, *1*(6), 487-495.

Ben-Salem, S., & Venkadakrishnan, V. B. 2021. Novel insights in cell cycle dysregulation during Prostate cancer progression. *Endocrine-related cancer*, *28*(6), R141-R155.

Bensimon, A., Aebersold, R., & Shiloh, Y. 2011. Beyond ATM: the protein kinase landscape of the DNA damage response. *FEBS letters*, *585*(11), 1625-1639.

Blackburn, J., Vecchiarelli, S., Heyer, E. E., Patrick, S. M., Lyons, R. J., Jaratlerdsiri, W., ... & Hayes, V. M. 2019. TMPRSS2‐ERG fusions linked to Prostate cancer racial health disparities: A focus on Africa. *The Prostate*, *79*(10), 1191-1196.

Blanco-Ameijeiras, J., Lozano-Fernández, P., & Martí, E. 2022. Centrosome maturation–in tune with the cell cycle. *Journal of Cell Science*, *135*(2), jcs259395.

Blattner, M., Liu, D., Robinson, B. D., Huang, D., Poliakov, A., Gao, D., ... & Barbieri, C. E. 2017. SPOP mutation drives Prostate tumorigenesis in vivo through coordinate regulation of PI3K/mTOR and AR signaling. *Cancer cell*, *31*(3), 436-451.

Bonollo, F., Thalmann, G. N., Kruithof-de Julio, M., & Karkampouna, S. 2020. The role of cancer-associated fibroblasts in Prostate cancer tumorigenesis. *Cancers*, *12*(7), 1887.

Bose, A., & Dalal, S. N. 2019. Centrosome amplification and tumorigenesis: cause or effect?. *The Golgi Apparatus and Centriole*, 413-440.

Brownlee, C. W., & Rogers, G. C. 2013. Show me your license, please: deregulation of centriole duplication mechanisms that promote amplification. *Cellular and Molecular Life Sciences*, *70*(6), 1021-1034.

Caillat, C., & Perrakis, A. 2012. Cdt1 and Geminin in DNA replication initiation. *The Eukaryotic Replisome: a Guide to Protein Structure and Function*, 71-87.

Campbell, K. J., & Leung, H. Y. 2021. Evasion of cell death: A contributory factor in Prostate cancer development and treatment resistance. *Cancer Letters*, *520*, 213-221.

Cappell, S. D., Chung, M., Jaimovich, A., Spencer, S. L., & Meyer, T. 2016. Irreversible APC^{Cdh1} inactivation underlies the point of no return for cell-cycle entry. *Cell*, *166*(1), 167-180.

Carlton, J. G., Jones, H., & Eggert, U. S. 2020. Membrane and organelle dynamics during cell division. *Nature Reviews Molecular Cell Biology*, *21*(3), 151-166.

Carver, B. S., Chapinski, C., Wongvipat, J., Hieronymus, H., Chen, Y., Chandarlapaty, S., ... & Sawyers, C. L. 2011. Reciprocal feedback regulation of PI3K and androgen receptor signaling in PTEN-deficient Prostate cancer. *Cancer cell*, *19*(5), 575-586.

Carver, B. S., Tran, J., Chen, Z., Carracedo-Perez, A., Alimonti, A., Nardella, C., ... & Pandolfi, P. P. 2009. ETS rearrangements and Prostate cancer initiation. *Nature*, *457*(7231), E1-E1.

Chan, J. Y. 2011. A clinical overview of centrosome amplification in human cancers. *International journal of biological sciences*, *7*(8), 1122.

Chan, S. C., & Dehm, S. M. 2014. Constitutive activity of the androgen receptor. *Advances in pharmacology*, *70*, 327-366.

Chang, D. C., Xu, N., & Luo, K. Q. 2003. Degradation of cyclin B is required for the onset of anaphase in Mammalian cells. *Journal of Biological Chemistry*, *278*(39), 37865-37873.

Chen, J. J., Sun, X., Mao, Q. Q., Jiang, X. Y., Zhao, X. G., Xu, W. J., & Zhong, L. 2020. Increased expression of hematological and neurological expressed 1 (HN1) is associated with a poor prognosis of hepatocellular carcinoma and its knockdown inhibits cell growth and migration partly by down‐regulation of c‐Met. *The Kaohsiung Journal of Medical Sciences*, *36*(3), 196-205.

Chen, J., Qiu, J., Li, F., Jiang, X., Sun, X., Zheng, L., ... & Zhang, Y. 2020. HN1 promotes tumor associated lymphangiogenesis and lymph node metastasis via NF-κB signaling activation in cervical carcinoma. *Biochemical and Biophysical Research Communications*, *530*(1), 87-94.

Chen, Z., Indjeian, V. B., McManus, M., Wang, L., & Dynlacht, B. D. 2002. CP110, a cell cycle-dependent CDK substrate, regulates centrosome duplication in human cells. *Developmental cell*, *3*(3), 339-350.

Cheng, H. H., Sokolova, A. O., Schaeffer, E. M., Small, E. J., & Higano, C. S. 2019. Germline and somatic mutations in Prostate cancer for the clinician. *Journal of the National Comprehensive Cancer Network*, *17*(5), 515-521.

Cheng, Y., Xiong, H. Y., Li, Y. M., Zuo, H. R., Liu, Y., & Liao, G. L. 2021. LncRNA HOXA11-AS promotes cell growth by sponging miR-24-3p to regulate JPT1 in Prostate cancer. *European Review for Medical and Pharmacological Sciences*, *25*(14), 4668-4677.

Chi, Y., Carter, J. H., Swanger, J., Mazin, A. V., Moritz, R. L., & Clurman, B. E. 2020. A novel landscape of nuclear human CDK2 substrates revealed by in situ phosphorylation. *Science advances*, *6*(16), eaaz9899.

Chow, J. P., Poon, R. Y., & Ma, H. T. 2011. Inhibitory phosphorylation of cyclin-dependent kinase 1 as a compensatory mechanism for mitosis exit. *Molecular and cellular biology*, *31*(7), 1478-1491.

Cimini, D. 2008. Merotelic kinetochore orientation, aneuploidy, and cancer. *Biochimica et Biophysica Acta (BBA)-Reviews on Cancer*, *1786*(1), 32-40.

Clijsters, L., Hoencamp, C., Calis, J. J., Marzio, A., Handgraaf, S. M., Cuitino, M. C., ... & Pagano, M. 2019. Cyclin F controls cell-cycle transcriptional outputs by directing the degradation of the three activator E2Fs. *Molecular cell*, *74*(6), 1264-1277.

Coelho, P. A., Bury, L., Shahbazi, M. N., Liakath-Ali, K., Tate, P. H., Wormald, S., ... & Glover, D. M. 2015. Over-expression of Plk4 induces centrosome amplification, loss of primary cilia and associated tissue hyperplasia in the mouse. *Open biology*, *5*(12), 150209.

Cosenza, M. R., & Krämer, A. 2016. Centrosome amplification, chromosomal instability and cancer: mechanistic, clinical and therapeutic issues. *Chromosome research*, *24*(1), 105-126.

Crasta, K., Lim, H. H., Giddings, T. H., Winey, M., & Surana, U. 2008. Inactivation of Cdh1 by synergistic action of Cdk1 and polo kinase is necessary for proper assembly of the mitotic spindle. *Nature cell biology*, *10*(6), 665-675.

D'Angiolella, V., Donato, V., Forrester, F. M., Jeong, Y. T., Pellacani, C., Kudo, Y., ... & Pagano, M. 2012. Cyclin F-mediated degradation of ribonucleotide reductase M2 controls genome integrity and DNA repair. *Cell*, *149*(5), 1023-1034.

D'Angiolella, V., Donato, V., Vijayakumar, S., Saraf, A., Florens, L., Washburn, M. P., ... & Pagano, M. 2010. $SCF^{Cyclin\ F}$ controls centrosome homeostasis and mitotic fidelity through CP110 degradation. *Nature*, *466*(7302), 138-142.

D'Angiolella, V., Esencay, M., & Pagano, M. 2013. A cyclin without cyclin-dependent kinases: cyclin F controls genome stability through ubiquitin-mediated proteolysis. *Trends in cell biology*, *23*(3), 135-140.

Dang, F., Nie, L., & Wei, W. 2021. Ubiquitin signaling in cell cycle control and tumorigenesis. *Cell Death & Differentiation*, *28*(2), 427-438.

Dankert, J. F., Rona, G., Clijsters, L., Geter, P., Skaar, J. R., Bermudez-Hernandez, K., ... & Pagano, M. 2016. Cyclin F-mediated degradation of SLBP limits H2A. X accumulation and apoptosis upon genotoxic stress in G2. *Molecular cell*, *64*(3), 507-519.

Datta, D., Aftabuddin, M., Gupta, D. K., Raha, S., & Sen, P. 2016. Human Prostate cancer hallmarks map. *Scientific reports*, *6*(1), 1-14.

Diffley, J. F. X. 2010 January. The many faces of redundancy in DNA replication control. In *Cold Spring Harbor symposia on quantitative biology* (Vol. 75, pp. 135-142). Cold Spring Harbor Laboratory Press.

Ding, L., Cao, J., Lin, W., Chen, H., Xiong, X., Ao, H., ... & Cui, Q. 2020. The roles of cyclin-dependent kinases in cell-cycle progression and therapeutic strategies in human breast cancer. *International journal of molecular sciences*, *21*(6), 1960.

Ditano, J. P., Sakurikar, N., & Eastman, A. 2021. Activation of CDC25A phosphatase is limited by CDK2/cyclin A-mediated feedback inhibition. *Cell Cycle*, *20*(13), 1308-1319.

Duensing, A., & Duensing, S. 2010. Centrosomes, polyploidy and cancer. *Polyploidization and Cancer*, 93-103.

Ekholm, S. V., & Reed, S. I. 2000. Regulation of G1 cyclin-dependent kinases in the mammalian cell cycle. *Current opinion in cell biology*, *12*(6), 676-684.

Facchini, L. M., & Penn, L. Z. 1998. The molecular role of Myc in growth and transformation: recent discoveries lead to new insights. *The FASEB Journal*, *12*(9), 633-651.

Faggioli, F., Vezzoni, P., & Montagna, C. 2011. Single-cell analysis of ploidy and centrosomes underscores the peculiarity of normal hepatocytes. *PloS one*, *6*(10), e26080.

Fan, G., Sun, L., Meng, L., Hu, C., Wang, X., Shi, Z., ... & Wang, C. 2021. The ATM and ATR kinases regulate centrosome clustering and tumor recurrence by targeting KIFC1 phosphorylation. *Nature Communications*, *12*(1), 1-16.

Filella, X., Fernández-Galan, E., Bonifacio, R. F., & Foj, L. 2018. Emerging biomarkers in the diagnosis of Prostate cancer. *Pharmacogenomics and personalized medicine*, *11*, 83.

Fine, S. W., & Reuter, V. E. 2012. Anatomy of the Prostate revisited: implications for Prostate biopsy and zonal origins of Prostate cancer. *Histopathology*, *60*(1), 142-152.

Fırat-Karalar, E. N., & Stearns, T. 2014. The centriole duplication cycle. *Philosophical Transactions of the Royal Society B: Biological Sciences*, *369*(1650), 20130460.

Fraser, M., Sabelnykova, V. Y., Yamaguchi, T. N., Heisler, L. E., Livingstone, J., Huang, V., ... & Boutros, P. C. 2017. Genomic hallmarks of localized, non-indolent Prostate cancer. *Nature*, *541*(7637), 359-364.

Fukasawa, K. 2011. Aberrant activation of cell cycle regulators, centrosome amplification, and mitotic defects. *Hormones and Cancer*, *2*(2), 104-112.

Gao, J., Aksoy, B. A., Dogrusoz, U., Dresdner, G., Gross, B., Sumer, S. O., ... & Schultz, N. 2013. Integrative analysis of complex cancer genomics and clinical profiles using the cBioPortal. *Science signaling*, *6*(269), pl1-pl1.

Gavet, O., & Pines, J. 2010. Progressive activation of CyclinB1-Cdk1 coordinates entry to mitosis. *Developmental cell*, *18*(4), 533-543.

Giacinti, C., & Giordano, A. 2006. RB and cell cycle progression. *Oncogene*, *25*(38), 5220-5227.

Godinho, S. A., & Pellman, D. 2014. Causes and consequences of centrosome abnormalities in cancer. *Philosophical Transactions of the Royal Society B: Biological Sciences*, *369*(1650), 20130467.

Godinho, S. A., Kwon, M., & Pellman, D. 2009. Centrosomes and cancer: how cancer cells divide with too many centrosomes. *Cancer and Metastasis Reviews*, *28*(1), 85-98.

Godinho, S. A., Picone, R., Burute, M., Dagher, R., Su, Y., Leung, C. T., ... & Pellman, D. 2014. Oncogene-like induction of cellular invasion from centrosome amplification. *Nature*, *510*(7503), 167-171.

Gong, D., & Ferrell Jr, J. E. 2010. The roles of cyclin A2, B1, and B2 in early and late mitotic events. *Molecular biology of the cell*, *21*(18), 3149-3161.

Gossen, M., & Bujard, H. 1992. Tight control of gene expression in mammalian cells by tetracycline-responsive promoters. *Proceedings of the National Academy of Sciences*, *89*(12), 5547-5551.

Gossen, M., Freundlieb, S., Bender, G., Müller, G., Hillen, W., & Bujard, H. 1995. Transcriptional activation by tetracyclines in mammalian cells. *Science*, *268*(5218), 1766-1769.

Grasso, C. S., Wu, Y. M., Robinson, D. R., Cao, X., Dhanasekaran, S. M., Khan, A. P., ... & Tomlins, S. A. 2012. The mutational landscape of lethal castration-resistant Prostate cancer. *Nature*, *487*(7406), 239-243.

Guderian, G., Westendorf, J., Uldschmid, A., & Nigg, E. A. 2010. Plk4 trans-autophosphorylation regulates centriole number by controlling βTrCP-mediated degradation. *Journal of cell science*, *123*(13), 2163-2169.

Hagting, A., Den Elzen, N., Vodermaier, H. C., Waizenegger, I. C., Peters, J. M., & Pines, J. 2002. Human securin proteolysis is controlled by the

spindle checkpoint and reveals when the APC/C switches from activation by Cdc20 to Cdh1. *The Journal of cell biology*, *157*(7), 1125-1137.

Hoffmann, I. 2021. Centrosomes in mitotic spindle assembly and orientation. *Current Opinion in Structural Biology*, *66*, 193-198.

Hubbard, G. K., Mutton, L. N., Khalili, M., McMullin, R. P., Hicks, J. L., Bianchi-Frias, D., ... & Bieberich, C. J. 2016. Combined MYC activation and Pten loss are sufficient to create genomic instability and lethal metastatic Prostate cancer. *Cancer research*, *76*(2), 283-292.

Icard, P., Fournel, L., Wu, Z., Alifano, M., & Lincet, H. 2019. Interconnection between metabolism and cell cycle in cancer. *Trends in biochemical sciences*, *44*(6), 490-501.

Inoue, H., Nojima, H., & Okayama, H. 1990. High efficiency transformation of Escherichia coli with plasmids. *Gene*, *96*(1), 23-28.

Inoue, H., Sawada, M., Ryo, A., Tanahashi, H., Wakatsuki, T., Hada, A., ... & Yamamoto, M. 1999. Serial analysis of gene expression in a microglial cell line. *Glia*, *28*(3), 265-271.

Jana, S. C. 2021, February. Centrosome structure and biogenesis: Variations on a theme?. In *Seminars in cell & developmental biology* (Vol. 110, pp. 123-138). Academic Press.

Janssen, A., van der Burg, M., Szuhai, K., Kops, G. J., & Medema, R. H. 2011. Chromosome segregation errors as a cause of DNA damage and structural chromosome aberrations. *Science*, *333*(6051), 1895-1898.

Jewett, C. E., & Pearson, C. G. 2021. Cancer biology: Messages in extracellular vesicles depend on centrosome number. *Current Biology*, *31*(7), R337-R340.

Jia, Q., Nie, H., Yu, P., Xie, B., Wang, C., Yang, F., ... & Ni, T. 2019. HNRNPA1-mediated 3′ UTR length changes of HN1 contributes to cancer-and senescence-associated phenotypes. *Aging (Albany NY)*, *11*(13), 4407.

Junior, J. P., Srougi, M., Borra, P. M., Dall'Oglio, M. F., Ribeiro-Filho, L. A., & Leite, K. R. 2010. E-cadherin and β-catenin loss of expression related to bone metastasis in Prostate cancer. *Applied Immunohistochemistry & Molecular Morphology*, *18*(2), 179-184.

Kalikin, L. M., George, R. A. V., Keller, M. P., Bort, S., Bowler, N. S., Law, D. J., ... & Petty, E. M. 1999. An integrated physical and gene map of human distal chromosome 17q24–proximal 17q25 encompassing multiple disease loci. *Genomics*, *57*(1), 36-42.

Kalkan, B. M., Ozcan, S. C., Quintyne, N. J., Reed, S. L., & Acilan, C. 2022. Keep Calm and Carry on with Extra Centrosomes. *Cancers*, *14*(2), 442.

Kallunki, T., Barisic, M., Jäättelä, M., & Liu, B. 2019. How to choose the right inducible gene expression system for mammalian studies?. *Cells*, *8*(8), 796.

Ko, M. S., Kitchen, J. R., Wang, X., Threat, T. A., Hasegawa, A., Sun, T., ... & Sano, Y. 2000. Large-scale cDNA analysis reveals phased gene expression patterns during preimplantation mouse development. *Development*, *127*(8), 1737-1749.

Kohlmaier, G., Lončarek, J., Meng, X., McEwen, B. F., Mogensen, M. M., Spektor, A., ... & Gönczy, P. 2009. Overly long centrioles and defective cell division upon excess of the SAS-4-related protein CPAP. *Current Biology*, *19*(12), 1012-1018.

Koniaras, K., Cuddihy, A. R., Christopoulos, H., Hogg, A., & O'Connell, M. J. 2001. Inhibition of Chk1-dependent G2 DNA damage checkpoint radiosensitizes p53 mutant human cells. *Oncogene*, *20*(51), 7453-7463.

Krämer, A., Maier, B., & Bartek, J. 2011. Centrosome clustering and chromosomal (in) stability: a matter of life and death. *Molecular oncology*, *5*(4), 324-335.

Krupina, K., Goginashvili, A., & Cleveland, D. W. 2021. Causes and consequences of micronuclei. *Current Opinion in Cell Biology*, *70*, 91-99.

Kulukian, A., Holland, A. J., Vitre, B., Naik, S., Cleveland, D. W., & Fuchs, E. 2015. Epidermal development, growth control, and homeostasis in the face of centrosome amplification. *Proceedings of the National Academy of Sciences*, *112*(46), E6311-E6320.

Kushner, E. J., Ferro, L. S., Yu, Z., & Bautch, V. L. 2016. Excess centrosomes perturb dynamic endothelial cell repolarization during blood vessel formation. *Molecular biology of the cell*, *27*(12), 1911-1920.

Kwon, M., Godinho, S. A., Chandhok, N. S., Ganem, N. J., Azioune, A., Thery, M., & Pellman, D. 2008. Mechanisms to suppress multipolar divisions in cancer cells with extra centrosomes. *Genes & development*, *22*(16), 2189-2203.

Lamb, A. D., Massie, C. E., & Neal, D. E. 2014. The transcriptional programme of the androgen receptor (AR) in Prostate cancer. *BJU Int*, *113*(3), 358-366.

Lara-Gonzalez, P., Moyle, M. W., Budrewicz, J., Mendoza-Lopez, J., Oegema, K., & Desai, A. 2019. The G2-to-M transition is ensured by a dual mechanism that protects cyclin B from degradation by Cdc20-activated APC/C. *Developmental cell*, *51*(3), 313-325.

Laughlin, K. M., Luo, D., Liu, C., Shaw, G., Warrington, K. H., Qiu, J., ... & Harrison, J. K. 2009. Hematopoietic-and neurologic-expressed sequence 1 expression in the murine GL261 and high-grade human gliomas. *Pathology & Oncology Research*, *15*(3), 437.

Leber, B., Maier, B., Fuchs, F., Chi, J., Riffel, P., Anderhub, S., ... & Krämer, A. 2010. Proteins required for centrosome clustering in cancer cells. *Science translational medicine*, *2*(33), 33ra38-33ra38.

Lee, J., Freddolino, P. L., & Zhang, Y. 2017. *Ab initio* protein structure prediction. In *From protein structure to function with bioinformatics* (pp. 3-35). Springer, Dordrecht.

Li, M., & Zhang, P. 2009. The function of APC/C^{Cdh1} in cell cycle and beyond. *Cell division*, *4*(1), 1-7.

Li, S., Meng, H., Zhou, F., Zhai, L., Zhang, L., Gu, F., ... & Qi, L. 2013. MicroRNA-132 is frequently down-regulated in ductal carcinoma in situ (DCIS) of breast and acts as a tumor suppressor by inhibiting cell proliferation. *Pathology-Research and Practice*, *209*(3), 179-183.

Li, X., Zhao, Q., Liao, R., Sun, P., & Wu, X. 2003. The SCFSkp2 ubiquitin ligase complex interacts with the human replication licensing factor Cdt1 and regulates Cdt1 degradation. *Journal of Biological Chemistry*, *278*(33), 30854-30858.

Lin, M., Xie, S. S., & Chan, K. Y. 2022. An updated view on the centrosome as a cell cycle regulator. *Cell Division*, *17*(1), 1-13.

Liu, Z., Yang, D., Li, Y., Jiao, Y., & Lv, G. 2020. HN1 as a diagnostic and prognostic biomarker for liver cancer. *Bioscience Reports*, *40*(7).

Loncarek, J., & Bettencourt-Dias, M. 2018. Building the right centriole for each cell type. *Journal of Cell Biology*, *217*(3), 823-835.

Lonergan, P. E., & Tindall, D. J. 2011. Androgen receptor signaling in Prostate cancer development and progression. *Journal of carcinogenesis*, *10*.

Lu, K. H., Patterson, A. P., Wang, L., Marquez, R. T., Atkinson, E. N., Baggerly, K. A., ... & Smith, D. 2004. Selection of potential markers for epithelial ovarian cancer with gene expression arrays and recursive descent partition analysis. *Clinical cancer research*, *10*(10), 3291-3300.

Luo, L., & Kessel, M. 2004. Geminin coordinates cell cycle and developmental control. *Cell cycle*, *3*(6), 709-712.

Mahjoub, M. R., & Stearns, T. 2012. Supernumerary centrosomes nucleate extra cilia and compromise primary cilium signaling. *Current Biology*, *22*(17), 1628-1634.

Malumbres, M., & Barbacid, M. 2001. To cycle or not to cycle: a critical decision in cancer. *Nature reviews cancer*, *1*(3), 222-231.

Martin, M., & Akhmanova, A. 2018. Coming into focus: mechanisms of microtubule minus-end organization. *Trends in cell biology*, *28*(7), 574-588.

Mateo, J., Seed, G., Bertan, C., Rescigno, P., Dolling, D., Figueiredo, I., ... & de Bono, J. S. 2020. Genomics of lethal Prostate cancer at diagnosis and castration resistance. *The Journal of clinical investigation*, *130*(4), 1743-1751.

Mavrommati, I., Faedda, R., Galasso, G., Li, J., Burdova, K., Fischer, R., ... & D'Angiolella, V. 2018. β-TrCP-and casein kinase II-mediated degradation of cyclin F controls timely mitotic progression. *Cell reports*, *24*(13), 3404-3412.

Melixetian, M., Ballabeni, A., Masiero, L., Gasparini, P., Zamponi, R., Bartek, J., ... & Helin, K. 2004. Loss of Geminin induces rereplication in the presence of functional p53. *The Journal of cell biology*, *165*(4), 473-482.

Mills, I. G. 2014. Maintaining and reprogramming genomic androgen receptor activity in Prostate cancer. *Nature Reviews Cancer*, *14*(3), 187-198.

Mittal, K., Kaur, J., Jaczko, M., Wei, G., Toss, M. S., Rakha, E. A., ... & Aneja, R. 2021. Centrosome amplification: A quantifiable cancer cell trait with prognostic value in solid malignancies. *Cancer and Metastasis Reviews*, *40*(1), 319-339.

Moser, J., Miller, I., Carter, D., & Spencer, S. L. 2018. Control of the Restriction Point by Rb and p21. *Proceedings of the National Academy of Sciences*, *115*(35), E8219-E8227.

Musacchio, A. 2015. The molecular biology of spindle assembly checkpoint signaling dynamics. *Current biology*, *25*(20), R1002-R1018.

Mustofa, M. K., Tanoue, Y., Tateishi, C., Vaziri, C., & Tateishi, S. 2020. Roles of Chk2/CHEK2 in guarding against environmentally induced DNA damage and replication‐stress. *Environmental and Molecular Mutagenesis*, *61*(7), 730-735.

Nakayama, K., Nagahama, H., Minamishima, Y. A., Matsumoto, M., Nakamichi, I., Kitagawa, K., ... & Hatakeyama, S. 2000. Targeted disruption of Skp2 results in accumulation of cyclin E and p27Kip1, polyploidy and centrosome overduplication. *The EMBO journal*, *19*(9), 2069-2081.

Nam, H. J., Chae, S., Jang, S. H., Cho, H., & Lee, J. H. 2010. The PI3K–Akt mediates oncogenic Met-induced centrosome amplification and chromosome instability. *Carcinogenesis*, *31*(9), 1531-1540.

Nigg, E. A. 2006. Origins and consequences of centrosome aberrations in human cancers. *International journal of cancer*, *119*(12), 2717-2723.

Ogden, A., Rida, P. C., & Aneja, R. 2013. Heading off with the herd: how cancer cells might maneuver supernumerary centrosomes for directional migration. *Cancer and Metastasis Reviews*, *32*(1), 269-287.

Otto, T., & Sicinski, P. 2017. Cell cycle proteins as promising targets in cancer therapy. *Nature Reviews Cancer*, *17*(2), 93-115.

Ovchinnikov, S., Kim, D. E., Wang, R. Y. R., Liu, Y., DiMaio, F., & Baker, D. 2016. Improved de novo structure prediction in CASP 11 by

incorporating coevolution information into Rosetta. *Proteins: Structure, Function, and Bioinformatics*, *84*, 67-75.

Ozturk, B.E. 2016. Investigating the role of HN1 in centrosome localization and duplication. Fen Bilimleri Enstitütü, Ege Üniversitesi. 96 s.

Pack, L. R., Daigh, L. H., & Meyer, T. 2019. Putting the brakes on the cell cycle: mechanisms of cellular growth arrest. *Current opinion in cell biology*, *60*, 106-113.

Pan, Z., Fang, Q., Li, L., Zhang, Y., Xu, T., Liu, Y., ... & Ge, M. 2021. HN1 promotes tumor growth and metastasis of anaplastic thyroid carcinoma by interacting with STMN1. *Cancer letters*, *501*, 31-42.

Pancione, M., Cerulo, L., Remo, A., Giordano, G., Gutierrez-Uzquiza, Á., Bragado, P., & Porras, A. 2021. Centrosome dynamics and its role in inflammatory response and metastatic process. *Biomolecules*, *11*(5), 629.

Pathan, M., Keerthikumar, S., Ang, C. S., Gangoda, L., Quek, C. Y., Williamson, N. A., ... & Mathivanan, S. 2015. FunRich: An open access standalone functional enrichment and interaction network analysis tool. *Proteomics*, *15*(15), 2597-2601.

Perdomo, H. A. G., Zapata-Copete, J. A., & Sanchez, A. 2018. Molecular alterations associated with Prostate cancer. *Central European Journal of Urology*, *71*(2), 168.

Pernar, C. H., Ebot, E. M., Wilson, K. M., & Mucci, L. A. 2018. The epidemiology of Prostate cancer. *Cold Spring Harbor perspectives in medicine*, *8*(12), a030361.

Pihan, G. A. 2013. Centrosome dysfunction contributes to chromosome instability, chromoanagenesis, and genome reprograming in cancer. *Frontiers in oncology*, *3*, 277.

Pihan, G. A., Purohit, A., Wallace, J., Malhotra, R., Liotta, L., & Doxsey, S. J. 2001. Centrosome defects can account for cellular and genetic changes that characterize Prostate cancer progression. *Cancer research*, *61*(5), 2212-2219.

Potapova, T. A., Daum, J. R., Byrd, K. S., & Gorbsky, G. J. 2009. Fine tuning the cell cycle: activation of the Cdk1 inhibitory phosphorylation

pathway during mitotic exit. *Molecular biology of the cell*, *20*(6), 1737-1748.

Qiao, R., Weissmann, F., Yamaguchi, M., Brown, N. G., VanderLinden, R., Imre, R., ... & Peters, J. M. 2016. Mechanism of APC/CCDC20 activation by mitotic phosphorylation. *Proceedings of the National Academy of Sciences*, *113*(19), E2570-E2578.

Rebello, R. J., Christoph, O., Knudsen, K. E., Loeb, S., Johnson, D. C., Reiter, R. E., ... & Bristow, R. G. 2021. Prostate cancer (Primer). *Nature Reviews: Disease Primers*, *7*(1).

Ren, S., & Rollins, B. J. 2004. Cyclin C/cdk3 promotes Rb-dependent G0 exit. *Cell*, *117*(2), 239-251.

Ren, S., Wei, G. H., Liu, D., Wang, L., Hou, Y., Zhu, S., ... & Sun, Y. 2018. Whole-genome and transcriptome sequencing of Prostate cancer identify new genetic alterations driving disease progression. *European urology*, *73*(3), 322-339.

Rhodes, D. R., Kalyana-Sundaram, S., Mahavisno, V., Varambally, R., Yu, J., Briggs, B. B., ... & Chinnaiyan, A. M. 2007. Oncomine 3.0: genes, pathways, and networks in a collection of 18,000 cancer gene expression profiles. *Neoplasia*, *9*(2), 166-180.

Risk, J. M., Evans, K. E., Jones, J., Langan, J. E., Rowbottom, L., McRonald, F. E., ... & Kelsell, D. P. 2002. Characterization of a 500 kb region on 17q25 and the exclusion of candidate genes as the familial Tylosis Oesophageal Cancer (TOC) locus. *Oncogene*, *21*(41), 6395.

Robins, D. M. 2012. Androgen receptor gene polymorphisms and alterations in Prostate cancer: of humanized mice and men. *Molecular and cellular endocrinology*, *352*(1-2), 26-33.

Robinson, D., Van Allen, E. M., Wu, Y. M., Schultz, N., Lonigro, R. J., Mosquera, J. M., ... & Chinnaiyan, A. M. 2015. Integrative clinical genomics of advanced Prostate cancer. *Cell*, *161*(5), 1215-1228.

Rodier, G., Coulombe, P., Tanguay, P. L., Boutonnet, C., & Meloche, S. 2008. Phosphorylation of Skp2 regulated by CDK2 and Cdc14B protects it from degradation by APCCdh1 in G1 phase. *The EMBO journal*, *27*(4), 679-691.

Rodrigues-Ferreira, S., & Nahmias, C. 2020. From tumorigenesis to cell death: the aneuploidy paradox. *Molecular & Cellular Oncology*, *7*(2), 1709390.

Romanuik, T. L., Wang, G., Morozova, O., Delaney, A., Marra, M. A., & Sadar, M. D. 2010. LNCaP Atlas: gene expression associated with in vivo progression to castration-recurrent Prostate cancer. *BMC medical genomics*, *3*(1), 43.

Rubin, S. M., Sage, J., & Skotheim, J. M. 2020. Integrating old and new paradigms of G1/S control. *Molecular Cell*, *80*(2), 183-192.

Ryniawec, J. M., & Rogers, G. C. 2021. Centrosome instability: when good centrosomes go bad. *Cellular and Molecular Life Sciences*, *78*(21), 6775-6795.

Sabat-Pośpiech, D., Fabian-Kolpanowicz, K., Prior, I. A., Coulson, J. M., & Fielding, A. B. 2019. Targeting centrosome amplification, an Achilles' heel of cancer. *Biochemical Society Transactions*, *47*(5), 1209-1222.

Sakaue-Sawano, A., Kurokawa, H., Morimura, T., Hanyu, A., Hama, H., Osawa, H., ... & Miyawaki, A. 2008. Visualizing spatiotemporal dynamics of multicellular cell-cycle progression. *Cell*, *132*(3), 487-498.

Sanches, B. D., Maldarine, J. S., Vilamaior, P. S., Felisbino, S. L., Carvalho, H. F., & Taboga, S. R. 2021. Stromal cell interplay in Prostate development, physiology, and pathological conditions. *The Prostate*, *81*(13), 926-937.

Santamaría, D., Barrière, C., Cerqueira, A., Hunt, S., Tardy, C., Newton, K., ... & Barbacid, M. 2007. Cdk1 is sufficient to drive the mammalian cell cycle. *Nature*, *448*(7155), 811-815.

Satyanarayana, A., & Kaldis, P. 2009. Mammalian cell-cycle regulation: several Cdks, numerous cyclins and diverse compensatory mechanisms. *Oncogene*, *28*(33), 2925-2939.

Schatten, H., & Ripple, M. O. 2018. The impact of centrosome pathologies on Prostate cancer development and progression. *Cell & Molecular Biology of Prostate Cancer*, 67-81.

Schatten, H., & Sun, Q. Y. 2015. Centrosome and microtubule functions and dysfunctions in meiosis: implications for age-related infertility and

developmental disorders. *Reproduction, Fertility and Development*, *27*(6), 934-943.

Schatten, H., & Sun, Q. Y. 2018. Functions and dysfunctions of the mammalian centrosome in health, disorders, disease, and aging. *Histochemistry and Cell Biology*, *150*(4), 303-325.

Schrock, M. S., Stromberg, B. R., Scarberry, L., & Summers, M. K. 2020, December. APC/C ubiquitin ligase: Functions and mechanisms in tumorigenesis. In *Seminars in Cancer Biology* (Vol. 67, pp. 80-91). Academic Press.

Seiki, M. 2003. Membrane-type 1 matrix metalloproteinase: a key enzyme for tumor invasion. *Cancer letters*, *194*(1), 1-11.

Serin, E. A., Nijveen, H., Hilhorst, H. W., & Ligterink, W. 2016. Learning from co-expression networks: possibilities and challenges. *Frontiers in plant science*, *7*, 444.

Silkworth, W. T., Nardi, I. K., Scholl, L. M., & Cimini, D. 2009. Multipolar spindle pole coalescence is a major source of kinetochore mis-attachment and chromosome mis-segregation in cancer cells. *PloS one*, *4*(8), e6564.

Silver, L. M. 1993. The peculiar journey of a selfish chromosome: mouse t haplotypes and meiotic drive. *Trends in Genetics*, *9*(7), 250-254.

Siu, K. T., Rosner, M. R., & Minella, A. C. 2012. An integrated view of cyclin E function and regulation. *Cell cycle*, *11*(1), 57-64.

Snow, O., Lallous, N., Singh, K., Lack, N., Rennie, P., & Cherkasov, A. 2019. Androgen receptor plasticity and its implications for Prostate cancer therapy. *Cancer Treatment Reviews*, *81*, 101871.

Stopsack, K. H., Nandakumar, S., Wibmer, A. G., Haywood, S., Weg, E. S., Barnett, E. S., ... & Abida, W. 2020. Oncogenic genomic alterations, clinical phenotypes, and outcomes in metastatic castration-sensitive Prostate cancer. *Clinical Cancer Research*, *26*(13), 3230-3238.

Sunchu, B., & Cabernard, C. 2020. Principles and mechanisms of asymmetric cell division. *Development*, *147*(13), dev167650.

Szklarczyk, D., Franceschini, A., Wyder, S., Forslund, K., Heller, D., Huerta-Cepas, J., ... & Von Mering, C. 2015. STRING v10: protein–

protein interaction networks, integrated over the tree of life. *Nucleic acids research*, *43*(D1), D447-D452.

T Das, A., Tenenbaum, L., & Berkhout, B. 2016. Tet-on systems for Doxycycline-inducible gene expression. *Current gene therapy*, *16*(3), 156-167.

Tan, M. H., Li, J., Xu, H. E., Melcher, K., & Yong, E. L. 2015. Androgen receptor: structure, role in Prostate cancer and drug discovery. *Acta Pharmacologica Sinica*, *36*(1), 3-23.

Tang, W., Lai, Y. H., Han, X. D., Wong, P. M., Peters, L. L., & Chui, D. H. 1997. Murine Hn1 on chromosome 11 is expressed in hemopoietic and brain tissues. *Mammalian genome*, *8*(9), 695-696.

Tang, Z., Li, C., Kang, B., Gao, G., Li, C., & Zhang, Z. 2017. GEPIA: a web server for cancer and normal gene expression profiling and interactive analyses. *Nucleic acids research*, *45*(W1), W98-W102.

Thompson, L. L., Rutherford, K. A., Lepage, C. C., & McManus, K. J. 2021. The SCF Complex Is Essential to Maintain Genome and Chromosome Stability. *International Journal of Molecular Sciences*, *22*(16), 8544.

Thu, K. L., Soria-Bretones, I., Mak, T. W., & Cescon, D. W. 2018. Targeting the cell cycle in breast cancer: towards the next phase. *Cell Cycle*, *17*(15), 1871-1885.

Van der Steen, T., Tindall, D. J., & Huang, H. 2013. Posttranslational modification of the androgen receptor in Prostate cancer. *International journal of molecular sciences*, *14*(7), 14833-14859.

van Leuken, R., Clijsters, L., van Zon, W., Lim, D., Yao, X., Wolthuis, R. M., ... & van Vugt, M. A. 2009. Polo-like kinase-1 controls Aurora A destruction by activating APC/C-Cdh1. *PLoS One*, *4*(4), e5282.

Varisli, L., 2012, Hücre döngüsü kontrolünde HN1'in rolü, Doktora Tezi, Ege Üniversitesi Fen Bilimleri Enstitüsü, 152 s

Varisli, L., Gonen-Korkmaz, C., Debelec-Butuner, B., Erbaykent-Tepedelen, B., Muhammed, H. S., Bogurcu, N., ... & Korkmaz, K. S. 2011. Ubiquitously expressed hematological and neurological expressed 1 downregulates Akt-mediated GSK3β signaling, and its

knockdown results in deregulated G2/M transition in Prostate cells. *DNA and cell biology*, *30*(6), 419-429.

Varisli, L., Gonen-Korkmaz, C., Syed, H. M., Bogurcu, N., Debelec-Butuner, B., Erbaykent-Tepedelen, B., & Korkmaz, K. S. 2012. Androgen regulated HN1 leads proteosomal degradation of androgen receptor (AR) and negatively influences AR mediated transactivation in Prostate cells. *Molecular and cellular endocrinology*, *350*(1), 107-117.

Varisli, L., Gonen-Korkmaz, C., Syed, H. M., Bogurcu, N., Debelec-Butuner, B., Erbaykent-Tepedelen, B., & Korkmaz, K. S. 2012. Androgen regulated HN1 leads proteosomal degradation of androgen receptor (AR) and negatively influences AR mediated transactivation in Prostate cells. *Molecular and cellular endocrinology*, *350*(1), 107-117.

Varisli, L., Ozturk, B. E., Akyuz, G. K., & Korkmaz, K. S. 2015. HN1 Negatively Influences the β‐Catenin/E‐Cadherin Interaction, and Contributes to Migration in Prostate Cells. *Journal of cellular biochemistry*, *116*(1), 170-178.

Vodermaier, H. C. 2004. APC/C and SCF: controlling each other and the cell cycle. *Current Biology*, *14*(18), R787-R796.

Vora, S. M., Fassler, J. S., & Phillips, B. T. 2020. Centrosomes are required for proper β-catenin processing and Wnt response. *Molecular biology of the cell*, *31*(17), 1951-1961.

Wakefield, J. G., Stephens, D. J., & Tavaré, J. M. 2003. A role for glycogen synthase kinase-3 in mitotic spindle dynamics and chromosome alignment. *Journal of cell science*, *116*(4), 637-646.

Wang, G., Zhao, D., Spring, D. J., & DePinho, R. A. 2018. Genetics and biology of Prostate cancer. *Genes & development*, *32*(17-18), 1105-1140.

Wright, P. E., & Dyson, H. J. 2015. Intrinsically disordered proteins in cellular signalling and regulation. *Nature reviews Molecular cell biology*, *16*(1), 18-29.

Wu, L., Grigoryan, A. V., Li, Y., Hao, B., Pagano, M., & Cardozo, T. J. 2012. Specific small molecule inhibitors of Skp2-mediated p27 degradation. *Chemistry & biology*, *19*(12), 1515-1524.

Xue, B., Dunbrack, R. L., Williams, R. W., Dunker, A. K., & Uversky, V. N. 2010. PONDR-FIT: a meta-predictor of intrinsically disordered amino acids. *Biochimica et Biophysica Acta (BBA)-Proteins and Proteomics*, *1804*(4), 996-1010.

Yamamoto, Y., Matsuyama, H., Furuya, T., Oga, A., Yoshihiro, S., Okuda, M., ... & Naito, K. 2004. Centrosome hyperamplification predicts progression and tumor recurrence in bladder cancer. *Clinical cancer research*, *10*(19), 6449-6455.

Yang, J., Yan, R., Roy, A., Xu, D., Poisson, J., & Zhang, Y. 2015. The I-TASSER Suite: protein structure and function prediction. *Nature methods*, *12*(1), 7-8.

Yang, S., Kim, C. Y., Hwang, S., Kim, E., Kim, H., Shim, H., & Lee, I. 2017. COEXPEDIA: exploring biomedical hypotheses via co-expressions associated with medical subject headings (MeSH). *Nucleic acids research*, *45*(D1), D389-D396.

Yoon, M. K., Mitrea, D. M., Ou, L., & Kriwacki, R. W. 2012. Cell cycle regulation by the intrinsically disordered proteins p21 and p27. *Biochemical Society Transactions*, *40*(5), 981-988.

Yu, Y., & Feng, Y. M. 2010. The role of kinesin family proteins in tumorigenesis and progression: potential biomarkers and molecular targets for cancer therapy. *Cancer*, *116*(22), 5150-5160.

Zhang, C., Xu, B., Lu, S., Zhao, Y., & Liu, P. 2017. HN1 contributes to migration, invasion, and tumorigenesis of breast cancer by enhancing MYC activity. *Molecular cancer*, *16*(1), 90.

Zhang, Z. G., Chen, W. X., Wu, Y. H., Liang, H. F., & Zhang, B. X. 2014. MiR-132 prohibits proliferation, invasion, migration, and metastasis in breast cancer by targeting HN1. *Biochemical and biophysical research communications*, *454*(1), 109-114.

Zhao, H. U. I., & Piwnica-Worms, H. 2001. ATR-mediated checkpoint pathways regulate phosphorylation and activation of human Chk1. *Molecular and cellular biology*, *21*(13), 4129-4139.

Zhao, J. Z., Ye, Q., Wang, L., & Lee, S. C. 2021. Centrosome amplification in cancer and cancer-associated human diseases. *Biochimica et Biophysica Acta (BBA)-Reviews on Cancer*, *1876*(1), 188566.

Zhou, G., Wang, J., Zhang, Y., Zhong, C., Ni, J., Wang, L., ... & Zhao, S. 2004. Cloning, expression and subcellular localization of HN1 and HN1L genes, as well as characterization of their orthologs, defining an evolutionarily conserved gene family. *Gene*, *331*, 115-123.

Zielke, N., & Edgar, B. A. 2015. FUCCI sensors: powerful new tools for analysis of cell proliferation. *Wiley Interdisciplinary Reviews: Developmental Biology*, *4*(5), 469-487.

Zyss, D., & Gergely, F. 2009. Centrosome function in cancer: guilty or innocent?. *Trends in cell biology*, *19*(7), 334-346.

RESUME

Education

PhD Biotechnology (2017-2022)

Department of Biotechnology, Graduate School of Natural and Applied Science, Ege University, Izmir, Turkey

MS Healthcare Biotechnology (2013-2015)

Department of Healthcare Biotechnology, Atta Ur Rahman School of Applied Biosciences (ASAB), National University of Sciences and Technology (NUST), Islamabad, Pakistan

B.S. (Hons.) Biotechnology & Bioinformatics (2009-2013)

Institute of Biochemistry & Biotechnology (IBBT), University of Veterinary and Animal Sciences (UVAS), Lahore, Pakistan

Research Experience

Researcher (2021-2022)

Scientific Research Project (BAP) (FGA-2021-21986), Department of Bioengineering, Ege University

Project Title: *Investigation of Anaphase Promoting Complex APCCcdh1 Activity and its Relationship with HN1*

Researcher (2019-2020)

TUBITAK 1001 Project (117S289), Department of Bioengineering, Ege University

Project Title: *Investigation of the Basis of Genetic Heterogeneity Developed by the Inflammatory Microenvironment in the Development of Prostate Cancer*

Research Scholar (2014-2015)

Atta Ur Rahman School of Applied Biosciences (ASAB), Department of Healthcare Biotechnology (Islamabad, Pakistan)

Project Title: *Mycosynthesis, Characterization, and Investigation of Therapeutic Potentials of Silver Nanoparticles*

Internship (April-June 2013)

Quality Operations Laboratory (QOL), University of Veterinary and Animal Sciences (UVAS)

Project Title: *Molecular Characterization of Newcastle Disease Virus and Development of Vaccine Approaches*

Final Year Internship

Faculty of Biosciences, Institute of Biochemistry and Biotechnology (IBBT), University of Veterinary and Animal Sciences (UVAS)

Title: *Hands-on Experience Practices in Different Laboratories including; Molecular Biology, Toxicology, Pathology, and Microbiology*

Publications

Review Article (First Author): **Javed, A**., Malagraba, G., Yarmohammadi, M., Barceló, C., & Rubio-Tomás, T. (2022). Therapeutic Potential Of Mitotic Kinases Inhibitors In Cancers Of The Gastrointestinal System. Future Pharmacology (Under Review)

Review Article (Co-first Author): Malagraba, G., Yarmohammadi, M., **Javed, A**., Barceló, C., & Rubio-Tomás, T. (2022). The Role of LSD1 and LSD2 in Cancers of the Gastrointestinal System: An Update. Biomolecules, 12(3), 462. DOI: 10.3390/biom12030462

Book Chapter (First Author): **Javed, A**., Niaz, K., Sideeq, O. (2021). Genetically engineered mouse models for COVID-19. In COVID-19: Different Models and Treatment Strategies (2) 1-19. Bentham Sciences. DOI: 10.2174/9781681089072121020004

Book Chapter (Last Author): Siqeeq, O., Niaz, K., Rahim, K., **Javed, A**. (2021). Stem cell therapy for COVID-19. In Different Models and Treatment Strategies (2) 266-287. Bentham Sciences DOI: 10.2174/9781681089072121020014

Research Article (Co-first Author): Varisli, L., **Javed, A**., Ozturk, B. E., Akyuz, G. K., Takir, G., Roumelioti, F. M., ... & Korkmaz, K. S. (2021). HN1 interacts with γ-tubulin to regulate centrosomes in advanced Prostate cancer cells. Cell Cycle, 1-22. DOI: 10.1080/15384101.2021.1962624

Research Article (Corresponding Author): Öztoprak, F., & **Javed, A**. (2020). Case fatality rate estimation of COVID-19 for European countries: Turkey's current scenario amidst a global pandemic; comparison of outbreaks with European countries. EJMO, 4(2), 149-159. DOI: 10.14744/ejmo.2020.60998

Book Chapter (First Author): **Javed, A**., Shahzad, M., Khan, F., & Niaz, K. (2020). Curcuminoids. In Recent Advances in Natural Products Analysis (1st ed., pp. 147-161). Elsevier.

Book Chapter (First Author): **Javed, A**., Umar, H., Khan, F., & Niaz, K. (2020). Stilbenoids. In Recent Advances in Natural Products Analysis (1st ed., pp. 117-131). Elsevier.

Review Article (Last Author): Khan, A. H., Khan, R., Saeed, M., & **Javed, A**. (2017). RHEUMATOID ARTHRITIS THERAPIES: PRESENT AND FUTURE. PAFMJ, 67(3), 483-87.

Review Article (First Author): **Javed. A**., Saeed, M. (2015). Introduction to Nano-technological Structures and their Potential Therapeutic Uses in Viral Diseases. Journal of Bio-Molecular Sciences 3(1), 1-17. Direct Sciences.

ACKNOWLEDGEMENT

I am thankful to my supervisor and mentor Prof. Dr. Kemal Sami Korkmaz for being the best supervisor any student can ask for, especially for a journey as tough and scientifically challenging as a PhD. I am thankful to my thesis committee members Prof. Dr. Petek Ballar Kırmızıbayrak and Doç. Dr. Buket Kosova for timely progress meetings and valuable suggestions throughout the period of this project.

I am thankful to all the members of the Cancer Biology Laboratory including Dr. Iroda Saydullaeva who introduced me to some of the aspects of the laboratory work. I am thankful to Sevda Altun, Elif İşel, Gülseren Özduman, Dilan Yerli, Doğan Duran, Büşra Dayıoğlu, Faruk Şimşek, and Tilbe Özar.

Moreover, I am grateful to the previous members of Cancer Biology lab for paving the way for us to carry out investigations on HN1. I am also grateful to Prof. Dr. Ayşe Nalbantsoy for letting us use flowcytometer of her lab, and thankful to Turkiye Bursları for supporting me personally to be granted for a doctoral program in Turkey.

I am also thankful to TUBITAK (project no: 113Z083 and partly 221Z202) and Ege BAP (thesis project) committees for financially supporting the projects undertaken in our Cancer Biology Laboratory, Department of Bioengineering, Ege University.

This journey could not have been possible without the constant support of my family. I am forever in debt to all my family members for letting me pursue my passion for higher education.

Aadil JAVED

10/06/22

IZMIR